Quantum chemical investigation of linear and nonlinear optical polarizabilities in organic molecular aggregates and inorganic clusters

A Thesis

Submitted For the Degree of

MASTER OF SCIENCE

as a part of the Integrated Ph. D Programme

in the Faculty of Science

by

Ayan Datta

CHEMISTRY AND PHYSICS OF MATERIALS UNIT
JAWAHARLAL NEHRU CENTRE FOR ADVANCED SCIENTIFIC
RESEARCH
Bangalore – 560 064

APRIL 2004

To my mother

DECLARATION

I hereby declare that the matter embodied in the thesis entitled "**Quantum chemical investigation of linear and nonlinear optical polarizabilities in organic molecular aggregates and inorganic clusters**" is the result of investigations carried out by me at the Chemistry and Physics of Materials Unit, Jawaharlal Nehru Centre for Advanced Scientific Research, Bangalore, India under the supervision of Dr. Swapan Pati and that it has not been submitted elsewhere for the award of any degree or diploma.
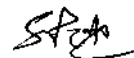
In keeping with the general practice in reporting scientific observations, due acknowledgement has been made whenever the work described is based on the findings of other investigators.

Ayan Datta

—————————

Ayan Datta

CERTIFICATE

I hereby certify that the matter embodied in this thesis entitled "**Quantum chemical investigation of linear and nonlinear optical polarizabilities in organic molecular aggregates and inorganic clusters**" has been carried out by Mr. Ayan Datta at the Chemistry and Physics of Materials Unit, Jawaharlal Nehru Centre for Advanced Scientific Research, Bangalore, India under my supervision and that it has not been submitted elsewhere for the award of any degree or diploma.

Dr. Swapan Pati
(Research Supervisor)

Acknowledgements

Who we are is not only comprised of the knowledge we have gathered, but also those who have influenced us. I am lucky to have been influenced by many incredible and loving people, and I want to thank all of them for being a part of whom I am today.

First, I remember my family. Mom, thank you for teaching me to never give up, and for being so patient with my curiosity and my desire to take things differently. You got up at five in the morning, 365 days a year whether it was winter or summer for making tiffin for my school. You will stay awake till midnight to make sure that I had put the mosquito net. Without your love and affection, life would have been really miserable. Dad and brother thank you for sparking my interest in science.

I would like to thank my supervisor, Dr. Swapan K. Pati for all the support, knowledge and encouragement that he has bestowed upon me. He has always cared for me and taught me how handle problems in science as well as in life. The independence and freedom that he has provided me in my work has helped me grow up from a novice to a research worker. He has provided me all the facilities and opportunities that I have not even dreamt of. Also, he has been very understanding and caring, and has forgotten and

Synopsis

In the present thesis, we have tried to elucidate the proper parameters upon which the nonlinear optical properties of materials depend. The thesis is divided into five chapters.

The first chapter provides a brief introduction to Nonlinear optics and its various applications. In the next chapter we have developed a model considering the orientation effects of the molecules in an assembly and discuss briefly how such different orientations can lead to changes in the optical properties of the molecular assemblies. We have also outlined the methods for stablilization of such assemblies due to Hydrogen - bonding interactions.

In the third chapter we consider a series of push-pull type organic chromophores and consider their various dipolar orientations and suggest the best orientation for maximizing their NLO responses based on the theory developed in chapter 2.

In the fourth chapter, we consider a series of bridged push-pull chromophores where orientation of the dipoles are restricted by the degrees of freedom (bonds connecting the push-pull moieties) and try to understand the factors that govern their behaviors in an electric field. We also suggest modifications to the experimental systems that will maximize their optical

polarizations.

Finally, in the fifth chapter, we extend our dipole interaction theory to finite-sized metallic clusters. These hetero-atomic metal clusters are interesting because of the ease by which they can be polarized due to out-of-plane charge transfer contrary to π- conjugated organic polymers which are polarized due to delocalization of the π-electrons. We compare and contrast the NLO properties of the conventional organic π-conjugated molecules to that of these metal clusters of similar sizes and geometries. We show that the NLO properties for these metal-clusters are orders of magnitude higher than their organic counterparts. We conjecture that these metal-clusters are good candidates for next generation NLO materials.

Nomenclature

e : Electron

ω : Frequency of applied field

χ : Optical Susceptibilities

η : Refractive Index

α : Linear Polarizability

β : First order Hyperpolarizability

γ : Second order Hyperpolarizability

$\alpha_2(\omega)$: Two-photon absorbtion coefficient

μ : Dipole Moment

au: Atomic Units

Contents

x

List of Figures

xv

List of Tables

Chapter 1

Nonlinear optical processes and related phenomena

A material undergoes distortion when exposed to an external electric field. The atoms develop an oscillating separation of charges that tend to counteract the field. The electromagnetic radiation thus induces a forced separation of the charges. This leads to a dipolar oscillation in the system, which emits radiation of the frequency of its oscillation. Thus as the wave field travels through the medium, it induces polarization whose oscillation launches an electromagnetic wave of its own. Since, there can be an out-of-plane component to this new wave, the net result is a phase shift in the emerging wave. This phase shift is the index of refraction of the material.

Under this external influence, the material becomes polarized with an induced dipole moment. Each constituent molecule of the material acts as a dipole with a dipole moment P_i. The dipole moment vector per unit volume

1

P is given by

$$P = \sum_i P_i \qquad (1.1)$$

where the summation is over the dipoles in the unit volume. The induced polarization in a material depends on the strength of the electric field. For a weak field, one can write the polarization as

$$P = \chi E \qquad (1.2)$$

where, χ is called the *polarizability* of the medium. The polarizability is related to the dielectric constant of the medium by

$$\epsilon = 1 + 4\pi\chi \qquad (1.3)$$

From an atomistic viewpoint, the electric field distorts the electron distribution of an atom or molecule. Thus the molecular polarization can be written as

$$\mu_i = \alpha E \qquad (1.4)$$

here, α corresponds to the polarizability of the atom or molecule. The polarizability of a system is directly proportional to the number of charges present in it. Thus, for atoms and molecules the polarizability increases with their size.

The wavelike properties of light are described by an oscillating electromagnetic field, $E(r,t)$. Consequently, the material response P and its linear susceptibility are also time and space varying quantities. Thus the previous

equation (1.2) modifies to

$$P(r,t) = \sum_{r_i} \chi_{rr_i} E(r_i, t) \qquad (1.5)$$

It can be seen that the polarization can be induced in a different direction to that of the applied field. This occurs because of the tensorial nature of the polarizability.

But, the whole story changed when the lasers produced fields much stronger than the atomic fields. With sufficiently intense laser radiation the previous relations require modification. The bulk polarization P, for a strong external field is then defined by a phenomenological power series expansion in terms of the applied electric field as [1-3]:

$$P = \chi^{(1)} E + \chi^{(2)} EE + \chi^{(3)} EEE + \ldots \qquad (1.6)$$

Here, $\chi^{(n)}$ is the nth-order susceptibility of the medium and E represents the total electric-field experienced by the system. The nth-order susceptibility is a tensor quantity of rank (n+1) which has 3^{n+1} elements [4]. Thus, $\chi^{(1)}$ is a second-rank tensor with nine elements, $\chi^{(2)}$ is a third-rank tensor with twenty-seven elements, $\chi^{(3)}$ is fourth-order tensor with eighty-one elements, and so on. This number is, of course, drastically reduced by symmetry requirements as not all elements are linearly independent and in most practical materials much fewer elements are required to describe the tensor. Thus, at a strong electric field, the optical characteristics of a medium, such as dielectric permittivity, refractive index etc., which depend on the susceptibility,

also become a function of the electric field E [5–8].

The possibility of exploiting a monochromatic light beam for the production of nonlinear optical phenomenon was first experimentally shown by Frenken *et al* [9]. They observed ultraviolet light at twice the frequency of a ruby laser (λ=6493 $\mathring{A}$), when the light was made to traverse through a quartz crystal. Also, at the same time there were reports of multi-photon absorption processes through which one could access high energy states that are otherwise forbidden by dipolar transitions, with relatively low-energy photons [10].

These experiments attracted huge attention from the science community and marked the beginning of a rich field called *Nonlinear optics* [11, 12]. The field witnessed a tremendous growth with the development of stronger lasers [13,14]. The evolution of lasers from their predecessors, the microwave beam and and the solid state masers, have been due to the phenomenal contribution by Townes, Basov and Prokhorov (they were awarded Nobel prize in 1964 for their discovery of laser) and N. Bloembergen (he was awarded the Noble prize in 1981). In short, lasers are sources of coherent light, characterized by a high degree of monochromaticity, high directionality and high intensity or brightness. With dye lasers it is possible to cover the range of wavelengths from 350-950 nm continuously, including the whole visible spectrum. A variety of nonlinear processes, including harmonic generation, extend the range of coherent sources throughout the infrared and into the vacuum ultraviolet.

Nonlinear optical (NLO) phenomena encompasses a broad range of light mediated processes like second harmonic generation, electro-optic Pockels

effect, optical rectification, third harmonic generation, optical Kerr effect and intensity dependent refractive index. It should be noted that the nonlinear optical processes were observed even before the discovery of lasers. Processes like the optical Kerr effect and the Pockels effect have been known for a very long period of time.

When an isotropic liquid comprising of asymmetric molecules (like nitrobenzene) is placed in an electric field, the molecules tend to align themselves parallel to the direction of the field. Because the molecules are not symmetrical, the alignment causes the liquid to become anisotropic and as a result bifringent. Thus, a light wave which enters the liquid, splits into two waves traveling at two different velocities with two different refractive indices. Thus the refractive index of a material can depend on the strength of the applied electric field. This is known as an *electro-optic effect*. The first order electro-optic effect (seen in crystals of KH_2PO_4) is known as Pockels effect. It is linear in the electric field. The quadratic process is called the Kerr effect. This is seen from the schematic figure (Fig 1.1) in the next page. A pockels cell, usually requires a small voltage of 1-5 kV while a Kerr cell requires a high voltage of 10-20 kV.
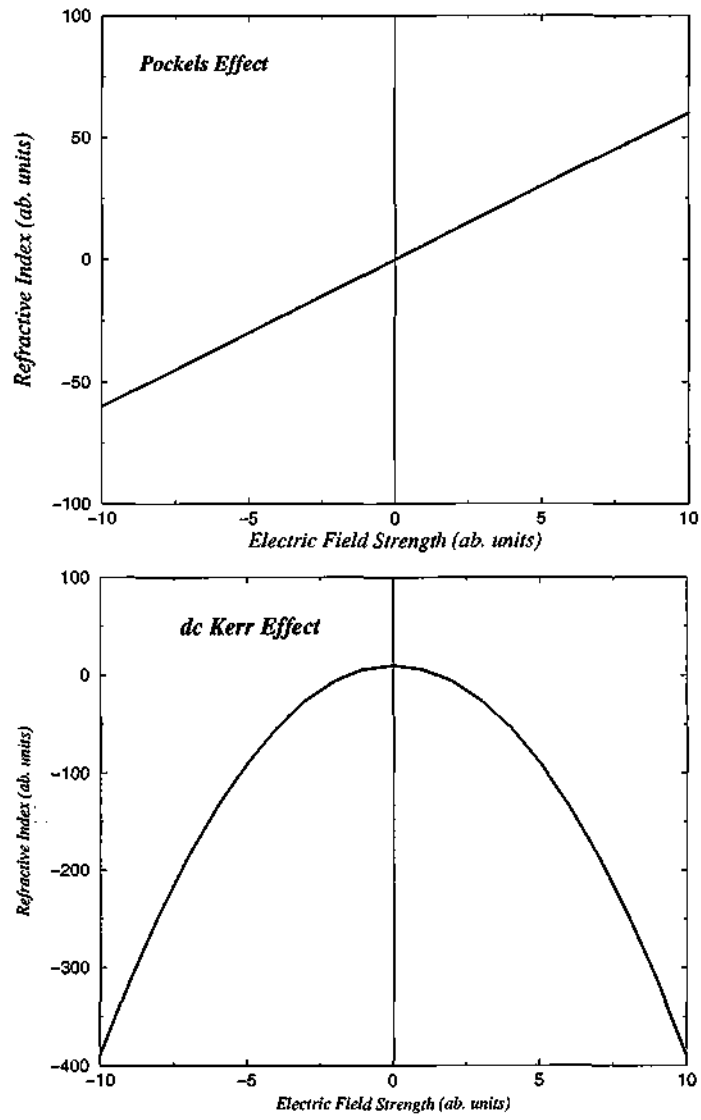
Figure 1.1: Pockel and dc Kerr Effects

For the present thesis, we limit ourselves to those NLO properties which are mostly governed by the polarizations of the electronic states. That is to say that the electric field does not distort the lattice nor does it couple to the vibronic structure of the system [15, 16].

The manifestation of the nonlinear optical behavior can be clearly seen by substituting a sinusoidal field $E = E_0 + E_1 \cos \omega t$ into the polarization. Substituting this in the previous equation (1.6) gives:

$$P = (E_0 + E_1 \cos \omega t)\chi^{(1)} + (E_0 + E_1 \cos \omega t)^2 \chi^{(2)}$$
$$+ (E_0 + E_1 \cos \omega t)^3 \chi^{(3)} + \dots \quad (1.7)$$

Rearranging the equation,

$$P = (\chi^{(1)} E_0 + \chi^{(2)} E_0^2 + \chi^{(3)} E_0^3)$$
$$+ (\chi^{(1)} E_1 + 2\chi^{(2)} E_0 E_1 + 3\chi^{(3)} E_0^2 E_1) \cos \omega t$$
$$+ (\chi^{(2)} E_1^2 + 3\chi^{(3)} E_0 E_1^2) \cos^2 \omega t$$
$$+ (\chi^{(3)} E_1^3) \cos^3 \omega t + \dots \quad (1.8)$$

Using the trigonometric relations, $\cos^2 \omega t = (1 + \cos 2\omega t)/2$ and $\cos^3 \omega t = (\cos 3\omega t + 3\cos \omega t)/4$, we get

$$P = \chi^{(1)}[E_0 + E_1 \cos \omega t]$$

$$+\chi^{(2)}[E_0^2 + (1/2)E_1^2 + 2E_0E_1 \cos \omega t + (1/2)E_1^2 \cos 2\omega t]$$

$$+\chi^{(3)}[E_0^3 + (3/2)E_0E_1^2 + 3E_0^2E_1 \cos \omega t + (3/4)E_1^3 \cos \omega t$$

$$+(3/2)E_0E_1^2 \cos 2\omega t + (3/4)E_1^3 \cos 3\omega t] + \ldots \qquad (1.9)$$

The 1st term in the brackets for all $\chi^{(n)}$ are constant factors. They give rise to a dc field across the medium.

1.1   Second-Order Optical Processes

Now let us consider the processes associated with the $\chi^{(2)}$ in details. From eqn (1.9)

$$P^{(2)} = \chi^{(2)}[E_0^2 + (1/2)E_1^2 + 2E_0E_1 \cos \omega t + (1/2)E_1^2 \cos 2\omega t] \qquad (1.10)$$

The coefficient E_0E_1 corresponds to the linear electro-optic effect and is represented as $\chi^{(2)}(-\omega;\omega,0)$. The sign attached to a frequency is negative if the photon is emitted and positive if it is absorbed. The last term which is square in the ac electric field and and has a frequency of 2ω is known as the second harmonic generation (SHG) process. Considering that two coherent light waves of unequal frequencies ω_1 and ω_2 are traveling in the material,

the 2nd and 4th terms from the previous equation (1.10) become

$$\chi^{(2)}(1/2)E_1^2[\cos(\omega_1 - \omega_2) + \cos(\omega_1 + \omega_2)] \qquad (1.11)$$

Thus we have now two new frequencies $(\omega_1 + \omega_2)$ and $(\omega_1 - \omega_2)$. This phenomenon is known as *optical mixing*. While, $\omega_1 + \omega_2$ is called the sum-frequency generation (SFG), $\omega_1 - \omega_2$ is called the difference- frequency generation (DFG). The second harmonic generation (SHG) process, actually, is a special case of SFG where the frequencies of the photons from the incident beams are equal $(\omega_1 = \omega_2)$. Similarly, *optical rectification (OR)* is a special case of DFG for $\omega_1 = \omega_2$. Thus the OR susceptibility, is represented as $\chi^{(2)}$ $(0;\omega,-\omega)$.

Three wave mixing (two inputs and one output) is known as a *parametric* process if the initial state and the final state of the system remains unchanged after interaction with the light. This is because in an emission process the system comes back to the same state after emission. The same is not true for an absorption process where the initial and the final states differ. The most prominent example of a *non-parametric* process is two-photon absorption, which will be discussed later.

Parametric processes can be used to make various devices (Fig 1.2). For example, *Optical Generators* can produce a wave of higher (up-conversion) or lower frequency (down-conversion) than the initial frequency. In *Parametric Amplifiers* three waves interact at frequency ω_1, ω_2 and ω_3 so that one wave at frequency ω_1 grows at the expense of the input frequency called, the pump frequency. A very important device using parametric amplification

is the *Optical Parametric Oscillator*. In this device, one uses a single pump source as an input and the output intensity can be controlled by changing the positions of the two mirrors surrounding the material.
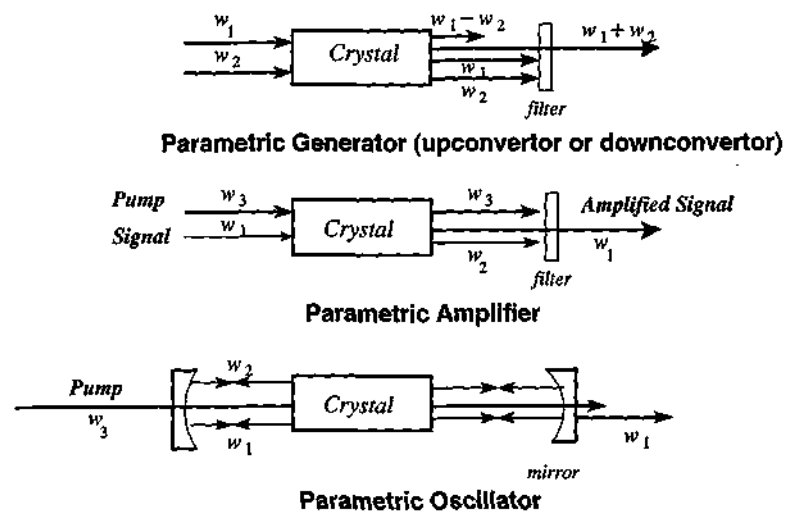
Figure 1.2: Some Important Parametric Processes

1.1.1 Symmetry Requirement for Second-Order Processes

In 1962, Kleinman found that in many nonlinear processes where all the interacting frequencies are far away from resonances, energy is simply exchanged between the fields and not dissipated in the medium [17,18]. Thus, the dispersion of the $\chi^{(n)}$ is negligible and therefore the susceptibility tensors are invariant under any permutation of their Cartesian indices. For instance, in the $\chi^{(2)}$, the symmetry relations give rise to:

$$\chi^{(2)}_{ijk} = \chi^{(2)}_{ikj} = \chi^{(2)}_{jik} = \chi^{(2)}_{jki} = \chi^{(2)}_{kij} = \chi^{(2)}_{kji} \qquad (1.12)$$

Thus due to Kleinman symmetry relations, the number of independent components of $\chi^{(2)}$ reduces from 27 to 10 and that of $\chi^{(3)}$ from 81 to 15.

For a medium to exhibit frequency conversion processes mediated by $\chi^{(2)}$, the medium must have $\chi^{(2)} \neq 0$. This condition requires that at a molecular level the nonlinear coefficient β must be nonzero. Furthermore, the orientationally averaged sum of β at all sites that gives rise to the macroscopic $\chi^{(2)}$ should not be zero. These two conditions lead to the following symmetry requirements for the realization of $\chi^{(2)} \neq 0$:

1. The molecules are noncentrosymmetric (do not possess an inversion symmetry). For such a structure, β - being an odd rank (3rd rank) tensor-is not zero (Fig 1.3).

2. The molecules in the bulk form are arranged in a noncentrosymmetric structure. Only then the overall $\chi^{(2)}$ is not zero.
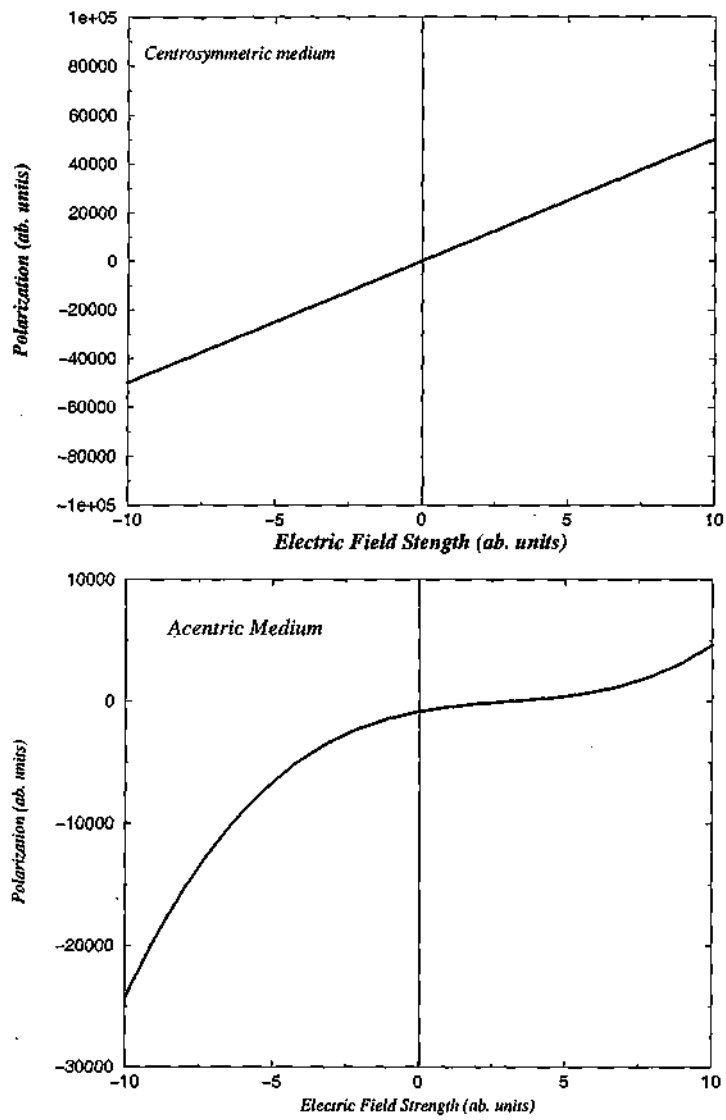
Figure 1.3: Polarization response of a material

A molecular design often used to make molecules with large β values is
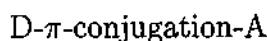
D-π-conjugation-A

where a molecular unit involving π-conjugation is connected to an electron donor, D (such as $-NH_2$), at one end and to an electron acceptor group, A (such as $-NO_2$), at the other end. A classic example is the *para*-nitroaniline molecule. We have performed extensive calculations on this molecule.

1.1.2   Methodologies for preparing a noncentrosymmetric crystal

A lot of efforts in the last two decades have been directed towards understanding and controlling the factors that may lead to an acentric crystal that shows large NLO response functions. It is quite a non-trivial task to arrange molecules in a noncentrosymmetric fashion in forming the crystal. One requires a combination of chemical intuition, theoretical understanding of intermolecular forces as well as very sound crystal engineering to tailor molecules for such applications.

D-π-conjugated-A molecular systems have a large NLO response because of the delocalized nature of the π-electrons resulting in low-energy excitonic levels with high oscillator strength. But these dipolar molecules tend to pack in an anti-parallel arrangement in the crystal thereby making the NLO response for the whole crystal almost zero. This drawback has led to search for other molecular materials. The most important of such molecules has

been the 3-methyl-4-nitropyridine-1-oxide (POM) shown in Fig 1.4. For this molecule there is a cancellation of the ground state dipole moment as the dipole moments for the pyridine-1-oxide and the nitrobenzene fragments are equal and opposite. So, the molecules have no urge to crystallize in a anti-parallel arrangement. Thus, for such a system even though the ground state dipole moment is zero, the excited states have a finite dipole moment. Such, molecules thus exhibit large β values. The crystal for POM thus have a substantial $\chi^{(2)}$ (about two times that of LiNbO$_3$).
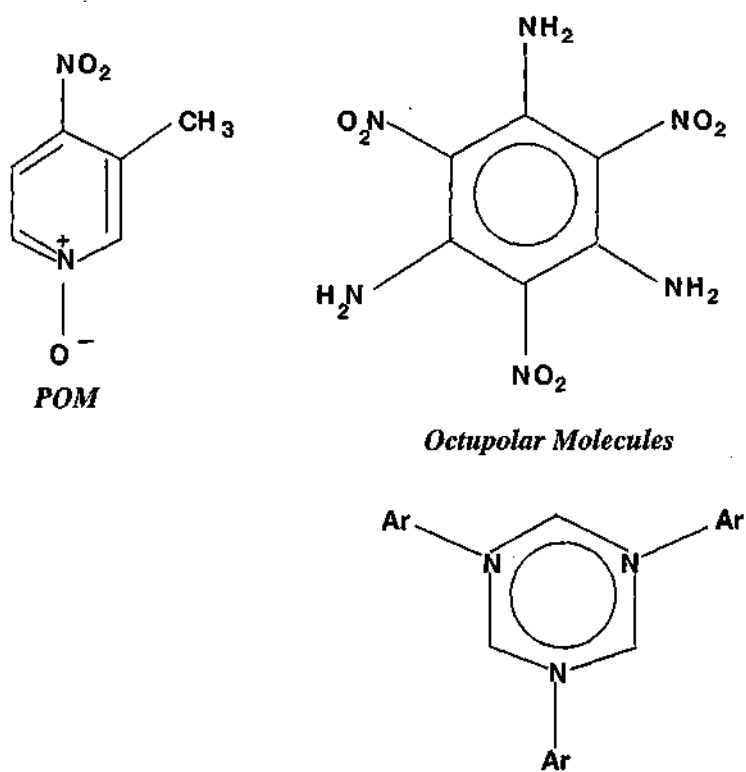
Figure 1.4: Molecules which exhibit significant $\chi^{(2)}$ in the bulk crystal

In 1993, Zyss had shown that molecules with *octupolar* moments are very promising candidates for NLO applications in crystals [19–21]. For these molecules even though the ground state dipole moment is zero, the higher order multipoles like the octupolar moment is non-zero. Very similar to that for POM, these molecules also have a non-centrosymmetric arrangements in the crystal structure. Some of such molecules exhibiting octupolar moments are shown in Fig 1.4.

Another way of ensuring noncentrosymmetricity in a crystal is the incorporation of chiral substituents in the molecular structure. Optically pure material, compounds which have only left-handed and/or right handed symmetry are inherently non-centrosymmetric. Such compounds are, in fact, readily available in the nature (amino acids, sugars and alkaloids are well known examples existing only in a single enantiomer). Thus, crystals of these materials are expected to be NLO active. Some of the best known examples are, methyl-2-(2,4-dinitroanilino)-propionate (MAP), *(+)*-camphor-10- sulfuric acid and N-(4-nitrophenyl)-L-prolinol (NPP). They are shown in Fig 1.5.
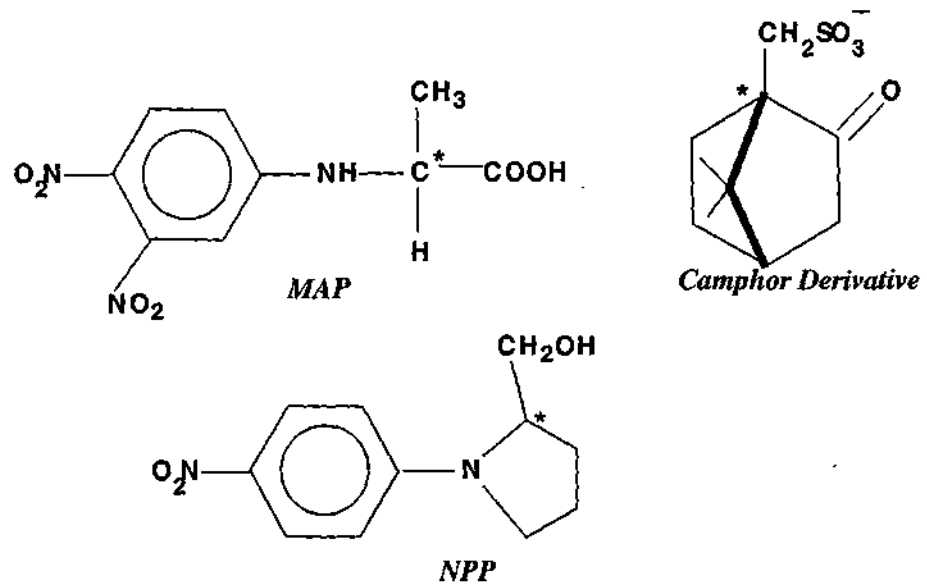
Chiral Molecules having non–centrosymmetric crystals

Figure 1.5: Chiral molecules forming non-centrosymmetric crystals

Thus, a solution or a glass, in its natural form being random, does not exhibit any second-order effect. For biological systems, important second-order effects are associated with the interface and with electric field poling. Surface second harmonic generation from a biological membrane provides a powerful method for second-harmonic imaging to selectively probing interactions and dynamics involving membranes. The electric-field- induced second harmonic generation provides an excellent probe for membrane potential. This has a very promising use in *bio-imaging* [22, 23].

1.2   Third-Order Optical Processes

The third-order polarization component from equation (1.9) has the form

$$P^{(3)} = \chi^{(3)}[E_0^3 + (3/2)E_0E_1^2(1 + \cos 2\omega t) +$$
$$3E_0^2E_1\cos\omega t + (3/4)E_1^3(\cos\omega t + \cos 3\omega t)]$$

$$(1.13)$$

The $E_0^2E_1$ term corresponds to the dc Kerr effect; the $E_0E_1^2$ term is the ac Kerr effect or the optical Kerr effect and is represented as $\chi^{(3)}(-\omega; 0,0,\omega)$. The E_1^3 with third-order response describes third harmonic generation (THG). THG is a special case of four wave mixing, which in general can be written as:

$$\chi^{(3)}(-\omega_\sigma; \omega_1, \omega_2, \omega_3)E(\omega_1)E(\omega_2)E(\omega_3) \qquad (1.14)$$

where three photons with frequencies, ω_1, ω_2 and ω_3, result in a fourth frequency of ω_σ. For $\omega_1 = \omega_2 = \omega_3$, the $\chi^{(3)}$ medium generates a new photon

of frequency 3ω. Thus, an incident fundamental light of wavelength at 1064 nm (from an Nd:YAG laser) will produce a third harmonic beam at 355 nm in the UV. Again, like in the case of second- harmonic generation, it is a coherent process with three incident frequencies and there is no resonance associated with it. A schematic representation of the third harmonic generation is shown in Fig 1.6.

Coherent anti-Stokes Raman Scattering (CARS) is also a $\chi^{(3)}$ process but contrary to THG, it is a resonant process (see Fig 1.6). In this process, three input light beams, two with frequency ν_1 and the third one with frequency ν_2, generate a new output beam at frequency $2\nu_1$-ν_2 and involves a vibration of the molecule at frequency $\nu_R = \nu_1$-ν_2. Thus, by observing the new output CARS signal at a frequency $\nu_{AS} = 2\nu_1$-ν_2, as a function of ν_1-ν_2, where one of the frequency is fixed and the other one is varied, one can obtain the Raman spectra of the molecule.

1. Third Harmonic Generation Process (THG).

2. Coherent anti—Stokes Raman Scattering (CARS).
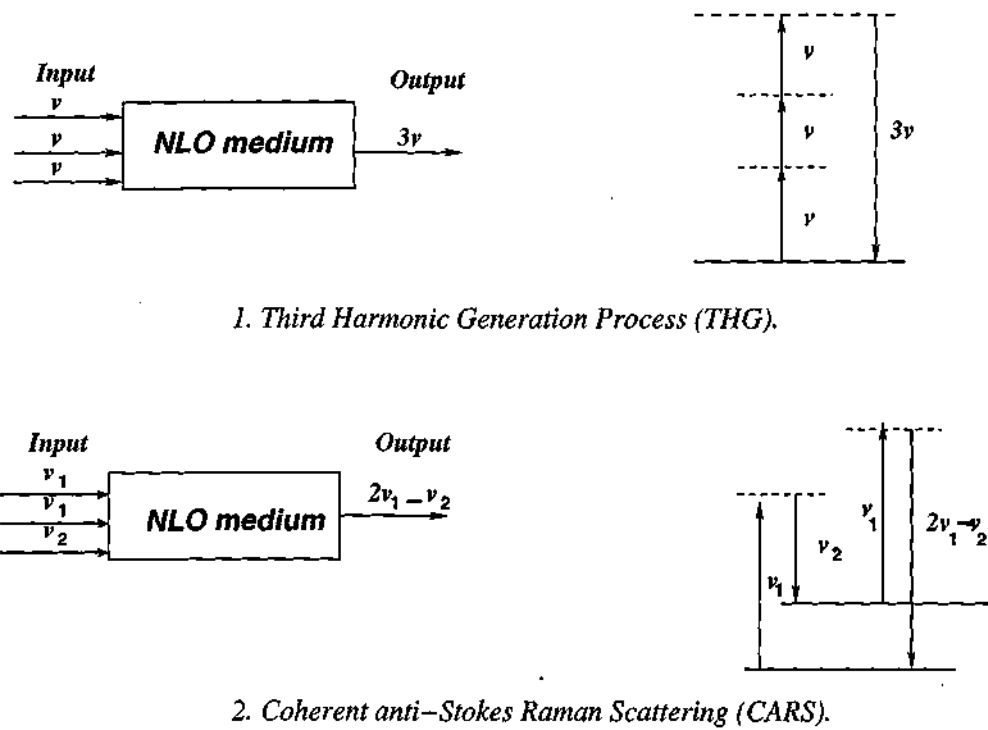
Figure 1.6: Representation of Third-order processes

Unlike the second-order nonlinear optical processes, which can take place only in a noncentrosymmetric oriented medium, the third-order processes can take place in any medium, random or ordered. But since it is a higher- order process, third harmonic generation is a less efficient process than second-harmonic generation, for a medium where both can occur.

1.3   Multi-photon Absorption

Multi-photon absorption is a nonlinear optical absorption process in which more than one photon, either of the same energy (frequency) or of different energies, are absorbed simultaneously or successively to access an excited state. Even though it is not necessary to have an intermediate state, exactly in between the ground state and the two-photon state, the transition probability is very sensitive to the detuning of the single-photon transitions. A two-photon absorption requires very fast recovery process. If we consider a system with three-levels, G, I and F, I being of opposite parity to both G and F, we can qualitatively understand why the transition probability for a two-photon absorption depends on the detunation of the one-photon emissions. On absorbing the first photon with frequency ω_i, the system can stay in the intermediate state I for a time of the order $(\omega_i)^{-1}$ because of the uncertainty principle. The two-photon transition can only take place if a second photon is absorbed during the time spent by the system in the state I. If a second photon is not absorbed within this time, the system decays to the ground state by a one-photon emission. The process is depicted in Fig 1.7.

Competition between Two–Photon Absorbtion and One–Photon emission.
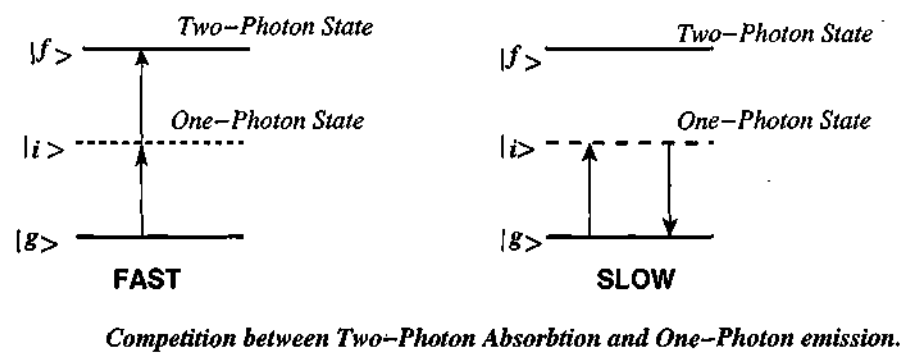
Figure 1.7: Detunation of excitation by one-photon emission reduces two-photon absorption processes

Two-photon absorption is a third-order nonlinear process, described by the imaginary component of the third-order nonlinear optical susceptibility $\chi^{(c)}$. Thus, this process has no symmetry restriction and can occur in any medium, symmetric or noncentrosymmetric. Also, as is true for extended π-conjugated systems, the π-electron frameworks, in general, show much higher two-photon absorptions.

If a beam of wavelength λ_1 and intensity I_1 transmitted from the system in the x-direction, and it went through a series of absorption processes in the system with intensity I_2, I_3, I_4, etc., corresponding to the wavelengths λ_1, λ_2, λ_3, λ_4, etc., the phenomenological equation for the intensity, I_1, takes the form

$$\frac{dI_I}{dx} = \alpha_1 I_1 + \alpha_2 I_1 I_2 + \alpha_3 I_1 I_2 I_3 + \alpha_4 I_1 I_2 I_3 I_4 + \ldots \qquad (1.15)$$

where the first term is for the linear absorption, which is proportional to the transmitted intensity. The 2nd term is the first nolinear absorption term, called two photon absorption, which is quadratic in the intensity variables. The above expansion is analogous to the power series expansion of the polarization, P, as a function of the electric field (eqn. 1.6),

$$P = \chi^{(1)} E + \chi^{(2)} EE + \chi^{(3)} EEE + \ldots \qquad (1.16)$$

where $\chi^{(n)}$ is the nth-order susceptibility tensor of the medium and E represents the electric field strength. Near a resonance, the susceptibility tensor becomes complex, and the imaginary part of which describes absorption (or gain) properties. As I is proportional to E^2, it is clear from the above expression that the two-photon absorption coefficient, α_2, is proportional to

the imaginary part of the 3rd-order susceptibility tensor. In the molecular level, the macroscopic susceptibility can be replaced by the third order molecular nonlinearity. Additionally, any absorption process is characterized by its cross-section, which is proportional to the corresponding coefficient. Therefore, the molecular two-photon absorption cross-section can be characterized by the imaginary component of the molecule's third order nonlinear polarizability, defined at the absorption frequency of ω as

$$\alpha_2(\omega) \propto Im[\gamma(-\omega_1; \omega_2, -\omega_2, \omega_1)] \tag{1.17}$$

The absorption is described by a two-photon absorption coefficient α_2 (unfortunately, the same letter α is used for the linear polarizability of the molecule). As discussed above, one can have a two-photon absorption involving simultaneous absorption of photons of different frequencies ω_1 and ω_2. The energy level diagram shows that a simultaneous two-photon absorption may be viewed as a absorption of one photon leading to a virtual intermediate level level I from where the absorption of another photon leads to a final level F. The appearance of the intermediate states reflect the possibility of attaining the final state *via* a series of intermediate states, which are connected with the final and initial states by non-zero matrix elements.

While dipole allowed transition occurs between states of opposite parity, a two-photon absorption occurs between states with same symmetry. States of same symmetry can in principle be accessed by quadrupolar moments. Thus, if two states G and F are of same parity, the quadrupolar transition moment, μ^2, can connect the F from G. Thus, the process can be represented

as, $<G|\mu^2|F>$. In principle, one can express it in terms of dipole moment operators as:

$$< G|\mu^2|F> = \sum_I < G|\mu|I> < I|\mu|F >$$ (1.18)

where I constitutes a complete set of states. A two photon process can thus be viewed as a sum of two one-photon processes wherein a *complete set* of one-photon states are involved.

Applying the Laporte selection rule for a ground state with g symmetry, I connecting to G has to have a u symmetry. Hence, the two-photon active state F has to have g symmetry. Therefore, while a one-photon absorption leads to a u-type of excited state, a two-photon absorption leads to g -type of excited state *not* accessible by one-photon absorption. Thus, two-photon absorption is a very powerful tool to study energy levels in molecules or atoms that are inaccessible by single-photon absorption.

For a multi-photon process, at the end of the process, the energy is conserved which means that the energy difference between the final and the initial state is $n\omega$. However, the initial and the final states of the systems are different. Thus it is a nonparametric process.

The probability of two-photon absorption is proportional to the square of the intensity of light, I^2, the probability of absorption of each photon absorption being proportional to I. In the case of an n-photon transition, the probability of excitation is proportional to I^n.

Similarly, *three-photon absorption* is a fifth-order optical process, described by $\chi^{(5)}$ (and it involves simultaneous absorption of three photons).

It is the imaginary part of the nonlinear refractive index η_4 or $\chi^{(5)}$. Three-photon absorption has found tremendous application in biophotonics [24]. Multi-photon processes are gaining popularity in spectroscopy of biological systems since one can probe the high energy excited states of light sensitive materials like cell by providing much less energy. For example to probe a three-photon state one needs to use an energy of only one-third of the optical gap.

Table 1.1: Some important processes involving Nonlinear Optical Spectroscopy

Process	Order	Frequency Relation
Linear Response	1	$-\omega; \omega$
Pockels Effect (EO effect)	2	$-\omega; \omega, 0$
Sum mixing	2	$-\omega_a; \omega_1, \omega_2$
Optical Rectification (OR)	2	$0; \omega, -\omega$
Intensity-dependent refractive index	3	$-\omega; \omega, -\omega, \omega$
Optical Kerr effect	3	$-\omega_1; \omega_2, -\omega_2, \omega_1$
dc Kerr effect	3	$-\omega; 0, 0, \omega$
Two-photon Absorption (TPA)	3	$-\omega_1; -\omega_2, \omega_2, \omega_1$
Third-harmonic generation (THG)	3	$-3\omega; \omega, \omega, \omega$
Coherent anti-stokes Raman scattering	3	$-(2\omega_1 - \omega_2); \omega_1, \omega_1, -\omega_2$
General four Wavemixing (FWM)	3	$-\omega_a; \omega_1, \omega_2, \omega_3$
Three-Photon Absorbtion (TPA)	5	$-\omega_1; -\omega_2, -\omega_3, \omega_3, \omega_2, \omega_1$
n^{th} harmonic generation	n	$-n\omega; \omega, \omega, \ldots\ldots, \omega$
Multi-photon Absorption (MPA)	2n-1	$-\omega; \ldots\ldots -\omega, \omega\ldots\ldots\omega$

1.4 Relationship between Macroscopic Susceptibilities and Microscopic Polarizabilities

For a bulk system (such as liquids, molecular solids or organic glasses) consisting of weakly interacting molecules, the bulk polarization P is derived from the distortion of electronic clouds in constituting molecules. The bulk nonlinear optical susceptibilities $\chi^{(2)}$ and $\chi^{(3)}$ are, therefore, obtained from the corresponding molecular nonlinear optical coefficients β and γ by using a sum of the molecular coefficients over all the molecular sites. The sum should consider their orientational distribution (different orientations at different sites). Furthermore, a local field correction factor F needs to be there to take into account the correction from the applied field E due to the interaction with surrounding molecules. Thus, the bulk $\chi^{(2)}$ and $\chi^{(3)}$ are related to the microscopic/molecular hyperpolarizability β and γ, by the relations

$$\chi^{(2)} = F \sum_i \beta_i(\theta, \phi) \qquad (1.19)$$

and

$$\chi^{(3)} = F \sum_i \gamma_i(\theta, \phi) \qquad (1.20)$$

where the sums are over the number of molecular sites and (θ, ϕ) measure the relative orientation of the molecules with respect to each other. Nonlinear optical interactions in a molecular medium, described by the bulk nonlinear optical susceptibilities, now become primarily molecular properties, described

by the values of β and γ. Thus for a material to have interesting NLO activity both the individual molecular hyperpolarizability and the orientation effects have to be optimized. In general, charge distribution due to π-electrons are readily deformable. Therefore, molecules with conjugated π-electrons give rise to large molecular hyperpolarizabilities (β and γ). In comparison, contribution due to σ-electrons are considerably smaller. But, the factors that govern their interactions in the supermolecule/ crystal are still unknown and it is a formidable task to predict the (θ,ϕ) for a crystal. It is therefore, of fundamental interest, to optimize the parameters that will provide large bulk nonlinear optical susceptibilities from molecular hyperpolarizabilities. There have been a lot of previous efforts to derive the bulk susceptibilities by both semi-empirical and *ab-initio* methods [25–29] but a proper understanding of the relation between the orientation and property is still elusive.

1.5   Calculation of Nonlinear Optical Polarizabilities

For the calculation of microscopic nonlinearities, there are many approaches. We will outline only two of them which have been used extensively in the subsequent chapters. They are the *Finite Field Approach* and the *Sum-Over-States Approach*.

1.5.1 Finite Field Approach

The finite field approach expands the energy of the system in terms of the static field, F as:

$$E(F) = E(0) - \mu_i F_i - \frac{1}{2}\alpha_{ij}[F_i F_j] - \frac{1}{6}\beta_{ijk}[F_i F_j F_k]$$
$$- \frac{1}{24}\gamma_{ijkl}[F_i F_j F_k F_l]\ldots \tag{1.21}$$

The optical response functions μ, α, β and γ are the 1st, 2nd, 3rd and 4th order derivatives of the energy with respect to the static field respectively. These derivatives are calculated numerically using a five-point formula, where the energies are calculated at five different fields; $F=0$, $F=$F, $F=$2F, $F=-$ F and $F=-$ 2F and a truncated series of the above expansion is used to derive the various order derivatives [30, 31].

$$\alpha_{ii} = [[\frac{5}{2}E(0) - \frac{4}{3}[E(F_i) - E(-F_i)]$$
$$+ \frac{1}{12}[E(2F_i) - E(-2F_i)]]/F_i^2 \tag{1.22}$$

$$\beta_{iii} = [[E(F_i) - E(-F_i)] - \frac{1}{2}[E(2F_i) - E(-2F_i)]]/F_i^3 \tag{1.23}$$

$$\gamma_{iiii} = [[-6E(0)] + 4[E(F_i) + E(-F_i)]$$
$$- [E(2F_i) + E(-2F_i)]]/F_i^4 \tag{1.24}$$

Though this method has been very popular, it suffers from the following limitations:

1. The numerical n-point formula for calculation of the energy derivatives are valid only for very low field strengths like 0.001 V.

2. The energies need to be extremely accurate for the calculation of their derivatives. For example, the calculation of γ_{iiii} requires the energy to be accurate to the order of 10^{-14} eV for even a small field of 0.0001 au. As the molecular integrals in quantum chemical calculations are seldom more accurate than 10^{-12} eV, finite field procedure for hyperpolarizabilities may not be reliable enough.

1.5.2   Sum-Over-States Approach

The sum-over-states (SOS) approach has its basis in a perturbation theory method developed by Ward and Orr to account for the effects of an externally applied electromagnetic field on the motions of electrons [32, 33]. Under the influence of the oscillating field the electrons will be perturbed and the resulting polarization in the molecule can be obtained by the inclusion of the field as a perturbation

$$H^1 = -e(Er)\sin \omega t \tag{1.25}$$

to the Hamiltonian and collecting terms of appropriate orders in the electric field. In this expression E is the amplitude of the field and r is a coordinate associated with the position of the electrons and is calculated from

$$r = \sum_a r_a \tag{1.26}$$

in which a is summed over all of the electrons and

$$-e.r = \mu \qquad (1.27)$$

The polarizability and hyperpolarizabilities are expressed as an infinite sums over various excited states in which the numerators contain dipolar integrals of the type

$$< m|\mu_{p=i,j,k}|n > \qquad (1.28)$$

where $m \neq n$. It corresponds to the *transition dipole moment* between the two states m and n.

The expression for the polarizability is given by

$$\alpha_{ij}(\omega) = \sum_m \frac{e^2}{\hbar}[\frac{< g|\mu_i|m >< m|\mu_j|g >}{(\omega_{mg} - \omega)} + \frac{< g|\mu_j|m >< m|\mu_i|g >}{(\omega_{mg} + \omega)}] \qquad (1.29)$$

In this expression g refers to the ground state and m refers to the excited state with $\omega_{mg} = \omega_m - \omega_g$.

The first hyperpolarizability term $\beta[-(\omega_p+\omega_q);\omega_p,\omega_q)]$, which is responsible for the second-harmonic generation, is given by

$$\beta_{ijk}[-(\omega_p + \omega_q), \omega_p, \omega_q] = P\sum_{mn} \frac{e^3}{2\hbar^2}[\frac{< g|\mu_i|n >< n|\mu_j|m >< m|\mu_k|g >}{(\omega_{ng} - \omega_p - \omega_q)(\omega_{mg} - \omega_p)}$$
$$+\frac{< g|\mu_j|n >< n|\mu_i|m >< m|\mu_k|g >}{(\omega_{ng} + \omega_q)(\omega_{mg} - \omega_p)}$$
$$+\frac{< g|\mu_j|n >< n|\mu_k|m >< m|\mu_i|g >}{(\omega_{ng} + \omega_q)(\omega_{mg} + \omega_p + \omega_q)} \qquad (1.30)$$

The symbol P indicates that the summations must be performed over all

permutations of the Cartesian indices i, j and k, with the electric field frequencies ω_p and ω_q. This summation generates terms that are products of transition dipole moment matrix elements and also sums and differences of dipole moments between the ground and excited states as well as between various excited states. The above expression simplifies into an intuitively appealing expression if we consider the properties of the molecule to be approximated by a simple two - level model. The two - level model is discussed in details in the next chapter.

The second hyperpolarizability term $\gamma(\omega_t;\omega_r,\omega_q,\omega_p)$ is expressed as

$$\gamma_{kjih} = P \sum_{mnv} \frac{e^4}{4\hbar^3} \left[\frac{<g|\mu_k|v><v|\mu_j|n><n|\mu_i|m><m|\mu_h|g>}{(\omega_{vg} - \omega_r - \omega_q - \omega_p)(\omega_{ng} - \omega_q - \omega_p)(\omega_{mg} - \omega_p)} \right.$$
$$+ \frac{<g|\mu_j|v><v|\mu_k|n><n|\mu_i|m><m|\mu_h|g>}{(\omega_{vg} + \omega_r)(\omega_{ng} - \omega_q - \omega_p)(\omega_{mg} - \omega_p)}$$
$$+ \frac{<g|\mu_j|v><v|\mu_i|n><n|\mu_k|m><m|\mu_h|g>}{(\omega_{vg} + \omega_r)(\omega_{ng} + \omega_r + \omega_q)(\omega_{mg} - \omega_p)}$$
$$\left. + \frac{<g|\mu_j|v><v|\mu_i|n><n|\mu_h|m><m|\mu_k|g>}{(\omega_{vg} + \omega_r)(\omega_{ng} + \omega_r + \omega_q)(\omega_{mg} + \omega_r + \omega_q + \omega_p)} \right] \quad (1.31)$$

The computation of the polarizabilities thus involves the evaluation of various dipole moment operators μ_{nm} and the energies, then summing over all the terms. These sums are infinite sums over all the excited states. However, in practice, one often utilizes the sum over the important excited states.

Chapter 2

Davydov splitting and H-bonding stabilizations in organic molecular aggregates

2.1 Introduction

The development of materials with large nonlinear optical (NLO) properties is a key to controlling the propagation of light by optical means. In particular, the response of the materials to the application of the electric field has found tremendous applications in designing materials for NLO devices [2]. These devices are being used in numerous applications, from lasers to optical switches and electronics.

Some of the best NLO properties are displayed by the organic π-conjugated materials [34,35]. The organic materials are of great interest because of their

low cost, ease of fabrication and integration into devices. One of the advantage in working with organic materials is that they allow one to fine tune the chemical structures and properties for the desired nonlinear optical properties [7]. Because of a delocalized pi-electron system, the macroscopic NLO polarizabilities of these materials are in almost all cases governed by the NLO characteristics of the constituent molecules. This is an added advantage of modeling organic systems with optimally required NLO properties. Recent paper on the use of azaphosphanes supports it [36]. The full realization of the prospects of the NLO active materials depend on, in one hand the optimization of the non-linear properties of the individual molecules at the microscopic level and on the other hand the efficiency of putting the molecules at the macroscopic level with a maximal chromophore density while achieving and preserving maximum acentricity of the micro-structures.

For a real application, the organic systems can be grown into molecular crystals, either in bulk or in the form of thin films on substrates or as amorphous systems which are polymeric. Although there exist a large number of articles discussing the relationship between the hyperpolarizabilities with structure or functionalizations of the organic molecules, the construction, design and understanding of multi-molecular arrays with desirable collective relationships between the constituent molecular blocks is still in its infancy [37–39]. The instability with respect to relaxation of the individual molecules to the equilibrium state of random orientation has been a serious problem associated with the various techniques to achieve this goal. Of the different known methods investigated experimentally, the self-assembly (SA) techniques are particularly promising and challenging, because, the resulting

materials offer the potential for far higher electro-optic coefficients and lower dielectric constant than those of established inorganic materials. These assembled materials are intrinsically noncentrosymmetric, and so they do not require electric field poling [8]. Moreover, growing chromophore arrays directly on silicon or related substrates would allow ready device integration. Chemisorptive siloxane-based SA can yield robust, densely packed organic films [40,41]. In such SA, the forces that act among the individual molecules, which eventually stabilize the assembly, are yet to be known clearly.

It would thus be of fundamental interest to explore theoretically the dependence of NLO response functions in organic aggregates to changing the nature and arrangement of the constituent chromophores. The energy shift due to the formation of various packing geometries reflect the change in polarization of the local environments. In the next section of this chapter, we present an exciton theory based on Davydov splitting for N molecular aggregates with a varying orientations of monomeric molecules. Later, we present a theoretical analysis for Hydrogen bonding in the aggregates. The Paranitroaniline (PNA) has been selected as a model although the energy decomposition analysis has been done on methyl amine-nitromethane cluster. Finally, we conclude the chapter with a brief discussion of the two-state model which is useful for a simplistic understanding of NLO in π-conjugated organic charge transfer compounds.

2.2 Exciton model for the molecular aggregates:

In this section we discuss a basic model which can explain the electronic excitations of one dimensional molecular aggregates. As it is quite well known in the field of strong correlations, an excitonic state is the result of electron correlation and exciton theory is an interaction theory between these excitonic states. In a self-assembled aggregates with low packing densities, the excitons are considered to be Frenkel type excitons where the electron and hole of a monoexcitation are located on the same molecular site. To develop a simple theory, we shall consider here the composite molecules, which includes van der Waals dimers, trimers, higher order aggregates. As has been pointed out in a number of previous works [42, 43], if the direct overlap between the chromophoric molecular orbitals (M.O.) is negligible, the exciton interactions can be expressed in the direct product basis of the chromophoric M.O.s.

Let us begin our discussion with the zeroth order Hamiltonian. The Hamiltonian for the mth molecule alone in an aggregate can be written as

$$H_m = \sum_k |k_m > (E^{k,m}) < k_m|$$

(2.1)

where k_m specifies the kth electronic state of the mth molecule. The wavefunction for the N number of molecules (in an aggregate) can be approximated as a linear combination of product functions $|k_1, k_2, \ldots, k_m, \ldots, k_N >$, where the k_m's are the kth electronic states for the molecule m. If we include

the electronic exchange interactions, the excitations will be the admixtures of charge transfer states which correspond to Wannier type excitons. However we assume here that the intermolecular distance is large enough to make electron exchange effects quite negligible, at least in low order. The ground state of N molecules is then the tensorial product of the molecular ground states.

$$|G >= |G_1, G_2, \ldots, G_m, \ldots, G_N >$$ (2.2)

Each molecular excitation gives rise to a band of N degenerate product states in the zeroth order. For excitation e in the mth molecule, it reads

$$|m, e >= |G_1, G_2, \ldots, G_{m-1}, e_m, G_{m+1}, \ldots, G_N >$$ (2.3)

In general the spatial structure of an aggregate is not quite well defined. However translational symmetry can be assumed to be valid in case of a molecular crystalline system. Here we consider the case of a perfect molecular aggregate. Let us denote the exciton coupling interaction term as $H_{m,n}$ for the interaction between the monomers, m and n. We derive the energy expression with the general $H_{m,n}$ terms now and introduce the particulars about this interaction later. For the N monomeric molecules, energy matrix

for any excitation e, for the perturbation $H_{m,n}$ will have the general form

$$[E_{mn}] = E_G(N-1) + \begin{bmatrix} E_e & H_{1,2} & H_{1,3} & \cdots & H_{1,N} \\ H_{2,1} & E_e & H_{2,3} & \cdots & H_{2,N} \\ H_{3,1} & H_{3,2} & E_e & \cdots & H_{3,N} \\ \vdots & \vdots & \vdots & \vdots & \vdots \\ H_{N,1} & H_{N,2} & H_{N,3} & \cdots & E_e \end{bmatrix} \qquad (2.4)$$

where E_G and E_e are the ground state energy and energy for the excitation e respectively. We assume the matrix to be symmetric so that $H_{m,n} = H_{n,m}$.

However the above matrix can be solved exactly only for a few cases. Imposing either periodic or open boundary condition in a one-dimensional case, the energies of the N perturbed states can be written as,

$$E(q) = (N-1)E_G + E_e + 2H_{m,m+1}\cos q + 2H_{m,m+2}\cos 2q + 2H_{m,m+3}\cos 3q + \ldots$$

$$(2.5)$$

where the energies are written in momentum space, q. Note that both for periodic and open boundary condition, the q-space energies are same, although the wavefunctions are completely different.

An analytical solution of the above expression can be obtained only for the nearest neighbor case. Assuming $H_{m,m+1}$ as the strongest coupling and neglecting all other types of coupling, the width of the excitation band e can be estimated to be $4H_{m,m+1}$ for periodic and $4H_{m,m+1}\cos(\pi/N + 1)$ for the open chain case. However if we include all the other($|m - n| > 1$) $H_{m,n}$ coupling, the width will be increased by 25% of the nearest neighbour values. Moreover the allowed transition is different for two different boundary

conditions. For an open chain, the allowed transitions are to the states with $q = \pi/(N+1), 2\pi/(N+1), \ldots, N\pi/(N+1)$. For the periodic chain however the transitions are to the momentum states with $q = 0, \pi/N, 2\pi/N, \ldots, (N-1)\pi/N$ values. Now let us first discuss the expression for $H_{m,n}$ coupling and then we shall come back to the consequences of the arrangement of monomer molecules and the allowed electric dipole transitions.

For dipolar molecules, the strongly allowed transition would be to the lowest exciton state and the coupling interactions can be approximated at large distances by a point dipole model. Assuming all molecules to be same, the coupling interactions can be written as

$$H_{m,n} = \frac{\vec{M}_{ij}.\vec{M}_{ij}}{r_{mn}^3} - \frac{3(\vec{M}_{ij}.\vec{r}_{mn})(\vec{M}_{ij}.\vec{r}_{mn})}{r_{mn}^5} \qquad (2.6)$$

where $\vec{M}_{ij}$ is the transition moment from state i to state j of the monomer molecule and r_{mn} is the distance between the two molecular centers m and n. It is to be noted that both the transition dipole and the molecular axis($\vec{r}_{mn}$) are vectorial quantities. Thus the magnitude of the interaction term will depend crucially on the relative orientations of the dipolar molecules as well as on the axis joining their centers. We shall give here a purely quasi-classical vector treatment to this interaction as we assume electrostatic interaction between the transition moments.

2.2.1 Excitonic Coupling in the Molecular Aggregates

In a molecular aggregate of N-molecules, the transition dipole moment of the aggregate depends on how well the individual molecules interact among

themselves. If the interaction among the molecules is finite, the intermolecular coupling leads to the splitting of the excited state rather than the ground state, since it corresponds to the electric field induced displacements. The schematics of the splitting is shown in Fig. 2.1.
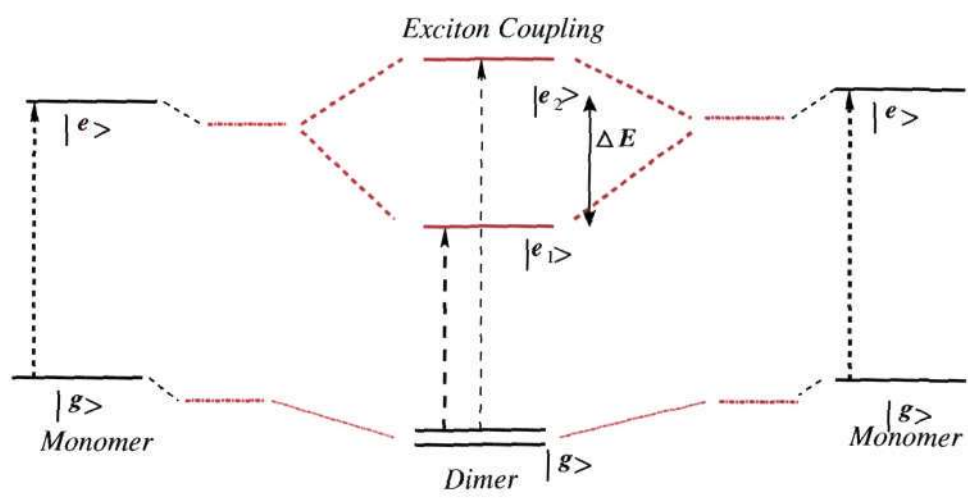
Figure 2.1: Excitonic Splitting for an aggregate

A number of cases can be analyzed where the dipolar molecules are arranged in various orientations. Let us assume that in the aggregate the chromophores are arranged as shown in Fig. 2.2. The directions shown there correspond to the polarization axis of the corresponding chromophores. The aggregate is constructed such that the chromophores are oriented with an angle ϕ between them and each monomer creates an angle θ with its molecular axis. It is quite simple to derive the splitting energy in this case from equation (2.6),

$$\Delta E = 2\frac{M_{gs}^2}{r_{mn}^3}(\cos\phi - 3\cos^2\theta) \tag{2.7}$$

where M_{gs} is the transition dipole from the ground state to the excited singlet state of the monomer.
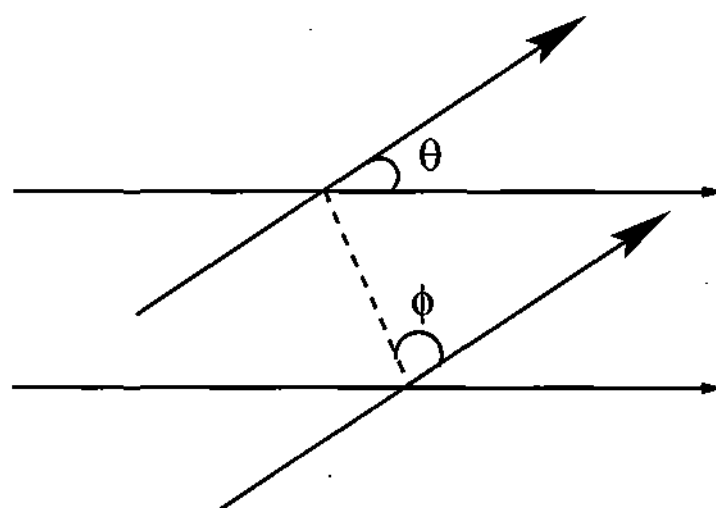
Figure 2.2: The arrows indicate the vector quantities. ϕ is the angle between the dipoles and the angle θ is between the dipole and its molecular axis

Let us now analyze few cases with the variance of angles θ and ϕ. Both the $(\theta, \phi) = (0°, 0°)$ and $(\theta, \phi) = (180°, 0°)$ cases correspond to the dipoles arranged in the same line as that of the molecular axis, while the $(\theta, \phi) = (0°, 90°)$ and $(\theta, \phi) = (180°, 90°)$ correspond to their perpendicular out-of-plane arrangements. Most importantly, for cases $(\theta, \phi) = (0°, 0°)$ and $(\theta, \phi) = (0°, 90°)$, the electrostatic interaction is attractive(repulsive) in nature for the lowest(highest) states but becomes repulsive(attractive) in nature when θ turns to $180°$ (i.e., other two cases). Note that the transition moments are finite for electric dipole transitions from the ground state to the state with attractive electrostatic interaction while it is vanishing to the state with repulsive interaction. As seen from equation (2.7), and the fact that the angle ϕ can not be greater than $90°$, the maximum splitting occurs when $(\theta, \phi) = (0°, 90°)$, and at $(\theta_c, \phi) = (\cos^{-1}(1/\sqrt{3}), 0°)$, the splitting vanishes, irrespective of the inter-chromophoric distance, r_{mn}. Explicitly as shown in the next figure (Fig. 2.3), with the continuous variation of the angle θ, for $\phi = 0°$, the excitonic state allowed for electric dipole radiation interchanges relative position with a forbidden excitonic state, while this is not the case for $\phi = 90°$. These remarkable effects can be realized just by changing the geometry of the aggregates.
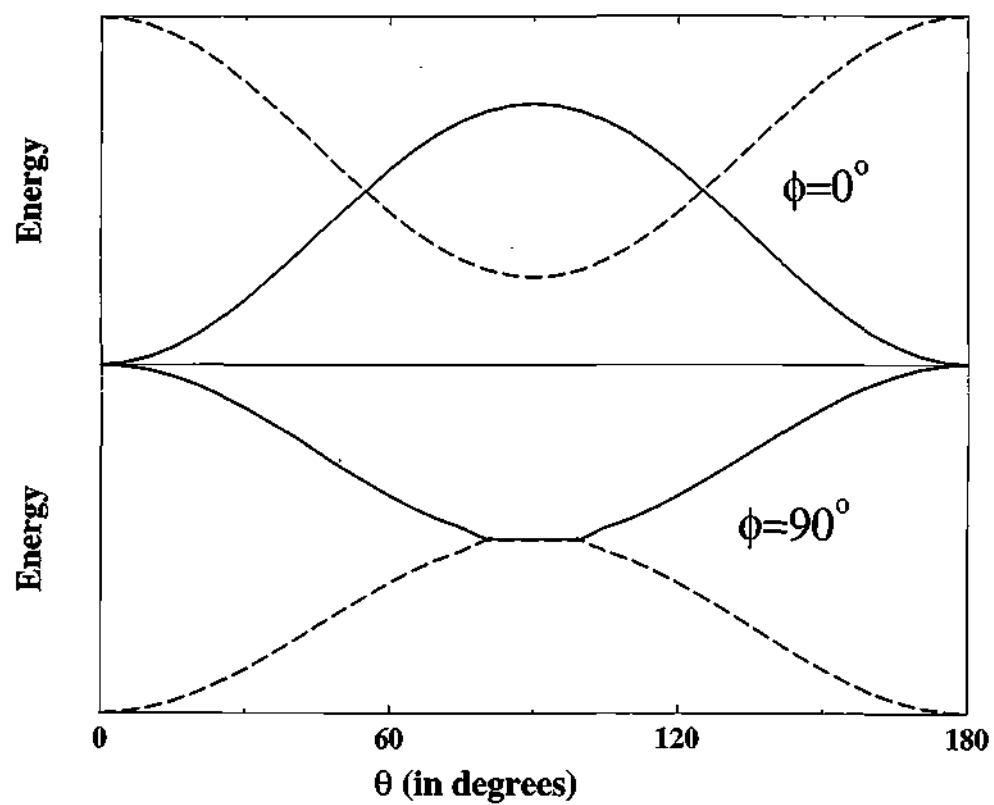
Figure 2.3: The splitting energy levels (solid and dashed lines) are plotted against the angle θ defined in the text, for two values of the angle ϕ

Therefore a singlet excited state of the monomer molecule would split according to the angles, (θ, ϕ). The intensities of the electric field transition to any q value can be written in terms of the transition moment correlations in momentum space. For a periodic chain of molecules, it can be written as,

$$I_q = |\frac{1}{\sqrt{N}} \sum_{m=1}^{N} e^{iqm} M_{gs}|^2 \tag{2.8}$$

while for the open chain it reads

$$I_q = \frac{2}{N+1} \frac{1 - (-1)^q}{2} \cot^2(\pi q/2(N+1)) M_{gs}^2 \tag{2.9}$$

Therefore for the cases with $\theta = 0°$, only the $q = 0$ transition is allowed for the periodic case while for the open boundary condition the $q = \pi/(N+1)$ transition is strongest but transitions to all odd q values are also allowed with weak intensities. However for cases with $\theta = 180°$, the transition to the upper band edge is only allowed. The most interesting point about the above expressions is that for the angle $\theta = 0$, either $q = 0$ state (for periodic chain) or $q = \pi/(N+1)$ (for open chain) state carries the entire oscillator strength of the system, which amounts to NM_{gs}^2. According to the definition of the absorptions at various energies, $\sum_q \frac{1}{E - E(q)} |M_{gs}|^2$, strong absorption band would appear in the absorption spectrum corresponding to the energy of that state. For the $\theta = 0$ case, this energy is shifted by an amount $\sim -1.25H_{12}(3 - \cos\phi)$ (considering all the other $H_{m,n}$) relative to the monomer excitation energy. Note that the above theory is valid only for aggregates where monomers are far apart from each other.

2.3   Hydrogen-Bonding Interaction in a Molecular aggregate

Apart from exciton coupling, there can be a different mode of stabilization of the monomer molecules in the aggregate: Hydrogen bonding. Hydrogen bonding stabilizes the molecular solids through electrostatic interactions. At small intermolecular distances (about 2.5-3.5 $\mathring{A}$), the strength of the hydrogen bonding is maximum.

We have performed extensive calculations based on both semi-empirical (AM1) [44] and *ab-initio* [45] level of theory for the head-to-tail arrangement of two paranitroaniline molecules. The optimal geometry corresponds to the *N...N* distance of 3.34 $\mathring{A}$ where two *N-H...O* hydrogen bonds are formed. The optimal molecular arrangements and the potential energy profile are shown in the attached figures (Fig. 2.4 and Fig. 2.5). The formation of the H-bonds at such distances facilitates other intermolecular interactions like the exciton and Davydov splitting discussed above to play a significant role in governing the Nonlinear Optical properties of the molecular solids.
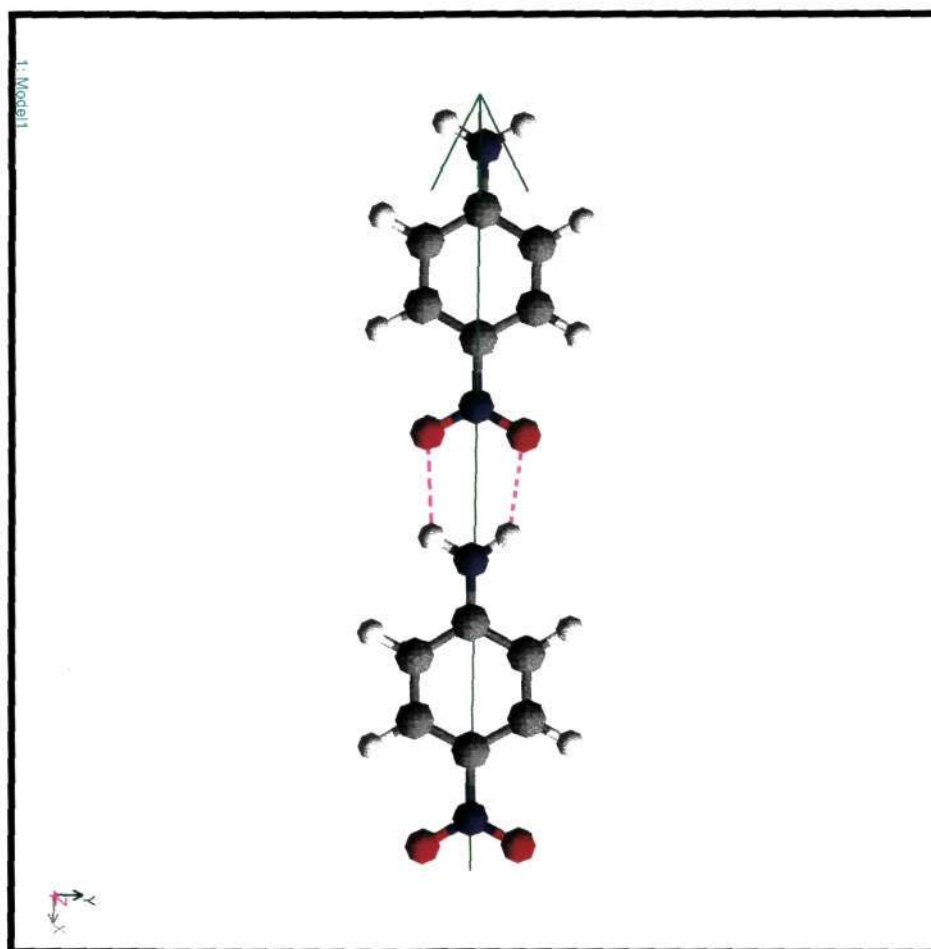
Figure 2.4: Minimum energy arrangement of Paranitroaniline molecules. Two *N-H...O* hydrogen bonds are formed. The arrow shows the direction of dipole moment

H−bond Energy Profile
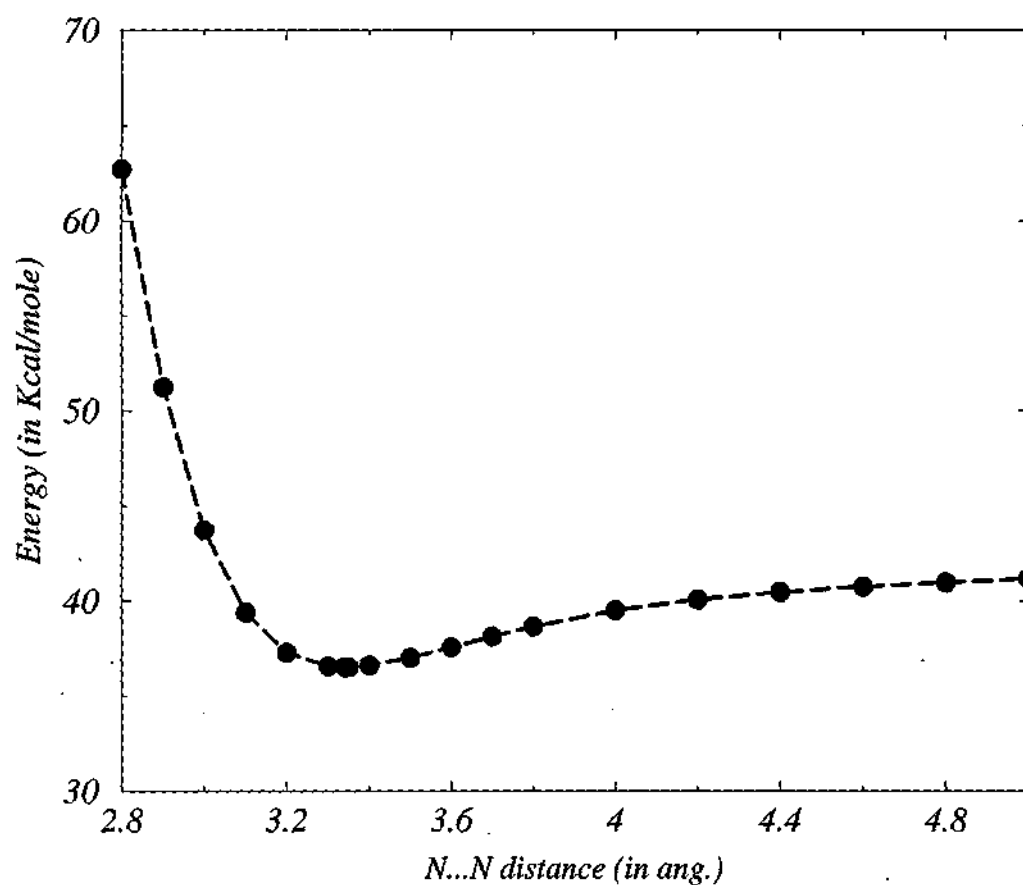
Figure 2.5: Potential energy plot for a Hydrogen bond with respect to the *N...N* distance in paranitroaniline in the head-tail arrangement

From a strictly electrostatic point of view, the molecules that eventually form a H-bond are associated with an electronic distribution which produces an electric field in the surrounding space. The interaction of the static fields of the two molecules corresponds to a purely Coulombic force between two charge distributions at long separation between the two subunits [46,47]. At such distances, one can write the full electrostatic interaction energy as a multipole series. That is, one may construct the charge distribution of each molecule as the sum of dipole moment vector, quadrupole moment tensor, and so on to higher and higher orders. The interaction between the dipoles of the two molecules decays as R^{-3}, where R is the distance between the centers of the charges. Dipole-quadrupole interaction dies off as R^{-4}, quadrupole-quadrupole interaction as R^{-5} and so on.

Indeed, for large separations, it is the dipole-dipole interaction which dictates the preferred angular orientation of the approach of one molecule towards the other. This is the exact reason why all the effects that we have discussed till now like the Davydov and excitonic splitting have dipole-dipole interactions only.

But, the situation becomes more and more complicated as the molecules approach the H-bonding distance. In the first place, the multipole series loses its utility since the higher and higher order terms become progressively larger and the series does not converge properly. For example, Ratajczak *et al.* have shown that for even a test case like the H_2O molecular dimer, at the H-bonding optimal distance of 3 $\mathring{A}$ between the O atoms in the $O - H \ldots O$, the R^{-7} term is also quite significant [48,49]. Thus, for a proper description of the H-bond, electrostatic interaction alone is clearly insufficient. One needs

to take into account covalent interactions like polarization, charge transfer and exchange interactions.

2.3.1   Morokuma Energy decomposition

In this method, the energy change on the formation of an intermolecular complex is partitioned into four components: electrostatic (E_{ES}), exchange (E_{EX}), polarization (E_{POL}) and charge transfer (E_{CT}) [50,51]. This decomposition allows one to quantitatively investigate the role of each interaction in between the molecules when a *supermolecule* is formed.

The Kitaura-Morokuma scheme first computes the wave functions of the two isolated subunits of the complex, ψ_A and ψ_B separately. This pair of wavefunctions is taken as the starting point for a Hartree-Fock calculation of the complex.

$$|\psi_1 >= |\psi_A \psi_B > \qquad (2.10)$$

The important point to note is that the electrons of A are antisymmetric within ψ_A, and similarly the B electrons in ψ_B. However, no exchange is permitted between ψ_A and ψ_B. The zeroth iteration of the SCF procedure yields an energy which differs from the total energy of the pair of isolated subunits by an amount E_{ES} since it permits the field of each monomer to interact with the density, ψ_A^2, of the partner molecule, without perturbing its density.

The exchange energy is extracted by again performing the SCF procedure,

however, this time permitting interchange of electrons between A and B:

$$|\psi_2 >= A_{AB}|\psi_A\psi_B >$$ (2.11)

where A_{AB} indicates the use of an antisymmetric combination of the wave-functions (like a Slater determinant). For the situation of a H-bonded system, the interaction is in between two closed shell systems. For such systems, the exchange interaction is repulsive in nature. This is similar to the classical picture of "steric repulsion" between the charge clouds.

Starting with ψ_1, and enforcing the restriction of no exchange between electrons in A and B, convergence of the iterative SCF procedure permits the electrons in each subunit to relax in the presence of the partner. The extra stabilization gained as a result of this relaxation is associated with the polarization of one subunit by another. It is labeled as E_{POL}.

A similar SCF relaxation, but now allowing the full antisymmetrization of all electrons, yields the charge transfer energy. This arises from the transfer of electrons from the occupied molecular orbitals of one subunit to the unoccupied orbitals of the other molecule.

In order to investigate the nature of these interactions in the H-bond dimers, we performed the energy decomposition analysis for a small H-bond system similar to paranitroaniline dimers, the methyl amine - nitromethane cluster $CH_3-NO_2\ldots H_2N-CH_3$. Full calculation for paranitroaniline dimer is not practical. Below, we present the results for the Morokuma analysis in the attached Table 2.1.:

Table 2.1: Energy decomposition for $CH_3 - NO_2 \ldots H_2N - CH_3$

Energy Component	Energy (in Kcal/Mol)
ELECTROSTATIC ENERGY	-1.31
EXCHANGE REPULSION ENERGY	+1.25
POLARIZATION ENERGY	-0.06
CHARGE TRANSFER ENERGY	-2.05
TOTAL INTERACTION ENERGY	-2.13

As can be seen from the table above, the classical electrostatic energy contributes only 61 percent of the total H-bond interaction energy. The $NO_2 \ldots NH_2$ system is a strongly charge-transfer system and the charge-transfer plays a very important role in stabilizing the supermolecule. This can be seen from the plots of the highest occupied molecular orbital (HOMO) and lowest unoccupied molecular orbital (LUMO) for the paranitroaniline dimer (Fig. 2.6 and Fig. 2.7). While, in the HOMO the charge is localized over the H-bond donors (NH_2) of one of the molecule, the LUMO has large contribution of the (NO_2) of the other molecule. Also can be seen from the plot of the charge densities (Fig. 2.8 and Fig. 2.9) that there is strong intermixing of the electron clouds when the two paranitroaniline are placed in a H-bonded distance. But when they are at a far away distance, the densities on each molecules are separated from each other. It is at this large separation that the dipole approximation becomes valid.
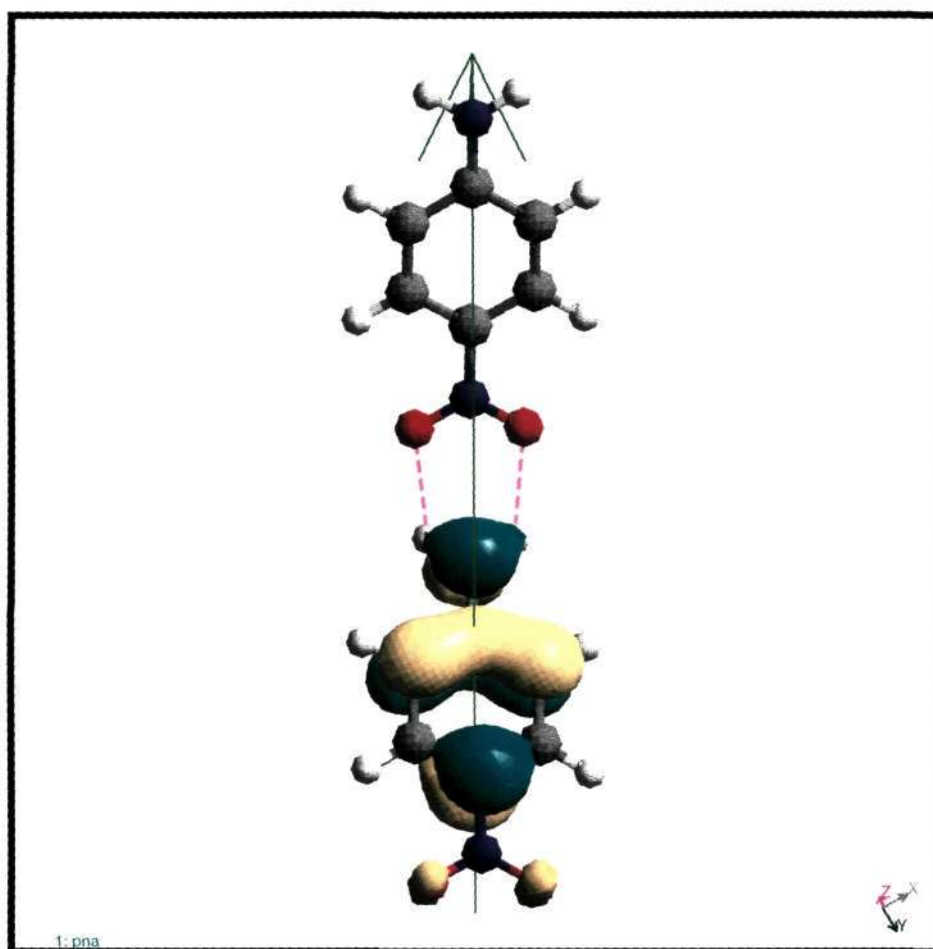
Figure 2.6: The HOMO orbital plot for the H-bonded Paranitroaniline dimer
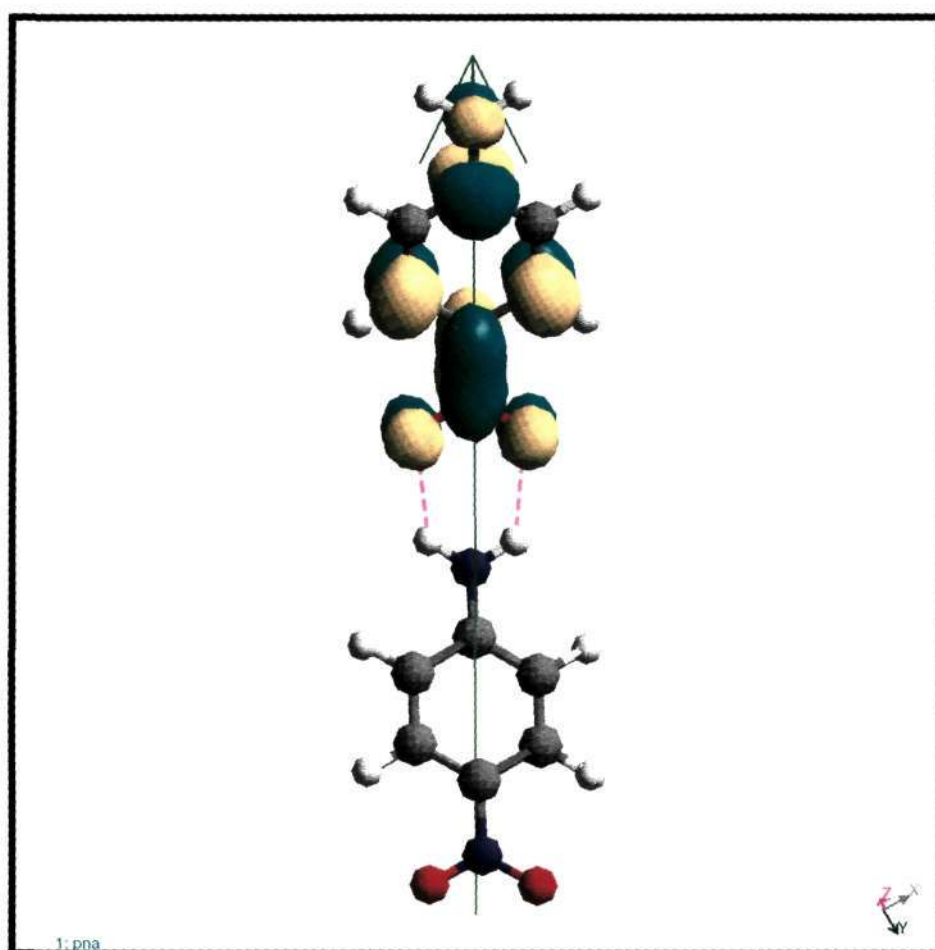
Figure 2.7: The LUMO orbital plot for the H-bonded Paranitroaniline dimer
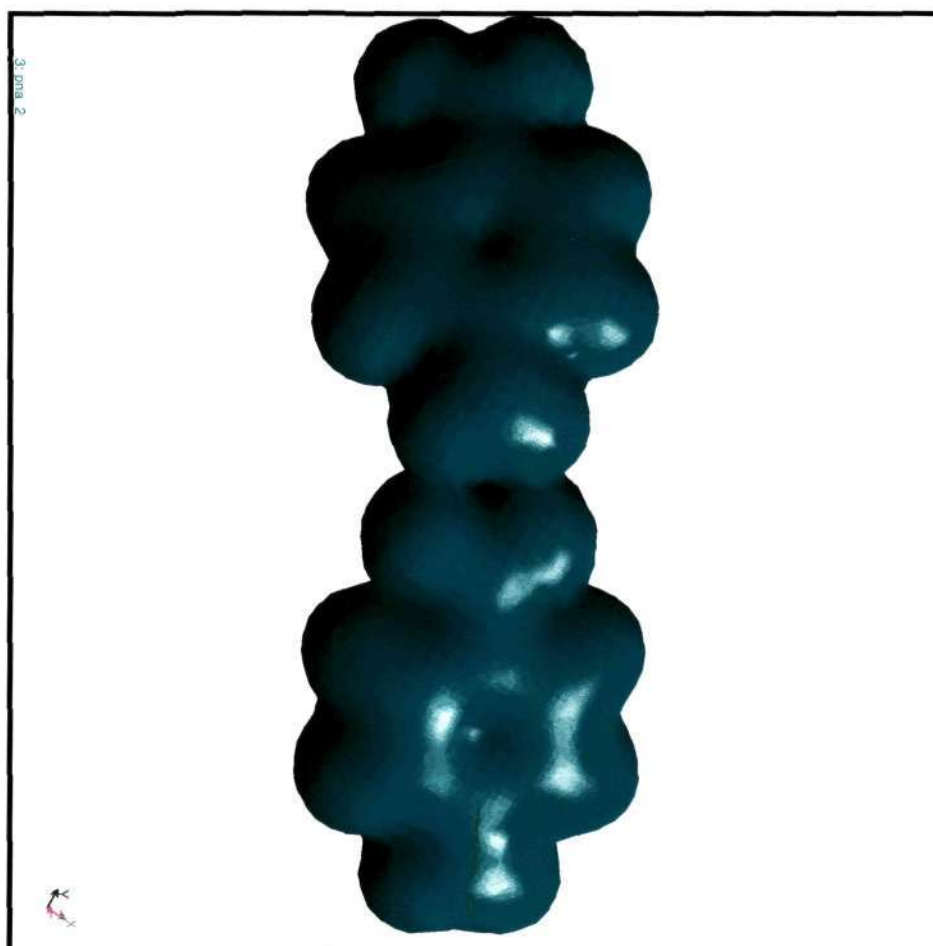
Figure 2.8: The orbital electron density plot for the Paranitroaniline dimers with H-bonding
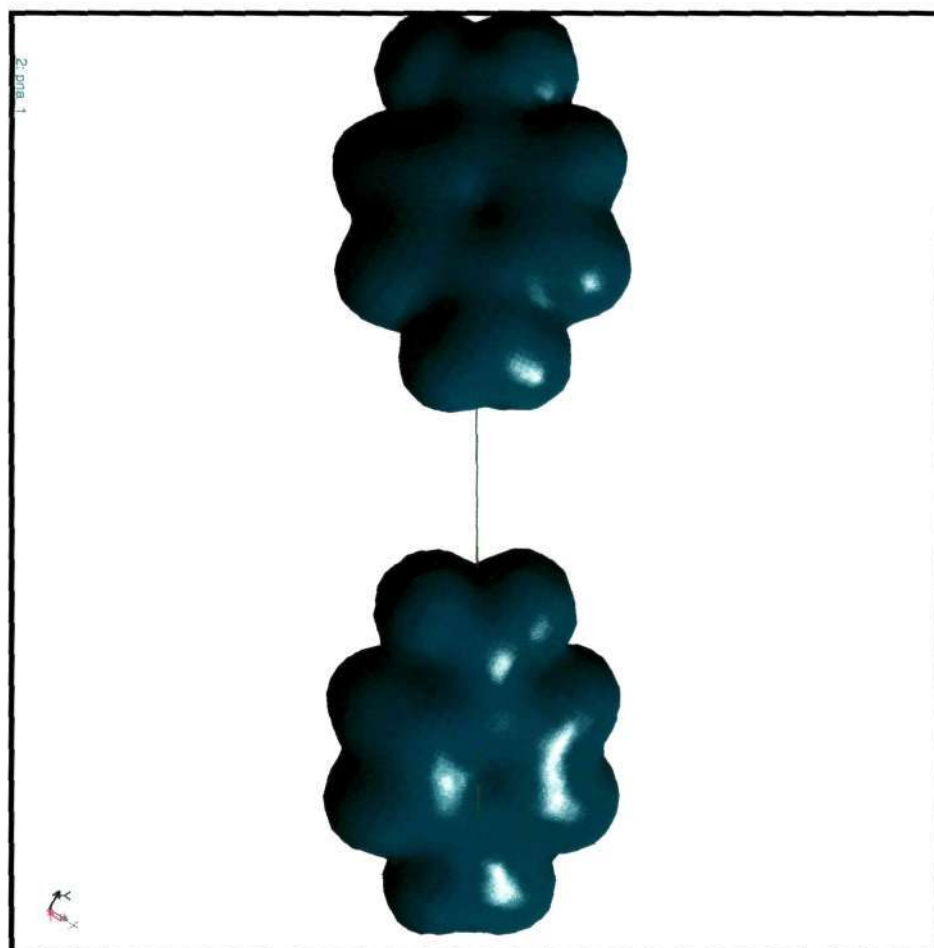
Figure 2.9: The orbital electron density plot for the Paranitroaniline dimers without H-bonding

Chapter 3

Organic π-conjugated molecular dimers: effects of dipole orientations

3.1 Introduction

To obtain a quantitative understanding in general cases with high to low packed monomer densities in an aggregate, we have carried out numerical calculations of the ground and excited singlet states of a few composite molecules. Computation work on a large aggregate is quite impossible and so we have considered only double molecules. However a dimer could give information which would be useful in predicting its behavior in a large aggregate structure. We have considered three model chromophoric molecules to estimate their aggregation effects quantitatively. They are shown in Fig 3.1. In van der Waals and hydrogen bonding aggregates, the observed electronic

spectra correspond to the exciton type interactions discussed in the previous chapter and the stabilization due to hydrogen bondings. As the exciton states are the fundamental excitations of interacting systems, for an accurate analysis, it is very important to know the correlated electronic spectra of the systems thoroughly. It is quite possible that some states which are weak in the monomer molecule may become active in the double molecule, due to reduced symmetry. This asks for a reliable quantitative interpretations.
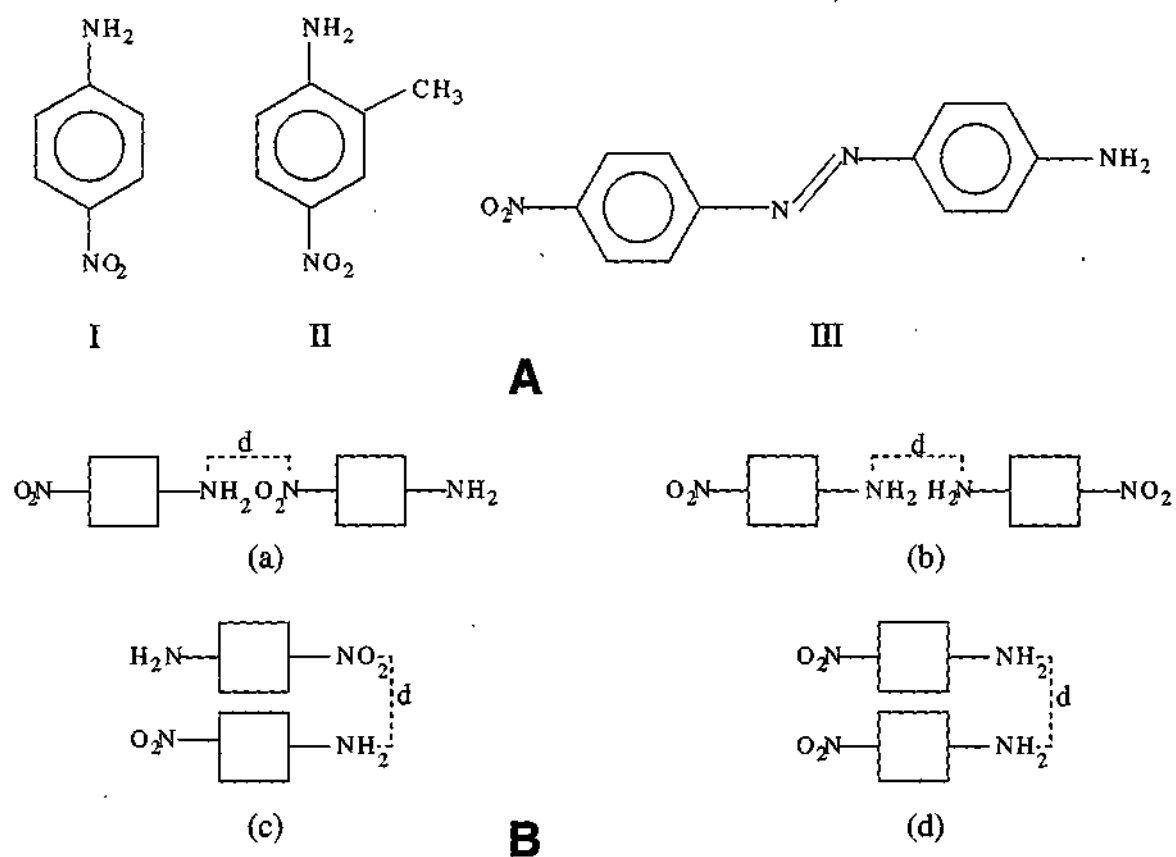
Figure 3.1: (A) Structure of the three molecules considered for the quantitative estimations (B) The distance, d, for each of the four dimeric configurations. In each case as shown, the distance is between the two inter-monomeric neighboring N-atoms

3.2 Dimer geometry and computations

Geometries of the monomer molecules were optimized using AM1 parameterized Hamiltonian, a part of semi-empirical MOPAC package. No symmetry constraints were used in the optimizations. However for the dimer configurations, although we use the optimized monomers, we do not optimize the composite structures, unless specified. These geometries were used to compute the SCF MO energies and then the spectroscopic properties using the Zerner's INDO method [52]. We have varied the levels of CI calculations, with singles(SCI) and multi-reference doubles CI (MRDCI), to obtain a reliable estimate of the second order optical response. The later method is particularly important since it includes correlation effects substantially. The MRDCI approach adopted here has been extensively used in earlier works, and was found to provide excitation energies and dipole matrix elements in good agreement with experiment [53, 54]. As reference determinants, we have chosen those determinants which are dominant in the description of the ground state and the lowest one-photon excited states [55]. We report below the MRDCI results with 4 reference determinants including the Hartree-Fock (HF) ground state. For each reference determinant, we use 5 occupied and 5 unoccupied molecular orbitals to construct a CI space with configuration dimension of 800 to 900. To calculate NLO properties, we use correction vector method, which implicitly assumes all the excitations to be approximated by a correction vector [56]. Given the Hamiltonian matrix, the ground state wave function and the dipole matrix, all in CI basis, it is straightforward to compute the dynamic nonlinear optic coefficients using either the first order

or the second order correction vectors. Details of this method have been published in a number of papers [57–59].

To study the double molecules, we generate first the optimized monomers. Then by translating and (or) rotating in long axis direction, we put together two of the same molecules. In some cases, we have also optimized the dimer structure. The distance between these two monomers is such that no covalent bonding is possible between the inter-monomeric nearest-neighbor atoms. Electronic excitation energies and spectroscopic properties are computed using the same method as discussed above. We also calculate the exciton interactions using the formalism developed in the previous chapter.

The NLO properties for organic charge-transfer complexes like D-π-A can be captured very nicely by a two state model [60]. This model assumes that the electronic properties of the molecule are determined by a ground state and a low-energy charge transfer excited state. Polarization results primarily from the mixing of the charge-transfer state with the ground state through the interaction of the molecule with the electric field. In the two-state formalism, the complicated β expression reduces to:

$$\beta_{two-level} = \frac{3e^2}{2\hbar} \frac{\omega_{12} f \Delta\mu_{12}}{(\omega_{12}^2 - \omega^2)(\omega_{12}^2 - 4\omega^2)} \tag{3.1}$$

where ω_{12} is the frequency of optical transition between states 1 and 2, f is the oscillator strength and is the square of the transition moment between the ground state and the charge transfer excited state $<1|er|2>$ and $\Delta\mu_{12}$ is the difference between the ground-state and the excited-state dipole moments. From this expression, it is evident that as the optical gap (energy difference

between the ground state and the 1st dipole allowed state) decreases (which can be implemented by increasing the conjugation length of the molecule) the magnitude for β increases. For, the favorable head-to-tail arrangement of the chromophores, the exciton level energies to the lowest dipole allowed state reduces. As a result, the optical response functions increase.

3.3   Comparison with *ab-initio* studies

Before we present our results on double molecules, we compare the dipole moments and the polarizabilities obtained from our MRDCI method and earlier ab *initio* calculations. For the PNA, the dipole moment from our MRDCI calculations (2.8au) compare fairly well with the ab *initio* value($\sim$ 3au). At a frequency of 0.028838au, the ab *initio* calculations give the polarizabilty $\sim$ 90au, compared to 57au from our calculations, for the PNA. For other frequencies too, the trend is very similar; for frequencies 0.077au, 0.1098au and 0.150au, the ab *initio*(MRDCI) values are 100(63), 107(73) and 134(115) respectively [61, 62]. For 4-amino-4′-nitro azobenzene, the higher level calculations with large basis functions [61] give a value of static linear polarizability close to 160au. At a small frequency (0.028au), our estimation gives a value of 140au. The hyperpolarizabilities too are comparable for the PNA molecule; for a frequency of 0.005au, the ab *initio* estimation gives 892au [63] while our calculations for the same frequency give 821au. It is to be noted that these values from the ab *initio* calculations vary $\pm$20% depending on the basis states used. Since MRDCI numbers have also been used to quantify the experimental results, and given the comparisons above, we believe that

the results presented below give an accurate picture for double molecules at various distances and configurations.

3.4   Results and Discussions

We first consider paranitroaniline (molecule-I in the Fig. 3.1) as our model molecule. The monomer molecule has a weak absorption band at 0.15798au with an oscillator strength of about 0.01, and a strong absorption band at about 0.169au with the oscillator strength ~ 0.43. The linear polarizability and the EFISH (electric field induced second harmonic) coefficients (product of transition dipole and the first hyperpolarizability, $\mu\beta$) of the monomer are 45au and 2604au respectively at an electric field frequency of 0.00367eV. For the detailed comparisons of the interaction effects, we consider four configurations of the PNA double molecules, out of which two are *in-plane* and the other two are *out-of-plane* configurations. These four configurations are also shown in Fig. 3.1.

In the Table. 3.1, we have shown the dependence of the ground state dipole moment, lowest singlet excitation gap, oscillator strength of the excitonic singlet, the linear polarizabilities and the EFISH coefficients($\mu\beta$), as a function of the nitrogen to nitrogen distance between two PNA molecules in all the four configurations (see Fig. 3.1B for the definition distance d in various cases). Note that the β is the tumbling average quantity, defined as $\beta = 1/3(\beta_{xyy} + \beta_{yyx} + \beta_{yxy})$.

Table 3.1: The dependence of the ground state dipole moment (μ_G in au), lowest singlet excitation gap (gap in au), oscillator strength (f), linear polarizability and the first hyperpolarizability (both in units of au), for a range of inter-PNA N-N distance, dist in Å. Four dimer configurations have been considered (see Figure 3.1, for the configuration structures)

θ=0 and ϕ=0						θ=180 and ϕ=0					
dist	μ_G	Gap	f	α	$\mu\beta$	dist	μ_G	Gap	f	α	$\mu\beta$
2.5	10.25	.111	1.65	104	39999.5	2.9	0.0	1.84	1.63	60.3	0.0
2.6	10.09	.119	1.63	101	39831.2	3.0	0.0	1.84	1.63	60.6	0.0
2.7	9.809	.132	1.60	96.5	38430.1	3.1	0.0	1.84	1.63	60.9	0.0
2.8	9.589	.142	1.56	93.1	36715.1	3.2	0.0	1.84	1.63	61.1	0.0
2.9	9.412	.148	1.53	90.4	35113.8	3.3	0.0	1.84	1.63	61.2	0.0
3.0	9.274	.155	1.40	88.4	33726.4	3.4	0.0	1.83	1.64	61.5	0.0
3.2	9.074	.158	1.49	85.3	31556.5	3.6	0.0	1.83	1.64	61.7	0.0
3.5	8.897	.161	1.47	82.3	28845.3	3.8	0.0	1.83	1.64	61.9	0.0
3.8	8.799	.163	1.45	79.6	27953.7	4.0	0.0	1.83	1.65	62.2	0.0
4.0	8.866	.161	0.97	79.6	21612.4	4.5	0.0	1.82	1.66	62.7	0.0
4.5	8.791	.163	0.94	78.3	20406.9	5.2	0.0	1.82	1.67	63.1	0.0
5.0	8.740	.164	0.92	76.9	19551.7	5.6	0.0	1.82	1.67	63.3	0.0
6.0	8.673	.166	0.90	74.9	18396.2	6.0	0.0	1.81	1.67	63.6	0.0
7.0	8.630	.168	0.88	74.3	17672.9	6.6	0.0	1.81	1.67	63.8	0.0
8.0	8.602	.169	0.86	73.6	17117.9	8.8	0.0	1.80	1.68	64.3	0.0
9.0	8.579	.169	0.86	72.9	16849.5	9.7	0.0	1.80	1.68	64.6	0.0

θ=0 and φ=90						θ=180 and φ=90					
dist	μ_G	Gap	f	α	$\mu\beta$	dist	μ_G	Gap	f	α	$\mu\beta$
3.9	8.052	.131	1.59	55.6	16390.0	4.0	0.0	.165	0.910	74.9	0.0
4.0	8.064	.131	1.60	56.0	16644.7	4.2	0.0	.165	0.880	73.5	0.0
4.5	8.091	.133	1.63	57.2	17463.5	4.5	0.0	.165	0.870	72.8	0.0
5.0	8.119	.134	1.64	58.2	18196.1	4.7	0.0	.166	0.870	72.8	0.0
5.5	8.146	.135	1.65	59.1	18832.9	5.2	0.0	.167	0.870	72.8	0.0
6.0	8.170	.136	1.65	59.9	19387.8	5.7	0.0	.168	0.870	72.8	0.0
6.5	8.190	.137	1.66	60.6	19860.1	6.2	0.0	.168	0.860	72.8	0.0
7.0	8.205	.137	1.66	61.2	20270.3	6.7	0.0	.169	0.750	72.8	0.0
7.5	8.221	.138	1.67	61.7	20616.1	7.1	0.0	.170	0.580	72.8	0.0
8.0	8.237	.138	1.67	62.2	20916.3	7.6	0.0	.170	0.530	72.2	0.0
8.5	8.245	.138	1.67	62.5	21171.1	8.1	0.0	.171	0.510	72.2	0.0
9.0	8.253	.139	1.68	62.8	21389.4	8.6	0.0	.171	0.500	72.2	0.0
9.5	8.264	.139	1.68	63.1	21575.8	9.1	0.0	.172	0.487	72.2	0.0
10.	8.268	.140	1.68	63.3	21739.6	9.6	0.0	.172	0.478	72.2	0.0
20.	8.319	.140	1.69	64.8	22795.1	10.	0.0	.172	0.470	72.2	0.0

In Fig. 3.1, the configurations (b) and (c) have a center of symmetry as the dipolar angle is 180°. The dipoles are facing opposite to each other resulting in exact cancellation of the corresponding dipoles of PNA monomers. Furthermore, in configuration (b), the same two groups (NH_2 in this case) are in the line next to each other, which results in repulsive interactions at short distances. On the other hand, in configuration (c), at short distances, there are attractive interactions due to hydrogen bonding. In the other two configurations, namely in (a) and (d), the corresponding monomeric dipoles create a 0° angle, resulting in a favorable quadrupolar configurations. However as in configuration (b), similar repulsive interactions exist at short distances in configuration (d) due to the same groups being next to each other. Similarly in configuration (a), as in (c), hydrogen bonding interactions stabilize the double molecular configuration at short distances.

Hydrogen bonding interactions stabilize the composite systems. Small positive and negative charges develop at the electropositive(hydrogen) and electronegative(nitrogen in our case) ends respectively in the composite structure. We have kept the distances such that there exist rooms for formation of two hydrogen bonds (strength being strongest to weakest), at least in the configuration (a), for N-N distances of up to 3.8Å. The splitting of the excitonic levels, where hydrogen bonding is possible, corresponds to the combined effects of the dipole-dipole as well as the attractive Coulomb interaction due to hydrogen bonding. Specifically, the Coulombic interactions play a major role in its quantitative estimation, due to the large charge transfer possibilities in the hydrogen-bonded configurations. Hydrogen bonding also effects the ground state dipole moment of the composite molecule. This

is the very reason for which in case (a), the ground state dipole reaches twice it's monomeric value only at large distances. However the repulsion due to the same group at close distances (cases b and d) reduces the ground state dipole of the double molecule, For case (a), the excitonic gap reduces while oscillator strength, α and $\mu\beta$ increase dramatically at small distance values where hydrogen bondings are possible. Although excitonic splitting corresponds to only $4\mu^2/r^3$ in this case, due to hydrogen bonding, the $\mu\beta$ value is almost 14 times greater than the monomeric $\mu\beta$. Considering the two-level β value, which is proportional to both $\Delta\mu$ and f, the Frenkel exciton estimate would give $\mu\beta \sim 22745$au at small distances. For case (d), at large distances, the $\mu\beta$ value is what is expected from exciton theory. Note that, the exciton splitting is maximum, $\Delta E \sim 6\mu^2/r^3$ for case (d). However, at small distances, because of the repulsion between the same groups, the $\mu\beta$ of case (d) is close to the $\mu\beta$ of (a) at large distances. Other cases are not quite interesting but note the excitation energy gap for cases (b) and (c). For case (c), hydrogen bonding is very weak at a N-N distance of $\sim 4\text{Å}$, while for case (b), the repulsion energy is very high for all the distances we have studied. The zero value of $\mu\beta$ signifies the symmetry effects as well as our computational accuracies, for both cases (b) and (c).

The configuration (a) is an asymmetric dimer. The exciton theory based on dipole-dipole interactions provide a small shift (maximum ~ 0.011au) even at small distances, with oscillator strength of the order 0.4. The strong red-shift at small distances is mainly due to hydrogen bonding. The lowest singlet excited state in the dimer is excitonic in character. These excitations posses appreciable intensity and are associated with an appreciable dipole

moment change, along the long axis of the dimer. The calculated low-energy excitonic character can be associated with the long-wavelength features observed in J-band aggregates [64, 65]. Previously a linear increase in the β value was reported for HF linear polymeric configurations. Coupled with the discussion above, we can thus safely conjecture that the PNA aggregates with hydrogen-bonded chromophores lying *in-line* can give rise to a large β value, with a one-photon absorption frequency deep inside the IR-region. A few experimental confirmatory examples of such planer (although not exactly *in-line*) monomeric stacks, with large SHG coefficients have been reported in [66, 67].

As the splitting energy strongly depends on the oscillator strength, we have considered two other dipolar molecules in their planar optimized structures. These molecules have high oscillator strengths. For 2-methyl paranitroaniline, the oscillator strength is 0.5, while it is 1.6 for the 4-amino-4′-nitro azobenzene. In the next figure (Fig. 3.2), the lowest excitation gap and the $\mu\beta$ value at an electric frequency of 0.00367au have been plotted for the double molecules (II) and (III) (as referred in the Fig. 3.1). We have considered the geometries of the dimer configuration at the most favored arrangement, i.e, the $\theta = 0$ and $\phi = 0$ configuration. Also given are the monomeric counterparts of the same quantities in each of the figure panel. As expected, due to the *in-line* arrangements of monomer molecules, the quantities like hyperpolarizabilities, and polarizability (not shown) increase drastically for the composite molecules, while the singlet-singlet gap reduces considerably.
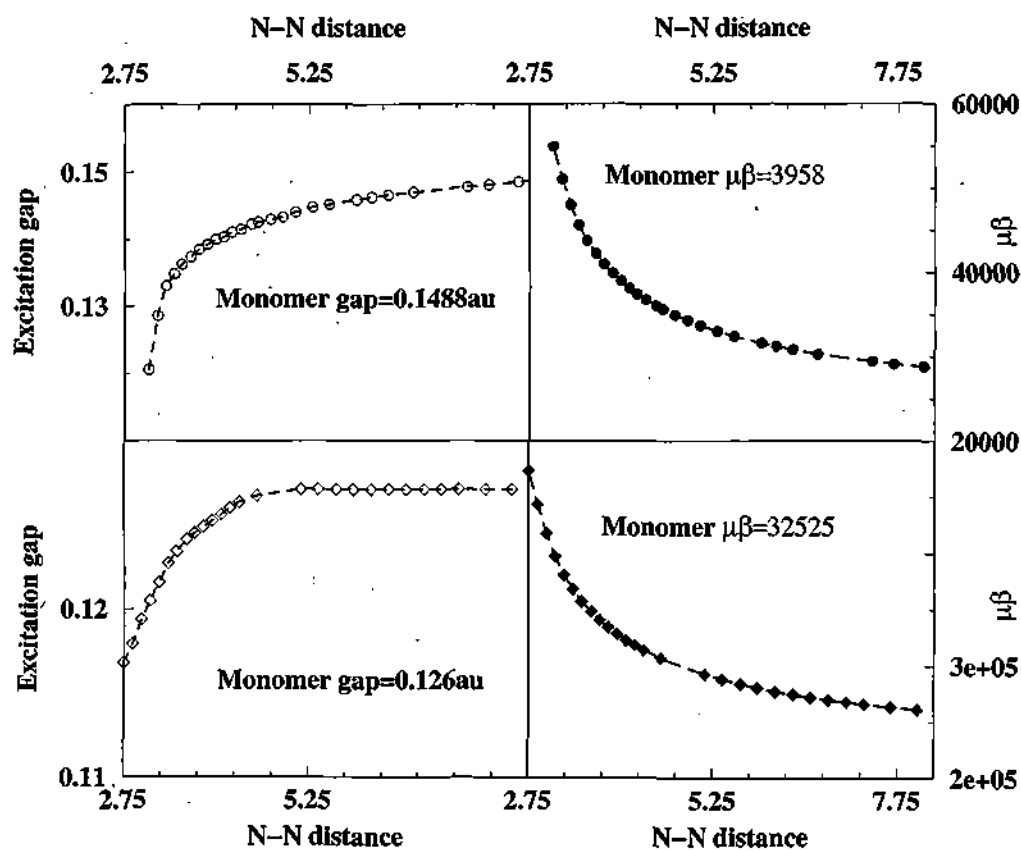
Figure 3.2: Plot of the excitation gap (in au) and $\mu\beta$ (in units of au), as a function of the distance, d (in Å). The upper panel (open and filled circles) is for the dimer with molecule-(II) as monomer and the lower panel (open and filled diamonds) is the same with molecule-(III) as monomer. In both cases, the $\mu\beta$ values are calculated for the oscillating frequency, $\omega = 0.00367$au

The present semi-empirical calculations go beyond the PNA dimer considered in *ab initio* calculations [63]. However, we consider the same optimized geometry of the PNA dimer as suggested by Peris et al to study the dispersion behavior. We have chosen the N-N distance to be $3.6\overset{\circ}{A}$ in the head-to-tail arrangement as in configuration (a), Fig. 3.1A. We find that the molecules are hydrogen bonded most efficiently at this distance and the dimers are in their global minimal of energy. For the other two molecules, we have considered similar distance as in $(PNA)_2$. On these dimer geometries, we have computed the dependence of α and $\mu\beta$ on the frequency of the applied electric field. The frequencies are chosen such that the system remains quite away from any resonance. Note that for β, the one-photon resonance occurs at frequency corresponding to one-half of the one-photon gap. In Fig. 3.3 we present the EFISH coefficients ($\mu\beta$) for a frequency range, 0.00183au to 0.0349au. For all three dimers, the $\mu\beta$ increases smoothly with the increase in frequency. We have verified the scaling by fitting the data in frequency power, which gives an exponent ~ 2 for all three cases.
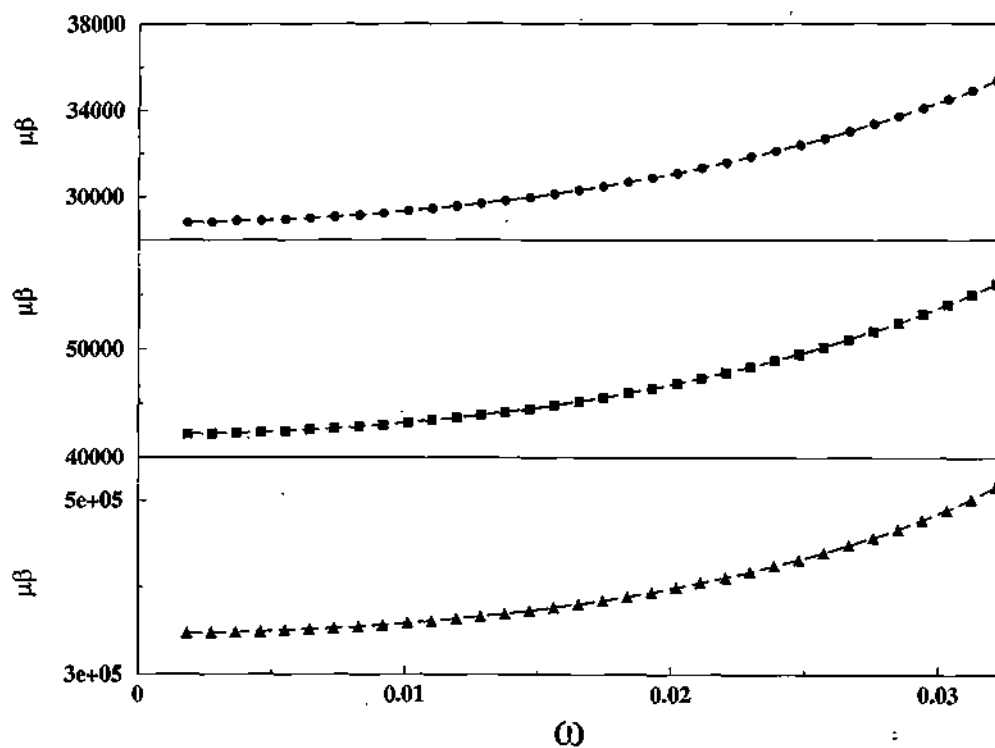
Figure 3.3: Dispersion curves for $\mu\beta$ (in units of au) for dimeric configurations of three molecules (see text for details); PNA dimer (filled circles), 2-methyl-paranitroaniline dimer (filled diamonds) and 4-amino-4′-nitro azobenzene dimer (filled triangles). Frequency is in au unit

3.5 Favorable arrangements of paranitroanilines in an assembly

We have already mentioned that the most stable arrangement for the paranitroaniline molecules involve the head-to-tail arrangement (arrangement a, Fig 3.1) and the π stacked complex (arrangement c, Fig 3.1, also Fig. 3.4). We calculate the energies for these two systems. The head-to-tail arrangement of two PNA molecules is the most stable arrangement (Table. 3.2) because it involves the formation of two H-bonds. For the π stacked complex, there are no H-bonds but the system is stabilized by the mixing of the orbital electrons between the two molecules.
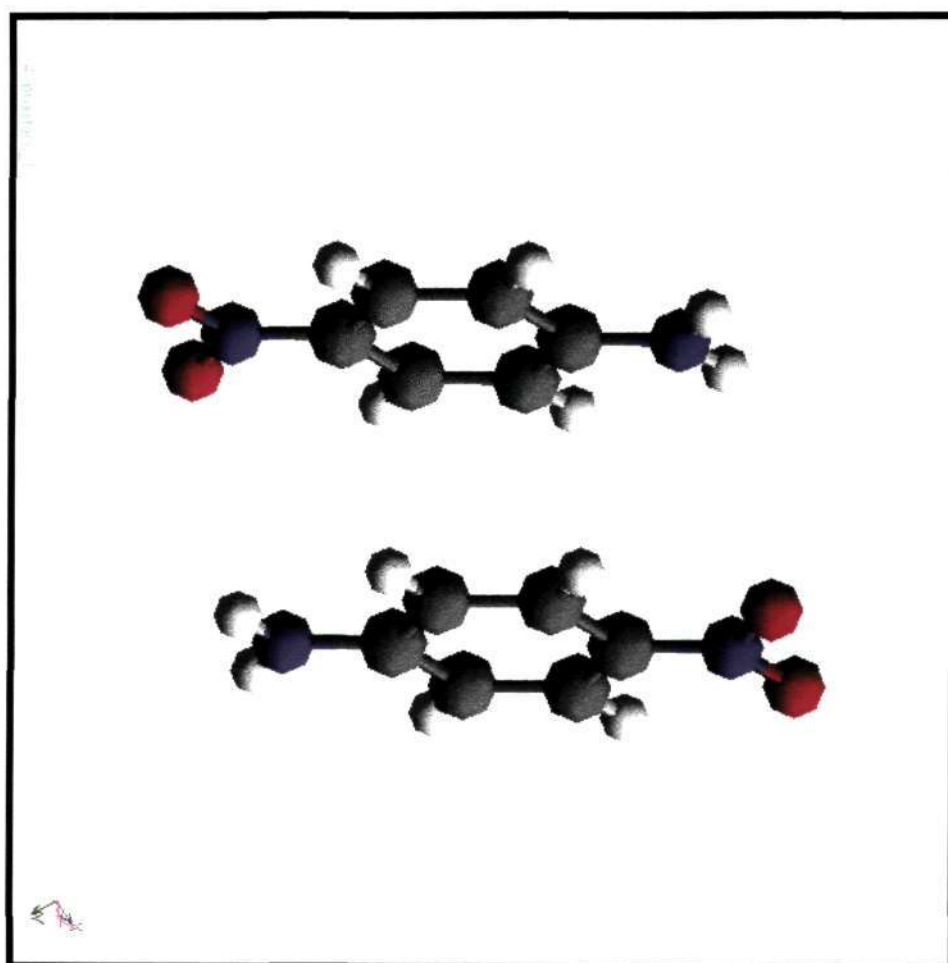
Figure 3.4: Arrangement of two PNA molecules having π stacked arrangement

Table 3.2: Energy analysis for the stacked dimer configuration for PNA

Molecular Arrangements	Energy (in eV)
Head-tail arrangement	-3806.364
π-Stacked arrangement	-3798.354
Optimal π-stacked arrangement	-3804.459

But, the most interesting case is for the optimal π-stacked arrangement. This arrangement is shown in Fig. 3.5. The two molecules are neither exactly π-stacked nor in a linear head to tail arrangement. One of the $-NO_2$ of a PNA molecule bends away from the planarity of the ring to interact through a H-bond with a $-NH_2$ of the other PNA molecule. The dimeric system relaxes by incorporating both the features: formation of a single H-bond and a tilted π-stacked complex. Thus, there is a very delicate balance between H-bonding interaction and π-stacking interaction.

Our calculation qualitatively explains the crystal-structure for paranitroaniline. The molecules are arranged along a line of head-to-tail arrangement so as to facilitate two H-bonds in plane for each molecule. This is the same arrangement as predicted by our calculations for two molecules that the linear head-tail arrangement corresponds to the global minima in the potential energy surface. Also, above each layer of such arrangement there is the second PNA layer that undergoes π-stacking with the lower layer.
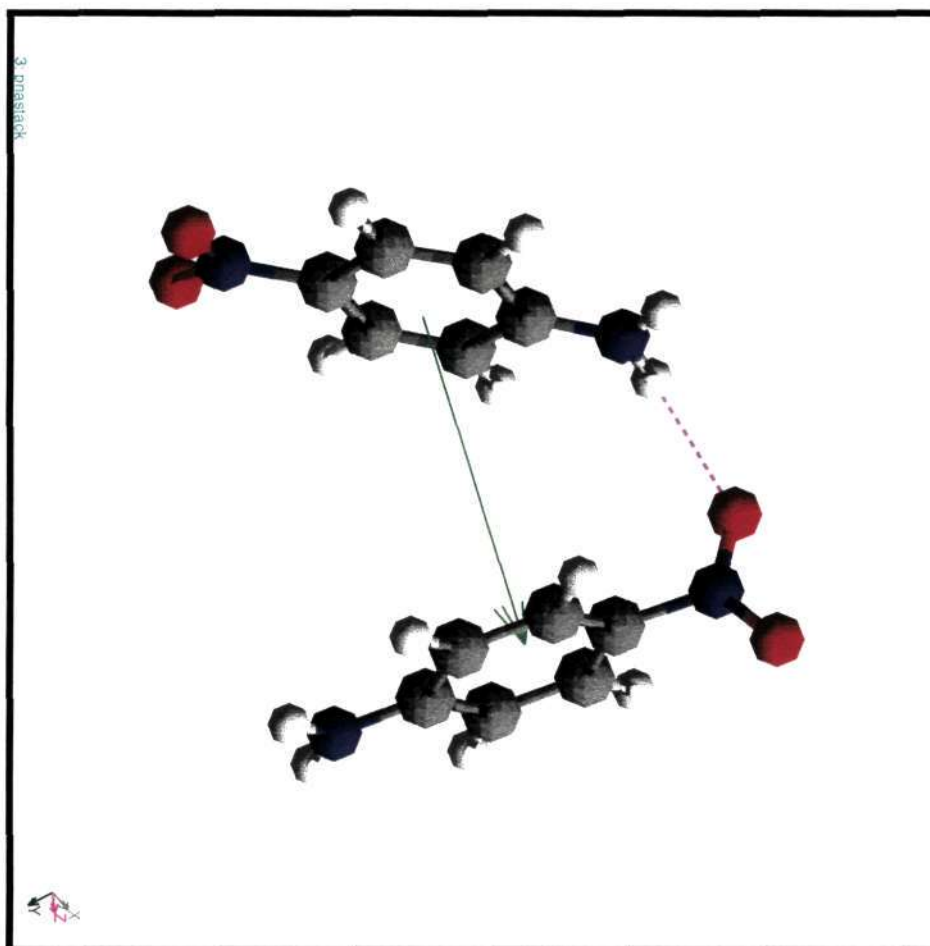
Figure 3.5: Optimal arrangement for two PNA molecules stacked

To conclude, we have carried out an extensive computations of a few dipolar organic molecules in a number of dimeric configurations to understand the aggregation effect. Although our results are based on semi-empirical computation, the use of a number of reference configuration interactions account for a substantial correlation effects, and thereby give rise to qualitatively (if not exact quantitative) accurate picture for double molecules at various distances and configurations. We find that the best arrangement is the *in-line* head-to-tail arrangement, which gives rise to an enormous increase in nonlinear optical properties. We have also shown that such a structure is extremely stabilized by hydrogen-bond formation and exciton-exciton interactions. This dimer configuration is associated with an appreciable absorption intensity, and for an aggregate, this would appear deep in the IR-region. For at least two molecules, PNA [68,69] and 2-methyl-paranitroaniline [70,71], the crystal structure shows that they crystallize in the most favored arrangement as per our discussion, but the whole crystal structure becomes unsuitable for serious consideration. This can be avoided through the self assembly techniques [8], building arrays of the compounds in the desired pattern. The problems associated with such self-assembly is the relatively low packing densities [72]. This could however be avoided to some extent by connecting the monomers through efficient hydrogen-bondings or π-stacking, to form an infinite network of one-dimensional chains or co-facial planer structures. But to achieve this, the molecular characteristics of the constituent monomers and their surrounding interaction effects have to be properly optimized. We stress that even if the monomers can not be arranged exactly *in-line* with each other, the effects discussed here will still be observed to some extent

below a certain critical angle. To determine this critical angle, one simply requires knowledge about the phase relations between each of the transition dipole pairs. Therefore, a synthetic scheme well suited for the best dipolar arrangements of various monomers can be fine tuned to obtain large nonlinear optical properties at extremely low-energy.

Chapter 4

Nonlinear optical properties of oxo-bridged di-nitroanilines

4.1 Introduction

Materials with large second harmonic coefficients are of huge current interest. Devices made up of these materials are finding a large number of applications in various disciplines, from lasers to optical switches and electronics [34].

Conjugated organic molecules have a lot of potential to be used as good nonlinear optical materials [1]. These molecules have delocalized π electrons over a large length scale of the molecule which can be very easily manipulated by substitution of electron donating (push) and electron withdrawing (pull) groups around the aromatic moieties. Apart from structural flexibility which allows fine tuning of chemical structures and properties for the desired nonlinear optical properties [7, 8], the organic materials are of great technological interest because of their low cost, ease of fabrication and integration

into devices.

Recently, a series of oxygen bridged organic dipolar molecules consisting of benzene rings with different donor and acceptor groups have been synthesized [73]. The nonlinear optical measurements show a wide variation in magnitudes, depending on the donor and acceptor strengths and their geometrical positions. For a proper understanding of the dependence of nonlinear optical properties on the constituent groups and their geometrical positions in similar group of structures, we have considered a series of nitroaniline systems where two nitroaniline molecules are connected by a bridged oxygen atom. This oxygen atom can be considered to be acting as a stitch between two nitroaniline molecules. Out of a large number of di-nitroaniline configurations, we find that the hyperpolarizability coefficient is maximum for the systems where the molecular dipoles make $0°$ angle between them and are on the same plane. However, in reality, these molecular systems are not planar due to steric interactions. Therefore, to put our predictions into maximum applicability, we connect the two nitroaniline rings by a covalent bond. This reduces the non-bonding interaction between the rings and makes them almost planar, thereby giving rise to desired nonlinear optical characteristics.

In the next section we modify the semi-classical theory based on point dipole interactions discussed in Chapter 2, so as to represent the interactions in these molecular structures. Next to that, we present a theoretical analysis of the nonlinear optical properties of the chromophores as a function of a number of dipolar orientations. This is done using established ZINDO/CV quantum chemical formalism. Finally,we conclude this chapter with a summary of all the results.

4.2 Dipolar model for the excitonic level splitting in oxo-bridged dinitroanilines

For organic dipolar molecules, the lowest optically allowed energy state is an exciton state, and the interactions between the excitonic states can be expressed in the direct product basis of the chromophoric molecular orbitals if the direct overlap between the chromophoric molecular orbitals is negligible [42, 43, 75–78]. This can be realized only at large distances and thus the coupling between dipolar molecules can be approximated at large distances by a point dipole model. If two molecular species, m and n, are same, the coupling interactions can be written as

$$H_{m,n} = \frac{\vec{M}_{ij}.\vec{M}_{ij}}{r_{mn}^3} - \frac{3(\vec{M}_{ij}.\vec{r}_{mn})(\vec{M}_{ij}.\vec{r}_{mn})}{r_{mn}^5} \tag{4.1}$$

where $\vec{M}_{ij}$ is the transition dipole moment from state i to state j of the monomer molecule and r_{mn} is the distance between the two molecular centers, m and n. It is to be noted that both the transition dipole and the distance $(\vec{r}_{mn})$ are vectorial quantities. Thus the magnitude of the interaction term will depend crucially on the relative orientations of the dipolar molecules as well as on the axis joining their centers. We shall give here a purely quasi-classical vector treatment to this interaction as we assume electrostatic interaction between the transition moments [79].

A number of cases can be analyzed considering the dipolar molecules in various orientations. We have considered the oxo-bridged di-nitroaniline systems as shown in Fig. 4.1. The chromophores are oriented with an angle

ϕ between the planes of the molecules and each molecule creates an angle θ with its molecular axis. Twisting of the C-O-C bridge, rotates one of the molecule (with an angle ϕ) while the other molecule remains fixed on the plane.
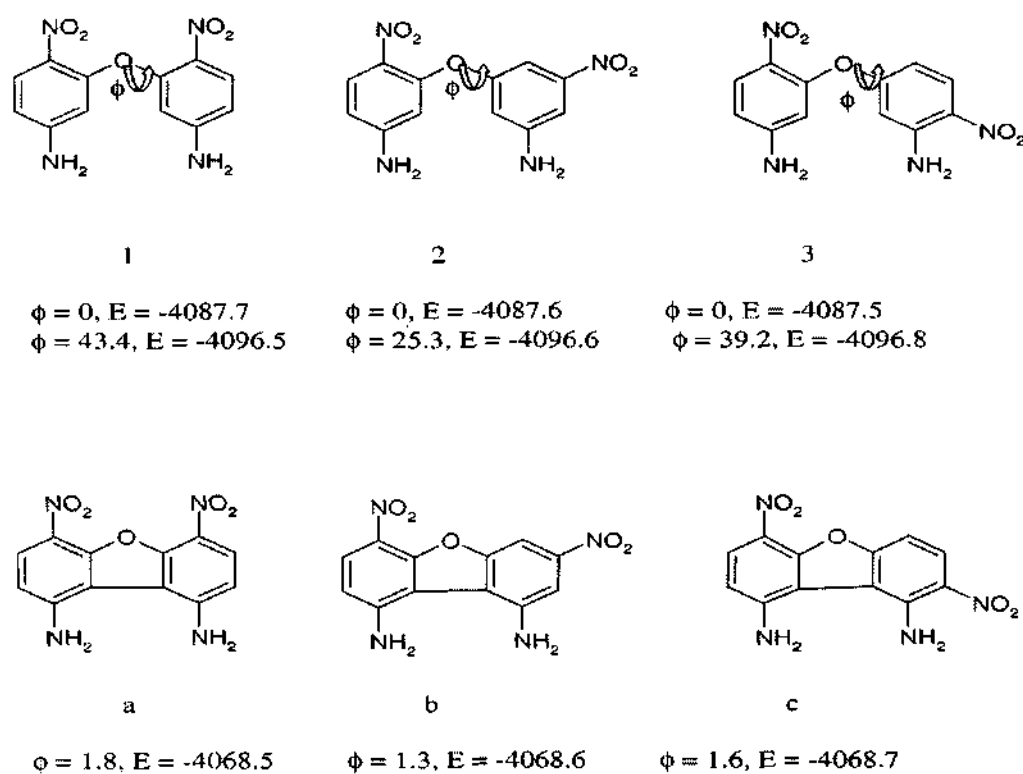
Figure 4.1: Structures of the three molecules 1, 2 and 3 considered for the quantitative estimations. The footnotes indicate the energies and twist angle (ϕ) of the systems. The 1st footnote shows the energies (eV) for parallel dipole $\phi=0$ (in degrees). The next footnote is for the optimized geometries. a, b and c are structures of the rigid molecules fixed by the C-C linkages. Their energies and twist angle (ϕ) are in the last footnote

It then becomes quite simple to derive the dipolar splitting energy of the lowest energy excitation

$$\Delta E = 2\frac{M_{gs}^2}{r_{mn}^3}(\cos\phi - 3\cos\theta_1\cos\theta_2) \qquad (4.2)$$

where M_{gs} is the transition dipole from the ground state to the excited singlet state of the monomer (excitonic state). Here θ_1 is the angle between the polarization axis and the molecular axis of molecule-1 and θ_2 is the same for the 2nd molecule.

Let us now analyze a few cases with the variance of angles θ_1, θ_2 and ϕ. We keep one of the molecules fixed so that the variance of θ_1 remains zero. Since, this fixed molecule is para-nitroaniline in our case, θ_1 itself is zero. Now the $(\theta_2, \phi) = (0°, 0°)$ case corresponds to the ideally planar pna-O-pna (paranitroaniline oxo bridged with another paranitroaniline), the case 1 in Fig. 4.1. For the planar pna-O-mna (paranitroaniline oxo bridged with metanitroaniline) and pna-O-ona (paranitroaniline oxo bridged with orthonitroaniline) however, the θ_2 angle is not well-defined. We determine the θ_2 by observing the angle that the dipole moment vector makes with the molecular axes for the optimized geometries of the individual molecules, i.e, 30° and 90° for mna (metanitroaniline) and ona (orthonitroaniline) respectively. Note that this is an approximatation, since in the presence of the bridged oxygen, the magnitude of this angle would be different. However, we find that the difference is quite small, and for simplicity we assume the θ_2 values from the individual optimized geometries, i.e., $(\theta_2) = 30°$ and $(\theta_2) = 90°$ for pna-O-mna and pna-O-ona (see cases 2 and 3 in Fig.4.1) respectively.

For cases where $(\theta_2, \phi) = (0°, 0°)[(90°, 0°)]$, the electrostatic interaction is attractive [repulsive] in nature for the lowest excited states. Note that the transition moments are finite for electric dipole transitions from the ground state to the state with attractive electrostatic interaction while it is vanishing for the states with repulsive interaction.

4.3 Results and Discussions

For a quantitative understanding of the phenomenon in general, we carry out extensive numerical calculations of the ground state and the excited states of the oxo-bridged di-nitroaniline systems.

We start our calculations by optimizing the geometries of all the molecules using the semi-empirical AM1 parameterized Hamiltonian [44] without any symmetry constraints available in the Gaussian-98 set of codes [45]. Due to the steric interactions between the nitroaniline rings, the angle connecting the two rings (ϕ) becomes non-zero for the optimized molecules 1, 2 and 3 in Fig. 4.1. The optimized geometry of the pna-O-pna and the C-C bridged pna-O-pna are shown in Fig. 4.2 and Fig. 4.3. Their bond lengths and bond angles are shown in Tables attached.
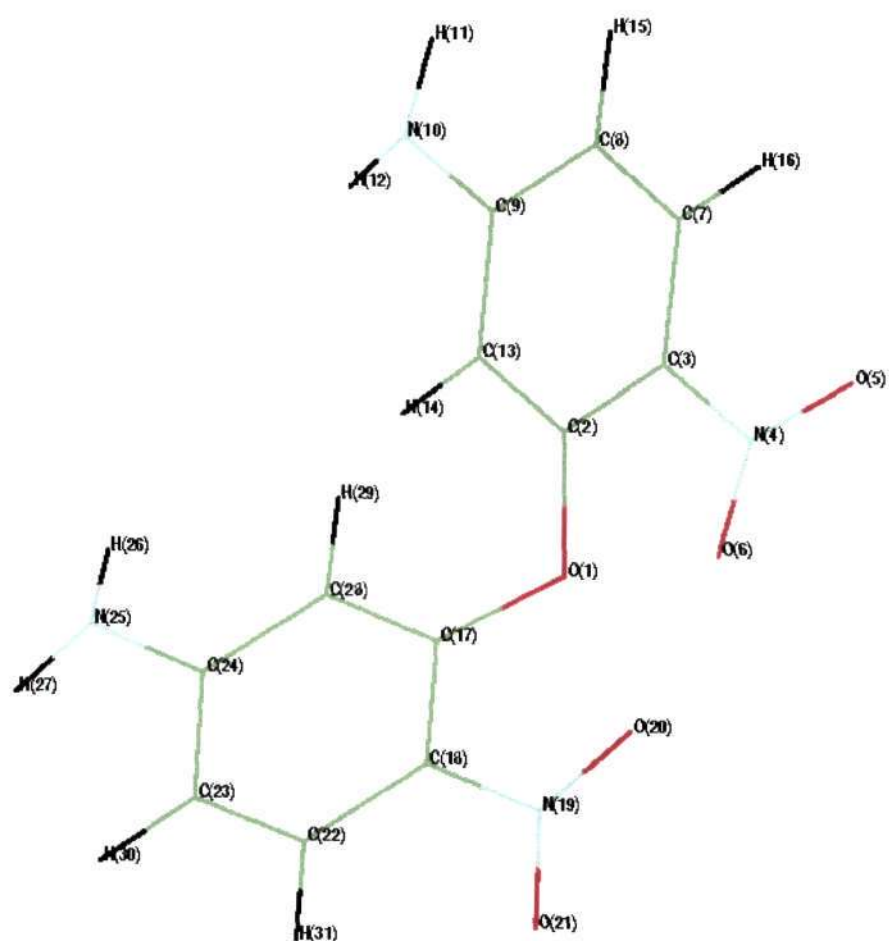
Figure 4.2: Optimized geometries of pna-O-pna. The numbers indicate atomic positions
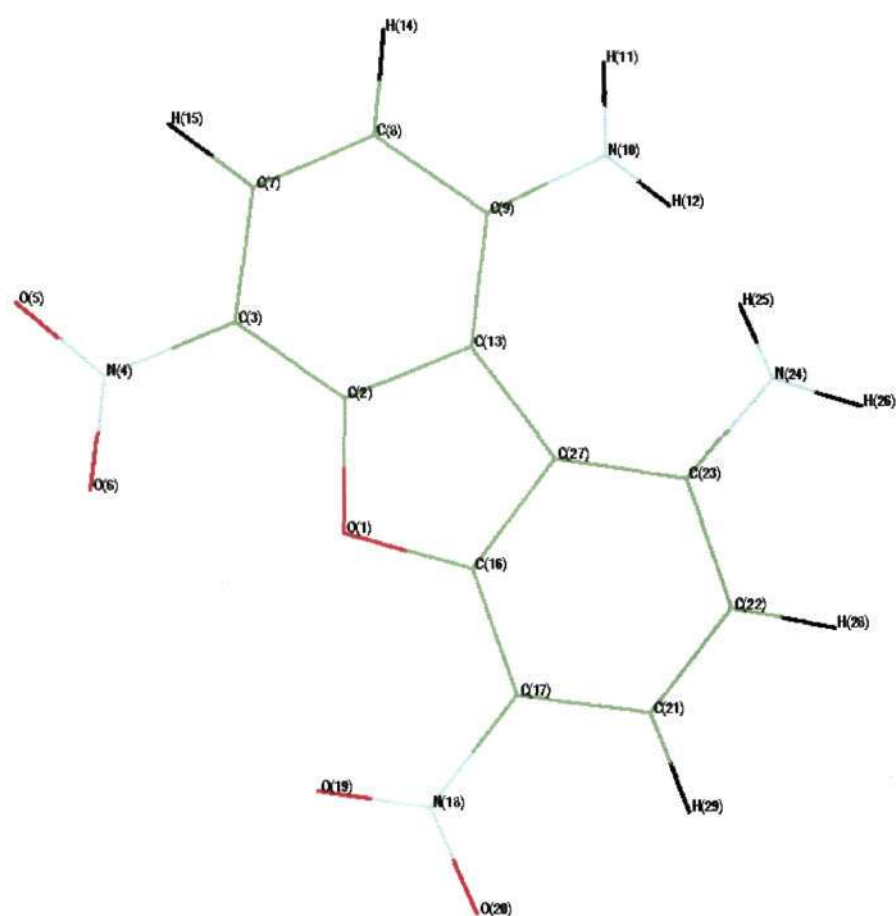
Figure 4.3: Optimized geometries for pna-O-pna bridged by C-C bond. The numbers indicate atomic positions

pna-O-pna			
bond	length	angle	degrees
C2-O1	1.388	C17-O1-C2	117.2
C17-O1	1.386	C2-C13-C9	120.7
C17-C28	1.416	C13-C9-C8	118.9
C28-C24	1.407	C9-C8-C7	119.8
C24-C23	1.384	C8-C7-C3	121.6
C23-C22	1.418	C7-C3-C2	119.5
C22-C18	1.423	C3-C2-C13	119.5
C18-C17	1.392	C3-N4-O5	119.6
C2-C13	1.398	C3-N4-O6	118.4
C13-C9	1.418	C13-C9-N4	120.3
C9-C8	1.423	C2-01-C17	117.2
C8-C7	1.379	C17-C28-C24	120.4
C7-C3	1.401	C28-C24-C23	118.9
C9-N10	1.374	C24-C23-C22	120.3
C3-N4	1.479	C23-C22-C18	120.7
N4-O5	1.201	C22-C18-C17	119.2
N4-O6	1.203	C18-C17-C28	120.5
C24-N25	1.376	C18-N19-O20	118.3
C18-N19	1.479	C18-N19-O21	119.8
N19-O20	1.204	C24-C23-N25	120.7
N19-O21	1.201	C28-C23-N25	120.5

pna-O-pna, C-C bridged			
bond	length	angle	degrees
C2-O1	1.398	C2-O1-C16	105.4
C16-O1	1.397	C16-C27-C23	118.4
C16-C17	1.395	C27-C23-C22	117.4
C17-C21	1.412	C23-C22-C21	122.5
C21-C22	1.382	C22-C21-C17	121.0
C22-C23	1.427	C21-C17-C16	116.8
C23-C27	1.409	C17-C16-C27	123.5
C27-C16	1.432	C2-C3-C7	116.8
C2-C3	1.395	C3-C7-C8	120.8
C3-C7	1.411	C7-C8-C9	122.7
C7-C8	1.383	C8-C9-C13	117.3
C8-C9	1.427	C9-C13-C2	118.4
C9-C13	1.410	C13-C2-C3	117.3
C13-C27	1.459	C8-C9-N10	122.8
C23-N24	1.386	C13-C9-N10	119.9
C17-N18	1.476	O5-N4-O6	122.3
N18-O19	1.198	O20-N18-O19	122.3
N18-O20	1.205	C16-C17-N18	120.5
C3-N4	1.476	C21-C17-N18	122.7
C9-N10	1.386	C7-C3-N4	120.5
N19-O21	1.201	C2-C3-N4	122.7
N4-O6	1.205	H12-N10-H11	114.1
N4-O5	1.198	H26-N24-H25	113.8

However to understand the effects of dipolar orientations on the nonlinear optical properties, we deliberately put the two rings planar and perform single point energy calculations. We then change the dihedral angle between the two rings by twisting the bond connecting the bridged oxygen and the carbon in one of the rings. These geometries were used to compute the SCF MO energies and then the spectroscopic properties using the Zerner's INDO method [52]. We use the singles CI (CIS), since the first nonlinear optical coefficients are derived from 2nd-order perturbation theory involving one-electron excitations. The CIS approach adopted here has been extensively used in earlier works, and was found to provide excitation energies and dipole matrix elements in good agreement with experiment [53,54]. To calculate nonlinear optical properties, we use the correction vector (CV) method, which implicitly assumes all the excitations to be approximated by a correction vector [56]. Given the Hamiltonian matrix, the ground state wave function and the dipole matrix, all in CI basis, it is straightforward to compute the dynamic nonlinear optical coefficients. Details of this method have been published in a number of earlier works [57–59].

Before presenting the nonlinear optical coefficients, we first show the variation of splitting energy (see Eq. 4.2) in each case as a function of dihedral angle or the twist angle. The distance between the molecular axis, r_{mn}, was obtained from the geometry of double molecule for the corresponding twist angle, as discussed in the previous paragraph. The Fig. 4.4 (upper portion) represents the variation of the modulus of the splitting energy with the variation in ϕ for the three systems 1, 2 and 3 with unit M_{gs}. As can be seen, for molecule 1 and 2, there is almost no variation in splitting energy, while

for molecule 3, the splitting energy decreases as a function of twist angle, ϕ. Furthermore, the splitting energy is negative for the cases 1 and 2, while it is positive for the case 3. However in all the cases the absolute value of the splitting energy is quite small.

In the lower panel of Fig. 4.4, we plot the total ground state dipole moment μ_G (in Debye) for these three systems as a function of angle ϕ. We find that while the dipole moment decreases with increase in ϕ for the case 1 and case 2, it increases for the case 3. This can be easily understood by considering the combined effects of ground state dipoles in each cases. If the two dipoles are parallel and in the same plane, the *in-phase* combination of the resultant dipole is the sum of the two individual dipoles. For the pna-O-ona (case 3), the two dipoles are pointing almost perpendicular to each other when they are in the same plane (ϕ=0 limit). Thus the *in-phase* combination of them give the net total dipole moment, μ_G, very small. However, as the ϕ increases from zero, the angle between the two dipoles reduces, increasing the *in-phase* combination of the total dipole moment (or equivalently, reducing the *out of phase* combination). Thus the μ_G increases with increase in ϕ for pna-O-ona. However, for pna-O-pna (case 1) and for pna-O-mna (case 2), the $\phi = 0$ configuration is the most favorable orientation in terms of their total ground state dipole moment. As ϕ increases from zero, the monomer dipoles rather oppose each other, *in-phase* combination of which reduces the μ_G.
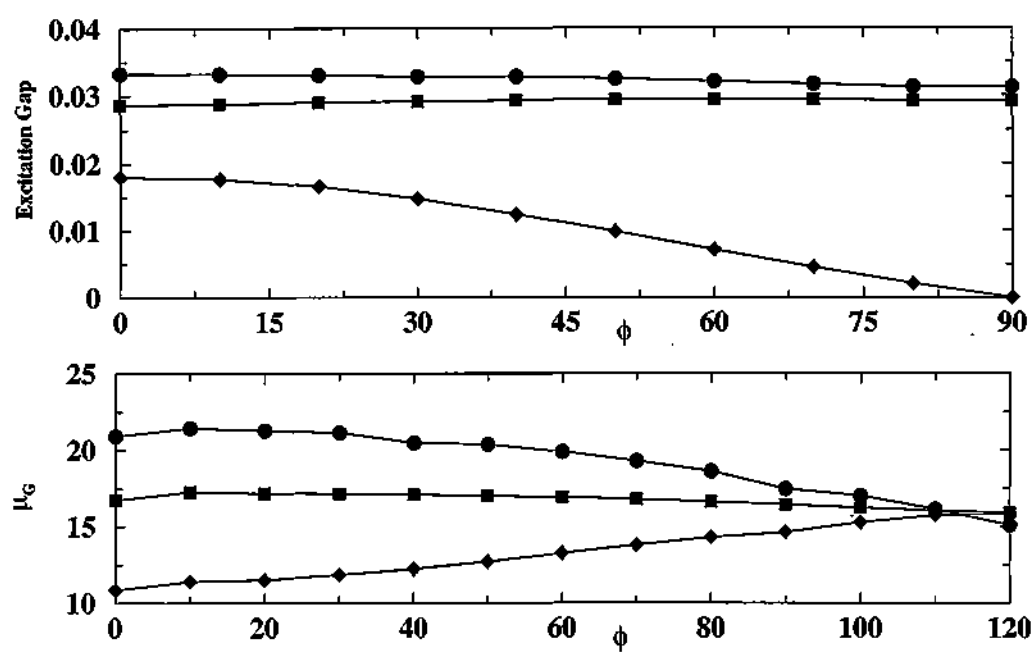
Figure 4.4: The upper panel shows the variation of the magnitude of the splitting energy (in eV) as a function of the dihedral angle for the three systems 1(circles), 2(squares) and 3(diamonds). The lower panel represents the variation of the ground state dipole moment μ_G (in Debye), as a function of the dihedral angle for the same three systems

To firmly establish the above qualitative discussions, we present in Fig. 4.5, the relative phases of the constituent molecules forming the dimer for the pna-O-pna cases. The ground and the lowest optically excited states are shown for pna-O-pna parallel dipoles ($\phi = 0$), the optimized geometry and the rigid molecule with C-C linkage (structure a in Fig. 4.1). The ground state (HOMO level) is an even-parity combination of the atomic orbitals from the individual rings, while for the LUMO level (the lowest optically active single excitation), the combination is out-of-phase or antisymmetric. From the figures, it is quite clear that with increase in ϕ, the magnitude of μ_G as well as the electric transition dipoles would reduce. In the MO picture, the electric field connects the ground state to a state with exactly opposite parity. The transition dipole strength will be maximum for the case where the change in parity is complete (even to odd) while going from HOMO to LUMO. Since the HOMO level for $\phi = 0$ pna-O-pna has the best in-phase combination (phase difference is zero), the μ_G is highest for this case. On the otherhand, for the optimized pna-O-pna geometry, the phase difference is 43.4°, which accounts for the small μ_G in this case. For the rigid geometry however, the phase combination in the HOMO level is almost symmetric (phase difference $\sim$ 1.8°), together with notable contribution from the C-C bond, although the dipoles are very close to being parallel. The phase difference in the HOMO level together with the parity difference between the HOMO and the LUMO level would account for the EFISHβ values found in various geometries, discussed later.

HOMO (parallel) LUMO (parallel)

HOMO (optimized) LUMO (optimized)

HOMO (rigid) LUMO (rigid)
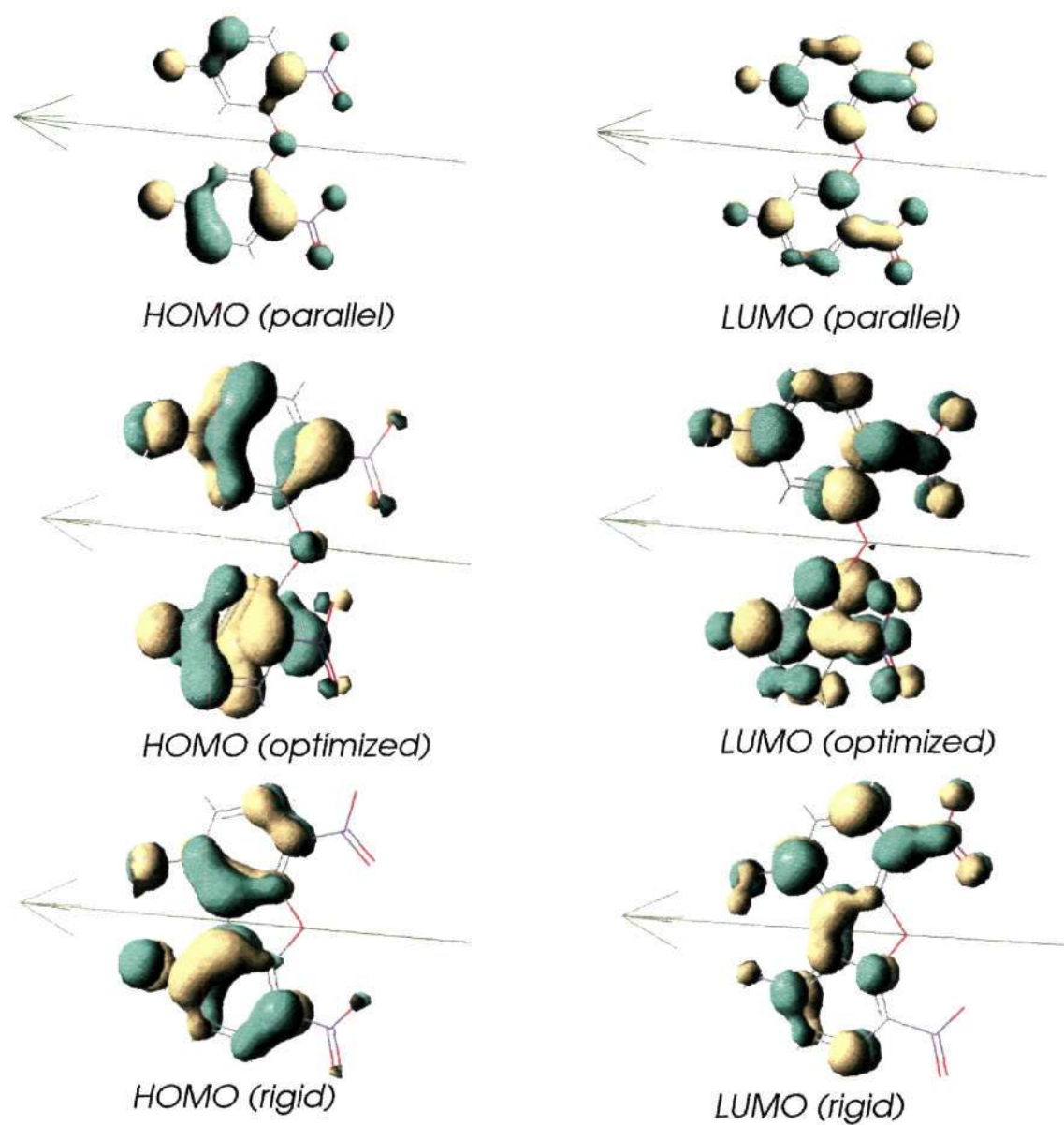
Figure 4.5: AM1 derived HOMO and LUMO molecular orbitals for: 1st row - the parallel dipoles(ϕ=0) for pna-O-pna. 2nd row - the optimized geometries. 3rd row - rigid pna-O-pna connected by C-C linkage. The shading represents the phase of the wavefunctions. The arrows indicate the directions of the dipole moments

The bridged oxygen atom does not play any significant role in determining the nonlinear optical coefficients. It basically controls the distance between the two nitroaniline dipoles. Due to its high electronegativity, it just increases the total dipole moment of the dimeric systems (it is roughly 1 Debye increase purely because of oxygen) to the same extent for all values of the dihedral angle, ϕ. Thus, even though our semi-classical theory of dipole-dipole interaction does not take into account the electronic properties of the bridged O atom, we find that the qualitative trend in splitting energy as a function of the angle ϕ is almost the same with those obtained from CIS calculations for the di-nitroaniline systems.

For the calculations of the optical coefficients, we have used 1064nm (1.17eV) as the excitation frequency of the oscillating electric field which corresponds to the frequency of the Nd-YAG lasers used in experiments. We plot the variation in EFISH (electric field induced second harmonic) coefficients with the angle ϕ in Fig. 4.6. The trend is very similar to that for the ground state dipole moment in Fig. 4.4. To be precise, the magnitude of EFISH coefficient decreases with increase in the torsional angle for the pna-O-pna and for the pna-O-mna, while for the pna-O-ona, the magnitude of the same increases.

The EFISH coefficients shown in Fig. 4.6 are the product of dipole moment (μ) and the SHG coefficients (β). The β is computed as the tumbling average quantity, defined as $\beta = 1/3(\beta_{xyy} + \beta_{yyx} + \beta_{yxy})$. From Fig. 4.4 (upper panel), it is clear that for pna-O-pna and for pna-O-mna, the energy difference between the ground and the one-photon state remains almost constant as a function of the torsional angle, ϕ. Thus, for this two systems, there is

very negligible effect of splitting energy on the magnitude of β. This suggests that the β values can be tuned to large extent according to the ground state dipole moment, if the oscillator strength is appreciable. This is precisely the EFISH coefficients trend observed for systems 1 and 2, as a function of ϕ. For pna-O-ona however, the EFISH coefficient increases with the increase in the angle ϕ. Interestingly, for this case, with the variation of ϕ, the increase in the ground state dipole is not much; the reduction in energy gap between the ground state and the one-photon state decides the trend for the EFISH coefficients.
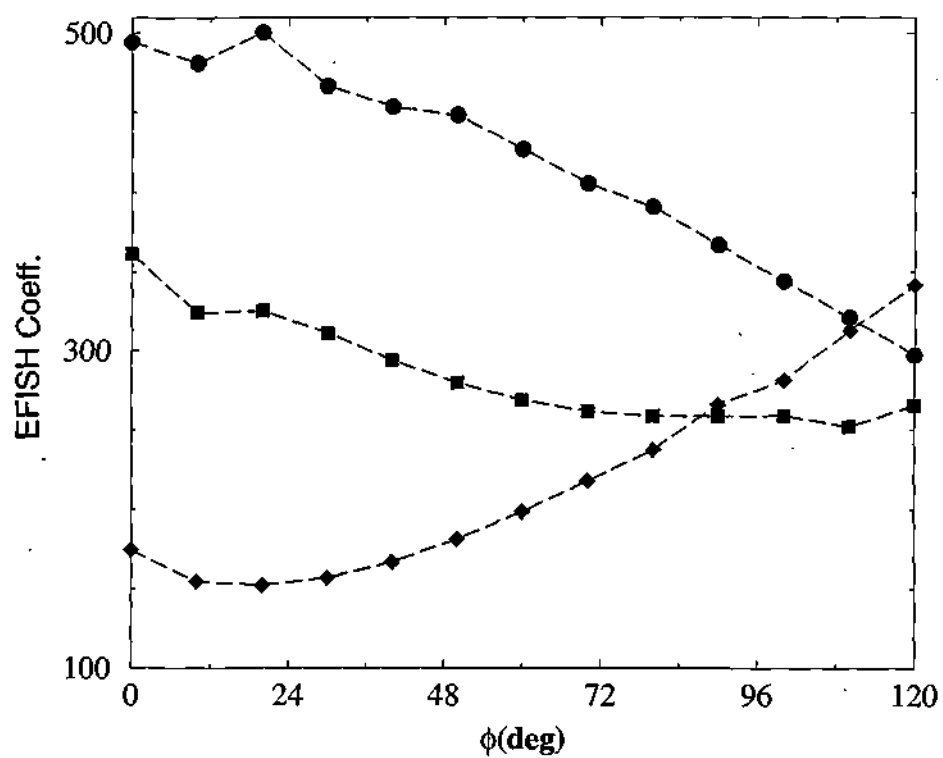
Figure 4.6: Plot of the EFISH coefficients (in units of 10^{-30}esu $\times$ Debye), as a function of the dihedral angle for the three systems 1(circles), 2(squares) and 3(diamonds). The input electric field frequency in all the cases is 1.17eV

We shall ask the question now as to how is it possible to achieve such high EFISH coefficients with desired dipole orientations in optimized oxo-bridged di-nitroaniline systems. The highest EFISH coefficients (494.4×10^{-30}esu) is obtained for pna-O-pna with zero dihedral angle. Such a high value of EFISH coefficient cannot be realized for the real molecular system as the optimized geometries of the di-nitroaniline molecules discussed above are not planar due to steric repulsions. Therefore, our best suggestion is to connect the oxo-bridged rings by a carbon-carbon bond in the *meta* position. Optimizations of the structures, (a) and (b) in Fig. 4.1 by the same method described earlier confirm that the nitroaniline rings are almost planar with the dihedral angle ϕ very close to zero. Thus one can make the two dipoles to be parallel to a large extent by bridging the two rings by a covalent bond. For the case (c) however, the optimized geometry is not planar. The rings themselves twist in the optimized structure of (c). This is due to the steric repulsion among the closely spaced three groups (see Fig. 4.1 c).

The EFISH coefficients for the optimized geometry of (a) is 471.5×10^{-30}esu, close to the parallel ($\phi = 0$) pna-O-pna dipole value. For the pna-O-mna cases, the values for parallel dipoles($\phi = 0$), and the optimized structure (b) are 307.8×10^{-30}esu and 301.6×10^{-30}esu respectively. Thus we can safely conclude that the C-C connected dipole provides a better choice of materials. However for the pna-O-ona systems, we find some different result. The values for parallel dipoles ($\phi = 0$), and the optimized structure (c) are 147.7×10^{-30} esu and 77.6×10^{-30} esu respectively. From the Fig. 4.6, we see that EFISH coefficient is least for the case 3 (Fig. 4.1) when the dihedral angle is zero and its magnitude increases with increase in ϕ. Thus we expect the optimized

structure (c) to give high values of EFISH coefficients compared to the $\phi = 0$, case 3 (Fig. 4.1). However, as we see, the magnitude is quite small. We attribute such a low value of the EFISH coefficient to the following. The C-C covalent connection would try to keep the rings planar; however this would enforce three groups (two NH_2 and one NO_2) to come close to each other. This results in strong steric repulsions and as a result the two NH_2 groups bend away from the plane of the benzene rings. Consequently, the π electron delocalization length decreases, decreasing the EFISH coefficient to a large extent.

Our results compare fairly well with the experimental values. For example, we have calculated the β for the optimized *Bis (2-amino-4-nitrophenyl) ether*, for which the experimental β value from Hyper-Rayleigh Scattering (HRS) experiments at the Nd:YAG frequency is 22.0×10^{-30}esu [73], while our estimate at the same frequency gives $\beta=16.4 \times 10^{-30}$esu.

Next we consider the dispersion relation for the first nonlinear polarizability coefficients (β). Since this needs to be done for a fixed geometry, we consider the optimized geometries of C-C connected oxo-bridged di-nitroaniline compounds (a), (b) and (c) as in Fig. 4.1. The dispersion relations for β are shown in Fig. 4.7. The magnitude of β coefficients increases rapidly with the increase in ω for all three cases. However, for (a) and (b), the increase of β is cubic in ω, $\beta = A + B\omega^3$, and for (c), it is quadratic, $\beta = C + D\omega^2$. The lowest one-photon excitation gap for these molecules are of the order of 4.0eV, and so we have carried out the β computations up to $\omega \sim 1.8$eV, well below the resonance frequency. From this, we can safely conjecture that while the C-C bonded pna-O-pna and pna-O-mna compounds are good candidates for

optical rectification, the corresponding pna-O-ona is not.
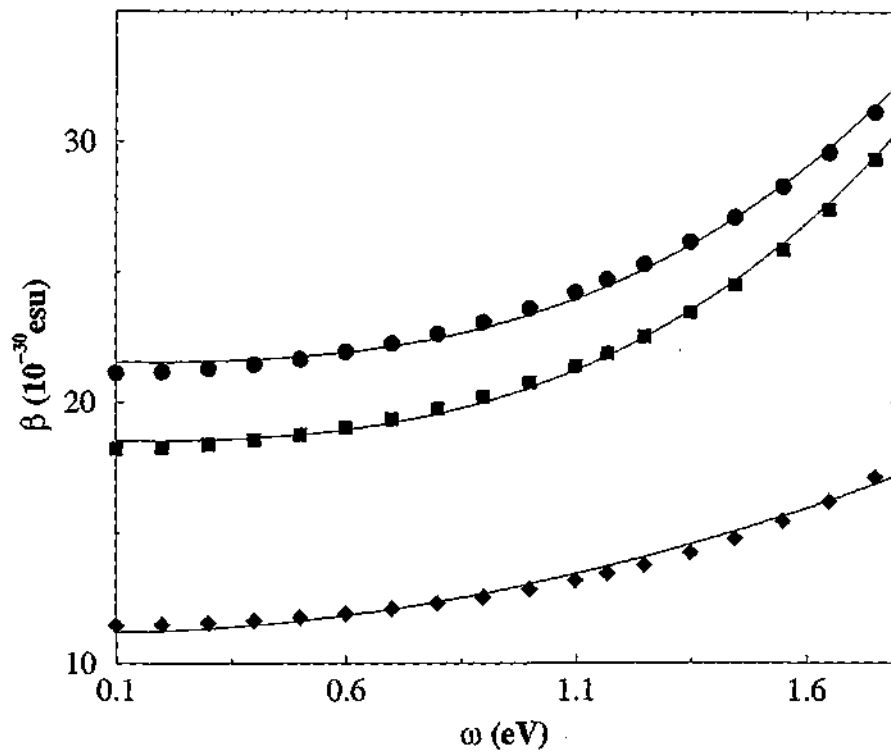
Figure 4.7: Dispersion curves for β (in units of 10^{-30} esu) for rigid configu-rations as in Fig.1, a(circles), b(squares) and c(diamonds). Frequency is in eV unit

4.4   Conclusion

We have considered a few dipolar organic molecules in a number of their dipolar configurations. Although our results are based on semi-empirical computations, the results have been verified with varying number of CIs. We find that the ground state dipole moment and the hyperpolarizability are governed by the extent of π-electron delocalization, which in turn depends on the structural details of the molecules. Based on our calculations, we have proposed molecular systems where large magnitudes of first order hyperpolarizabilities can be realized. From a synthesis point of view, these molecules are rather simple to prepare; analogous systems have been synthesized with good yield [73]. Therefore, we believe that a synthetic scheme well suited for the best dipolar arrangements can be fine tuned to obtain large nonlinear optical properties at extremely low-energy.

Chapter 5

Charge-transfer induced large linear and nonlinear optical properties of small Al Clusters: Al_4M_4 (M=Li, Na and K)

5.1 Introduction

The development of materials with large nonlinear optical (NLO) properties is a key to controlling the propagation of light by optical means. In particular, the response of the materials to the application of the electric field has found tremendous applications in designing materials for NLO devices [4]. These devices are being used in numerous applications, from lasers to optical switches and optoelectronics. The NLO properties of organic π-conjugated materials have been studied in great details in the last few decades [7, 8, 79].

The first and second order non-linear optical properties, β and γ for the π-conjugated polymers increase with the conjugation length (L) roughly as L^3 and L^5 respectively [80]. Therefore, the general strategy to model NLO materials has been to increase the conjugation length. However, there exist an upper limit for every off-resonant susceptibilities [81]. Alternatives to these π-conjugated compounds are yet to be explored theoretically in a detailed fashion. But, with the gaining popularity of various *ab-initio* level methods [82], there has been a tremendous impetus in investigating the structure and electronic properties of both homogeneous and heterogeneous small clusters in recent years [83,84].

Small Al_4 rings like Al_4M_4 and their anions $Al_4M_3^-$, M=alkali metals, have been a subject of current interest [85,86] because of their unique characteristics and close structural resemblance with the C_4H_4. However, although C_4H_4 is an anti-aromatic species, these Al_4-clusters are recently reported to be σ aromatic [87]. Thus, it would be interesting to ask whether these rings are better polarizable than their organic counterpart; whether the structural characteristics has any role in their polarization response functions. Organic π-conjugated systems are stabilized due to π-electron delocalizations, while the inorganic metal complexes reduce their energy through strong charge transfer. There have been no previous efforts to study in details the NLO properties of these all-metal clusters. We describe in the following that these metal clusters offer a unique polarization response due to their ionic character, contrary to conventional π-conjugated systems, leading to large optical coefficients.

5.2   Geometry Optimizations

We begin our calculations by optimizing the ground state geometries of the Al_4-clusters (Al_4Li_4, Al_4Na_4 and Al_4K_4). All the optimizations have been done using the B3LYP//RHF/6-31G(d,p) method available in the GAMESS electronic structure set of codes [88]. Since, we want to compare the optical properties of these small four-membered rings with their organic analogue C_4H_4, we start with a planar initial geometry for the optimizations. We have varied the level of basis set from 6-31G(d,p) to 6-311G+(d) to ensure that these geometries correspond to the minima in the potential energy surface. The final geometries indeed remain independent of the selection of the basis set. Contrary to that of C_4H_4 having a rectangular ring, these Al_4-clusters are found to have a rhombohedral structure with four Al atoms forming a rhombus and the four alkali atoms around the four Al-Al bonds forming four Al-M (Li, Na, K)-Al triangles. One of the diagonals of the Al_4 ring are also connected by Al-Al bond. The equilibrium geometries are shown in Fig. 5.1 [1(a), 1(b) and 1(c)].
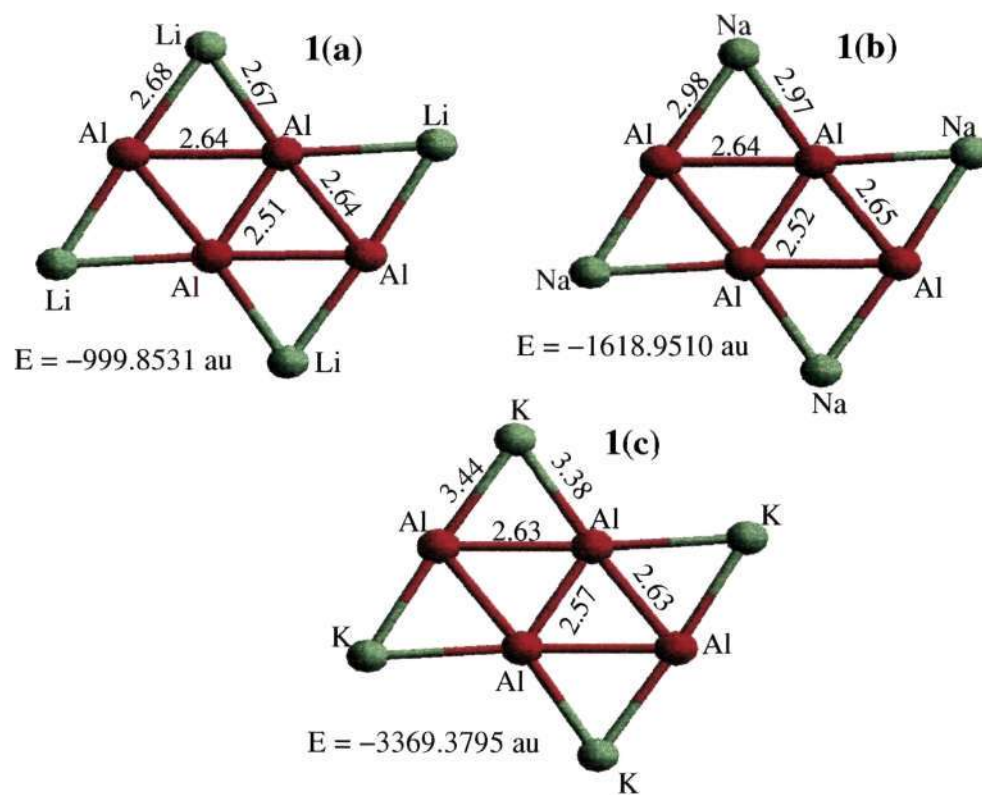
Figure 5.1: Equilibrium ground state geometries for Al_4Li_4, Al_4Na_4 and Al_4K_4. The footnote of each structure contains the ground state energies in au

While Al_4Li_4 and Al_4K_4 have a planar structure (D_{2h}), Al_4Na_4 has a distorted structure, with the four Na atoms arranged in a non-planar geometry around the planar ring (the Na atoms are distorted by 13 degrees from the plane of Al_4 ring). This can be understood by considering the increase in size of the alkali ions and the distances of the ions from the Al_4-ring. With the progressive increase in the ionic radii of counter-ion, Li to K(Li=0.68 $\mathring{A}$, Na=0.97 $\mathring{A}$ and K $=$ 1.33 $\mathring{A}$), the structures are expected to be distorted and the four alkali atoms should arrange in a non-centrosymmetric geometry around the Al_4 ring to minimize steric repulsion. But, the average Al-M distance increases while going from Al_4Li_4 (2.65 $\mathring{A}$) to Al_4Na_4 (3.00 $\mathring{A}$) to Al_4K_4 (3.35 $\mathring{A}$). Although the ionic radii of K ion is more than that of Li and Na, in Al_4K_4, the four K ions are far separated from the Al_4 ring, allowing a planar structure. For Al_4Na_4, both the ionic radius of Na and the average Al-M distance fall in between Al_4Li_4 and Al_4K_4 and thereby minimizes the steric repulsion through distortion.

Also, very close in energy to these planar rhombohedral structures for these Al_4-clusters are the capped octahedron structures for the Al_4Li_4 [2(a)] and Al_4Na_4 [2(b)] (with C_{2h} symmetry) and a distorted tricycle-like structure for Al_4K_4 [2(c)]. These geometries are shown in Fig.5.2.

At the footnote of each structure, the corresponding ground state energies are given. It has however not escaped our attention that previous works on alkali derivatives of Al_4-clusters have predicted more than one unique structures for these systems [89]. This calls for a study to elucidate whether the optical properties for these Al_4-clusters for different geometries are substantially different or are very similar. Hence, both the geometries for each
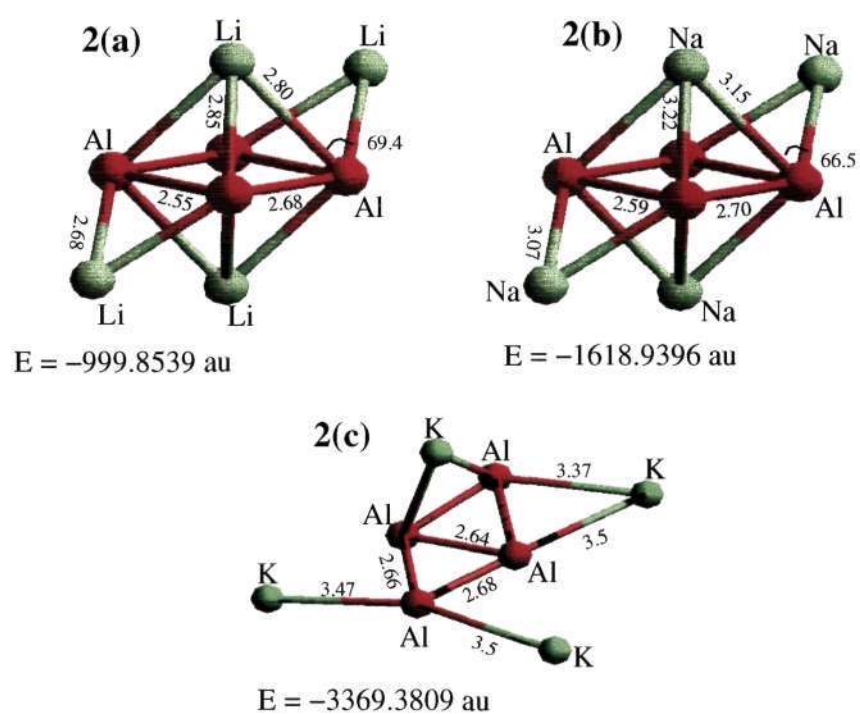
Figure 5.2: Equilibrium ground state geometries for the other set of Al_4Li_4, Al_4Na_4 and Al_4K_4, very close in energy to Figure 1. The footnote of each structure contains the ground state energies in au

cluster were considered for computing the optical response functions.

5.3   Results and Discussions

We calculate the linear and nonlinear polarizabilities by three different methods: ZINDO, B3LYP and MP2. We first report the results with the Zerner's INDO method [52] with multi-reference doubles CI (MRDCI) calculations. The MRDCI is particularly important since it includes correlation effects substantially, as reported by us earlier [79]. All the ZINDO calculations are performed with 4 reference determinants including the Hartree-Fock ground state, at an electrical frequency of 0.001 au, much below any optical resonance.

Table 5.1, shows the bond-length alternation (BLA), Δr (defined as the average difference between the bond lengths of two consecutive Al-Al bonds), the optical gap (energy difference between the ground state and the optically active state i.e, having finite oscillator strength) and the average Mulliken charge on the Al_4 ring for all the geometries.

Table 5.1: The bond length alternation, Δr (in Å), Optical Gap (in a.u.) and the average Mulliken charge (Δq) on the ring for the clusters from ZINDO calculations

Molecule	Δr	Gap	Δq
Al_4Li_4 1(a)	0.1283	0.0819	-0.592
Al_4Li_4 1(b)	0.1276	0.024	-0.506
Al_4Na_4 2(a)	0.1302	0.0909	-0.174
Al_4Na_4 2(b)	0.1103	0.0607	-0.127
Al_4K_4 3(a)	0.0656	0.0663	-0.634
Al_4K_4 3(b)	0.06487	0.0867	-0.618
C_4H_4	0.245	0.2410	0.000
C_6H_6	0.000	0.2588	0.000

To directly compare the efficiency of these Al_4-clusters with the conventional π conjugated systems, we calculate the optical properties of the 1,3-cyclobutadiene (C_4H_4) and benzene (C_6H_6) at the same level of theory. It is evident that for the Al_4-clusters, the Δr is very small compared to the C_4H_4 (anti-aromatic) but larger than C_6H_6 (aromatic, $\Delta r = 0$). For the Al_4-clusters there is a substantial amount of charge transfer from the alkali atoms to the Al atoms (negative charge), making them act as donor and acceptor respectively. Such a charge transfer induces polarization in the ground state structure and reduces the optical gap. On the other hand, the C-H bond being perfectly covalent, there is almost no charge transfer in case of C_4H_4 and C_6H_6 and thus have a large optical gap due to finite size molecular architecture.

Charge transfer stabilizes the system with very small changes in the bond lengths. The chemical hardness, η, defined as, one half of (ionization potential-electron affinity), decreases as one moves from Li to K. More specifically, the η for Li, Na and K are 2.39eV, 2.30eV and 1.92eV respectively [90]. So, the extent of charge transfer from the alkali atom to the Al_4-ring should increase with the decrease in the chemical hardness of the alkali atoms which is evident from Table 5.1. From Al_4Li_4 to Al_4Na_4 to Al_4K_4, the Mulliken charge on the Al_4-ring increases leading to decrease in the BLA along the series with the exception of Al_4Na_4 [1(b) and 2(b)] which has much lower Mulliken charge on the Al_4-ring. For, the Al_4Na_4 [1(b)] as mentioned above, there is a substantial distortion of the Na atoms from the Al_4-ring. For the Al_4Na_4, with C_{2h} symmetry [2(b)] even though there is no distortion, the large Al-Na distance reduces the ionicity of the bond. As a result the

extent of charge transfer is lesser for Al_4Na_4.

Although BLA can not be regarded as the sole measuring index of aromatic character, the small BLA found for the Al_4-clusters (together with large BLA for the anti-aromatic C_4H_4) tend to suggest that the Al_4-clusters are more like aromatic but most certainly not anti-aromatic species, as has been proposed recently [86]. The distorted Al_4K_4 structure [2(c)] is very interesting. The Al_4-ring is distorted from planarity by 9.5 degrees. Such a distortion arises to minimize the steric repulsion in accommodating four bulky K atoms on a plane, very similar to that of cyclooctatetraene, which undergoes a distortion from planar to tub-shaped geometry to minimize the ring-strain [91]. Thus, this structure of Al_4K_4 is neither aromatic nor anti-aromatic but can be considered to be non-aromatic just like cyclooctatetraene. This is supported by the energies for the structures for Al_4K_4 [1(c) and 2(c)]. The distorted structure is more stable than the planar structure. Thus, the steric repulsion for the four large K atoms overwhelms the stability of the planar undistorted aromatic Al_4K_4 making the Al_4K_4 cluster non-aromatic.

In Table 5.2, the magnitudes of the ground state dipole moment, μ_G, the linear(α), and nonlinear (β and γ) polarizabilities for the clusters are reported from the ZINDO calculations. Note that we report the magnitudes

for the tumbling averaged $\bar{\alpha}$, $\bar{\beta}$ and $\bar{\gamma}$, defined as

$$\bar{\alpha} = \frac{1}{3} \sum_i (\alpha_{ii})$$

$$\bar{\beta} = \sqrt{\sum_i \beta_i \beta_i^*}; \quad \beta_i = \frac{1}{3} \sum_j (\beta_{ijj} + \beta_{jij} + \beta_{jji})$$

$$\bar{\gamma} = \frac{1}{15} \sum_{ij} (2\gamma_{iijj} + \gamma_{ijji}) \tag{5.1}$$

where the sums are over the coordinates x, y, z $(i, j = x, y, z)$ and β_i^* refers to the conjugate of β_i vector.

Table 5.2: The ground state dipole moment, μ_G, linear polarizability, α, 1st hyperpolarizability, β and the 2nd hyperpolarizability, γ, (isotropic average) for the clusters and for *trans-* polyacetylene chain from ZINDO-MRDCI calculations. The units are in a.u. 'n' is the number of $-CH = CH-$ units

Molecule	μ_G	$\bar{\alpha}$	$\bar{\beta}$	$\bar{\gamma}$
Al_4Li_4 1(a)	0.000	4.9×10^3	542.5	1.91×10^7
Al_4Li_4 1(b)	0.000	5.5×10^3	244.9	5.33×10^8
Al_4Na_4 2(a)	0.076	5.9×10^3	8465.2	1.09×10^7
Al_4Na_4 2(b)	8.6×10^{-4}	8.7×10^3	1098.5	2.00×10^8
Al_4K_4 3(a)	0.004	5.4×10^3	79.3	2.60×10^7
Al_4K_4 3(b)	5.720	4.7×10^3	1.2×10^5	1.90×10^7
C_4H_4	0.000	2.9×10^2	0.000	4.76×10^3
C_6H_6	0.000	5.4×10^2	0.000	8.44×10^3
$(CH=CH)_n$, n=1	0.000	136.3	0.000	2.78×10^4
$(CH=CH)_n$, n=2	0.000	421.0	0.000	4.15×10^4
$(CH=CH)_n$, n=3	0.000	852.4	0.000	6.17×10^5
$(CH=CH)_n$, n=4	0.000	1455.2	0.000	2.82×10^6
$(CH=CH)_n$, n=5	0.000	2203.2	0.000	8.41×10^6
$(CH=CH)_n$, n=6	0.000	3074.9	0.000	2.07×10^7

The ground state dipole moment μ_G and $\bar{\beta}$ are zero for the C_4H_4 and C_6H_6 due to its perfect centrosymmetric geometry, although, the $\bar{\alpha}$ and $\bar{\gamma}$ have finite values. For the Al_4-clusters with the progressive increase in the ionic radii of counter-ion, the ground state dipole moment increases. Thus, while Al_4Li_4 has no ground state dipole moment, Al_4Na_4 and Al_4K_4 have substantial ground state dipole moment (particularly 1(b) and 2(c) due to their non-centrosymmetric structures discussed above). For Al_4K_4, while the rhombohedral geometry has a very low ground state dipole moment but the distorted tricycle-like structure has a very high dipole moment. Thus, due to the out-of-plane charge transfer, the dipole matrix elements are also larger, resulting in large values of the $\bar{\alpha}$, $\bar{\beta}$ and particularly the $\bar{\gamma}$. For Al_4Li_4 and Al_4Na_4 [2(b)] the polarization is in the excited state as the ground state dipole moment is zero. However, it is not the case for the insulating C_4H_4 and C_6H_6 which have zero polarization both in the ground and the optical excited states. Thus, $\bar{\beta}$ is zero for C_4H_4 and C_6H_6.

The optically active states are the low-energy states of these metallic clusters and the lowest optical gap is about 0.07 au for Al_4-clusters compared to 0.25 au for the C_4H_4 and C_6H_6. Since the optical coefficients are inversely proportional to the optical gaps and proportional to the dipolar matrices, a large optical gap implies low magnitudes for the optical coefficients. C_4H_4 has the highest magnitude of BLA and optical gap and the least charge transfer on the ring structure, thereby smallest magnitude of $\bar{\gamma}$. On the otherhand, although BLA is zero for C_6H_6 due to complete π-electron delocalization, there is no charge transfer in the finite molecular structure leading to large optical gap and weak polarization. Consequently, $\bar{\gamma}$ is very less also for C_6H_6.

In contrast, the optical coefficients in general are quite large for the Al_4-clusters. For example, the $\bar{\gamma}$ for the Al_4-clusters are roughly 10^4 times more than that for C_4H_4 and C_6H_6. This is because the $\bar{\gamma}$ is a third order property with 4 dipolar matrices in the numerator and 3 optical gaps in the denominator [59]. The $\bar{\gamma}$ for the Al_4-clusters increases with the increase in the polarization of the Al-M bonds and follows the trend: $\bar{\gamma}$ of $Al_4Li_4 < \bar{\gamma}$ of $Al_4Na_4 < \bar{\gamma}$ of Al_4K_4 (same trend as η). But, the distorted structures for Al_4Na_4 and Al_4K_4 [1(b) and 2(c)] have less $\bar{\gamma}$ due to less polarization of the Al-M bonds. For C_4H_4 ($\Delta r = 0.245\mathring{A}$), C_6H_6 ($\Delta r = 0.00\mathring{A}$) and linear chain, $(-CH=CH-)_n$, n=3 ($\Delta r = 0.1\mathring{A}$) the $\bar{\gamma}$ are 2.21, 2.63 and 192.85 (all in au) per CH bond, respectively. This is in agreement with previous findings that the magnitude of γ varies nonlinearly with Δr and its maximal occurs at an optimal $\Delta r \neq 0$ [92]. For the Al_4-clusters we believe that the magnitudes of Δr are the optimal values leading to high nonlinear electric polarizations.

To further verify that these Al_4-clusters are really better NLO materials than their organic counterparts, we carry out finite field calculations using the B3LYP [93, 94] and MP2 [95] methods. This is done at a static electric field of 0.001 au by taking energy derivatives with respect to the external field numerically [96], along the X-axis (the axis across which the electric field induced polarization is maximum). The results are shown in Table 5.3.

Table 5.3: Same as in Table 5.2, by B3LYP and MP2 methods (units in au). The electric field is applied along the polarization axis and we report only the diagonal components of the tensorial quantities.

	μ_G		α_{xx}		β_{xxx}		γ_{xxxx}	
Molecule	DFT	MP2	DFT	MP2	DFT	MP2	DFT	MP2
Al_4Li_4 1(a)	0.00	0.00	544	533	0.15	0.15	2.2×10^6	1.9×10^6
Al_4Li_4 1(b)	0.00	0.00	497	454	9.02	13.7	3.4×10^6	3.4×10^6
Al_4Na_4 2(a)	0.004	0.004	729	749	0.13	0.12	4.2×10^6	5.5×10^6
Al_4Na_4 2(b)	0.0	0.0	905	857	9.84	5.24	9.3×10^6	1.2×10^7
Al_4K_4 3(a)	0.004	0.003	1109	1279	0.10	0.173	1.8×10^7	4.7×10^7
Al_4K_4 3(b)	2.57	3.19	1285	1320	19100	49400	4.5×10^7	7.9×10^7
C_4H_4	0.000	0.000	37.9	37.0	0.000	0.000	1.8×10^2	1.4×10^3
C_6H_6	0.000	0.000	71.7	70.1	0.000	0.000	2.2×10^2	1.1×10^3

	μ_G	α_{xx}	β_{xxx}	γ_{xxxx}
Molecule	MP2	MP2	MP2	MP2
$(CH=CH)_n$, n=1	0.00	29.8	0.00	8.84×10^2
$(CH=CH)_n$, n=2	0.00	69.7	0.00	1.36×10^4
$(CH=CH)_n$, n=3	0.00	129	0.00	1.11×10^5
$(CH=CH)_n$, n=4	0.00	206	0.00	4.45×10^5
$(CH=CH)_n$, n=5	0.00	300	0.00	1.25×10^6
$(CH=CH)_n$, n=6	0.00	408	0.00	2.83×10^6

The trends are very much the same, i.e, the γ for the Al_4M_4 are orders of magnitude more than that for C_4H_4 and C_6H_6. The differences in the absolute magnitudes for the three different methods, particularly between the ZINDO and the B3LYP/MP2 methods, is understandable because in B3LYP/MP2 methods the static electric field is applied about one axis-direction, while ZINDO performs dynamical frequency calculations. Furthermore, the NLO coefficients due to static field is calculated based on the ground state energy alone (in absence and in presence of a few appropriate multiples of the field), while in ZINDO, the computation of the coefficients involve all the dipole allowed and forbidden states with MRDCI improving accuracy of these states. However, the conclusion from all the methods is still the same: Al_4M_4 are better NLO materials than the similar organic systems. Also, the fact that the different geometries with different structural symmetries have similarly high NLO coefficients for the Al_4-clusters confirm that Al_4M_4 are indeed better NLO materials.

To compare and contrast these clusters with their organic counterparts, we calculate the NLO properties of the well-known π-conjugated systems, the *trans*-polyacetylene chain, $(-CH=CH-)_n$, by varying the number of spacers, n, from n=1 to 6, and thereby extending the length of conjugation from 2.65 au to 29.11 au. The geometries were optimized by the AM1 parameterized Hamiltonian [44]. The linear and nonlinear polarizations are calculated at the same frequency (0.001 au) with MRDCI implementation of ZINDO and using static electric field (0.001 au). We report the calculations with ZINDO and MP2 only, as DFT is known to be less reliable for the optical properties

for 1-D systems [97]. Our calculated values for the optical properties compare fairly well in trends with the experimental results that the linear (α) and nonlinear (γ) optical properties increase steadily with the increase in the conjugation-length of the chain (see Table 5.2 and Table 5.3). For example, for ethylene, $\gamma_{expt}=$ 1504.9 au, for butadiene (n=2), $\gamma_{expt}=$ 4566.4 au and for hexatriene (n=3), $\gamma_{expt}=$ 14950.1 au [98]. Note that our calculations are done at a much higher frequency compared to the laser frequency used in the experiment. However, the magnitudes of all the polarization quantities are much higher for the charge-transfer complex (Al_4M_4 clusters) compared to the conventional π conjugated chains with comparable conjugation length. Only when there are very large number of spacers (n=5-6), that the magnitudes become comparable to the much smaller Al_4-clusters.

5.4 Stabilization of Al-clusters: Sandwich-like complex formation

From the discussion above, it is clear that these Al_4M_4 clusters are certainly better NLO materials. But, for a material to be useful for a successful experiment, it must be stable. Though we find that these small clusters are stable in gas-phase, we try to investigate modes to stabilize these materials by various chemical means.

Since, these Al_4 clusters have both strong σ as well as π electron delocalizations, one way of stabilizing them will be to incorporate them into

sandwich-type complexes where the delocalized electrons will tend to inter-
act with the central metal ion [99, 100]. The same idea has been widely
used in organometallic chemistry where one can stabilize an unstable organic
ligand by complexing it with a metal ion. For example, one can stabilize
the cyclopentadiene ligands by complexing it with a metal like Fe to form
Ferrocene [101, 102].

We first try to stabilize the structure of C_4H_4 in a sandwich-like geome-
try. Since C_4H_4 has 4π electrons, a simple effective electron number (EAN)
counting scheme tells us that the metal in between the two ligands needs to
have 10 electrons to stabilize a sandwich of the type: $(C_4H_4)_2M$ [103]. The
simplest species with 10 electrons in the valence shell is Nickel. Elements
in the same group like Pd or Pt have a strong spin-orbit coupling and are
stabilized in a square-planar geometry. Thus a coordination number of 8 as
that in a sandwich complex is unfavorable. The energy minimized structure
for the $(C_4H_4)_2Ni$ is indeed a sandwich geometry with the two C_4H_4 rings
above and below the Ni atom (see Fig. 5.4). The Ni atom sits symmetrically
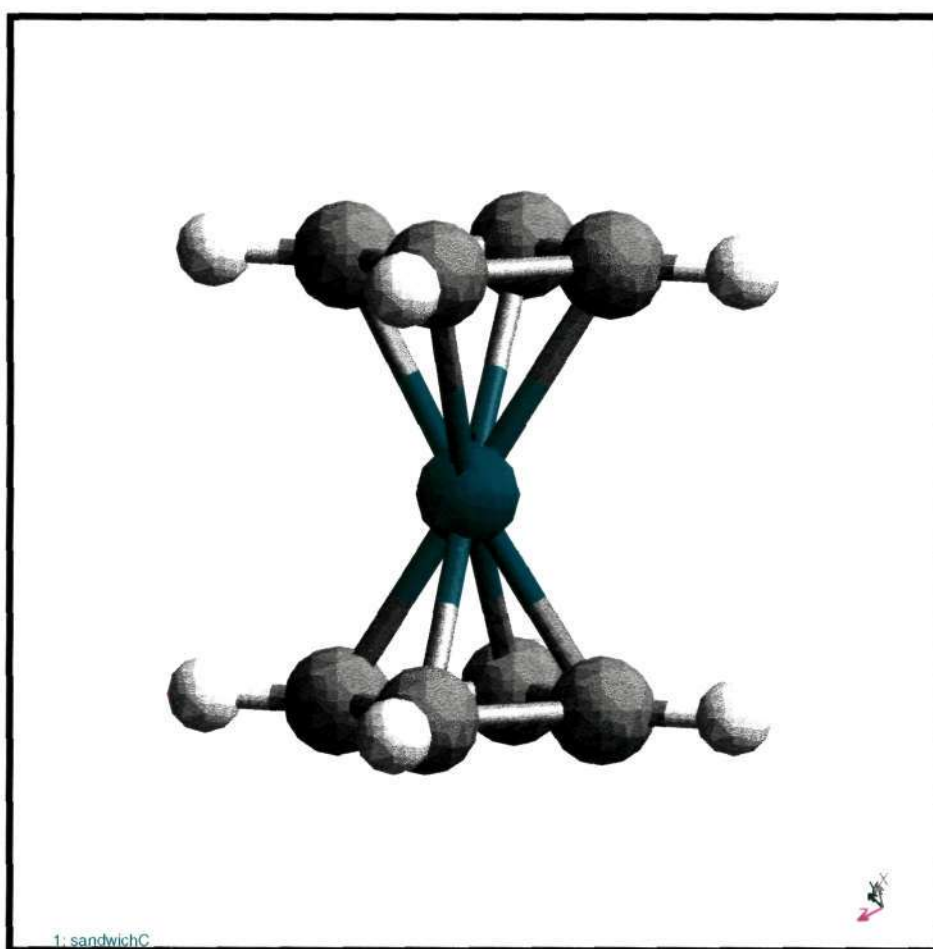inside the cavity of the two C_4H_4 rings with a distance of $2\mathring{A}$ from each C
atom.

Figure 5.3: Equilibrium ground state geometry for the $(C_4H_4)_2Ni$ species

The same logic is used by us to try to stabilize the Al_4M_4 cluster. We have been able to stabilize the Al_4Li_4 cluster by introducing it in a sandwich of the type: $(Al_4Li_4)_2Ni$. The geometry is shown in Fig 5.5. The central Ni atom sits exactly in the cavity of the two Al_4Li_4 rings. Very interestingly, the Al atoms in the rings bend towards the Ni atom and the planarity of the Al_4Li_4 is lost. This is understood from the fact that when the 4π electrons of each of the two Al_4Li_4 rings interact with the central Ni atom, the requirement of the Al atoms to be in plane with the Li atom is no longer important. Instead, the sandwich like structure with 18 electrons give an extra stabilization while the whole system remains electrically neutral.
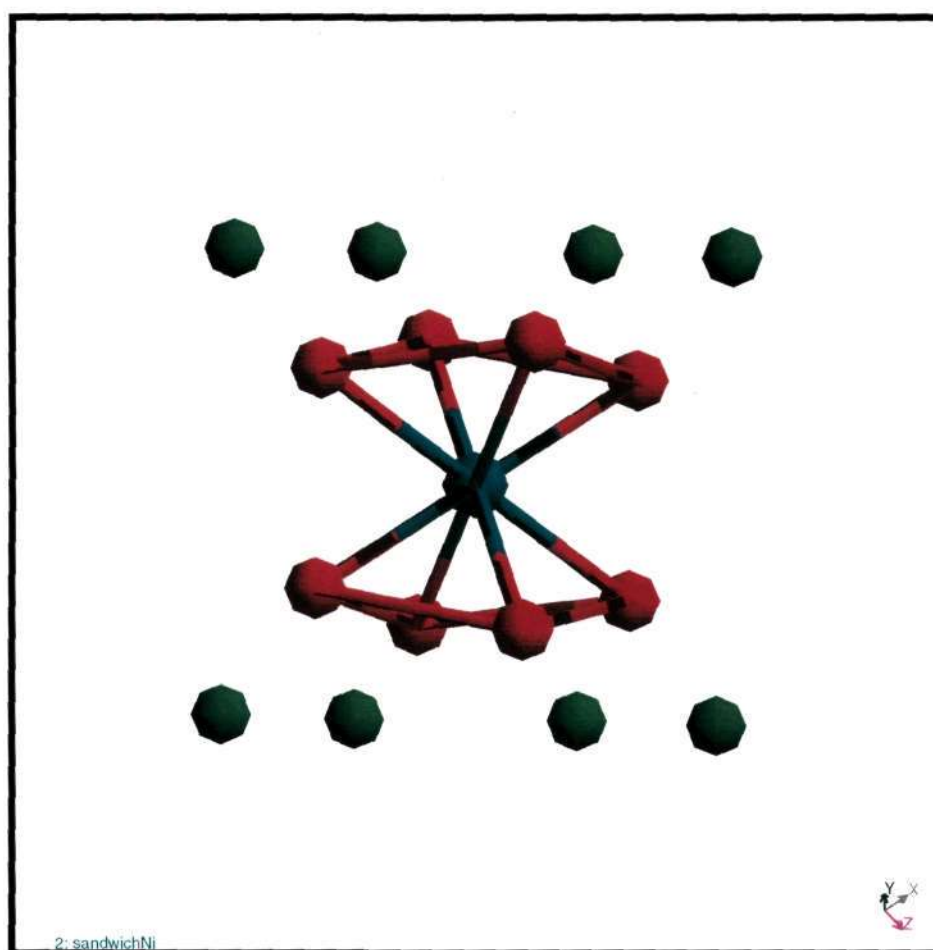
Figure 5.4: Equilibrium ground state geometry for the $(Al_4Li_4)_2Ni$ species

5.5   Summary and Outlook

To conclude, our theoretical study shows that the small four membered Al_4-clusters functionalized with various metal cations provide an innovative route for selection of materials with very high nonlinear optical properties. Also, the method of stabilization of these clusters in a sandwich-like structure suggested by us will motivate experiments on these systems. Since, some of the compounds have already been synthesized [86], we believe that these inorganic materials will be competing for the next generation NLO materials.

Bibliography

[1] *Nonlinear Optical Properties of Organic Molecules and Crystals*, D. S. Chemla and J. Zyss, *Academic Press*, (1987).

[2] *Introduction to Nonlinear Optical Effects in Molecules and Polymers*, P. N. Prasad and D. J. Williams (Wiley, New York, 1991).

[3] *Lasers and Nonlinear Optics*, B. B. Laud, (New Age Int, 1991).

[4] *Nonlinear Optical Materials*, ACS Symposium Series 628, Eds. S.P.Karn a and A.T.Yeates, Washington DC, 1996.

[5] Optical Nonlinearities in Chemistry, edited by D. M. Burland, *Chem. Rev.*, **94**, *special volume*, (1994).

[6] *Nonlinear Optics*, R. Boyd, 2nd Edition, Academic Press, 2003.

[7] D. J. Williams, *Angew. Chem. Int. Ed. Engl.*, **23**, 690, (1984).

[8] T. J. Marks and M. A. Ratner, *Angew. Chem. Int. Ed. Engl.*, **34**, 155, (1995).

[9] P. A. Franken, A. E. Hill, C. W. Peters and G. Weinrich, *Phys. Rev. Lett.*, **7**, 118, (1961).

[10] (a). M. Goppert-Mayer, *Annu. Phys*, **9**, 273, (1931); (b). W. Kaiser and C. G. B. Garrett, *Phys. Rev. Lett.*, **7**, 229, (1961).

[11] N. Bloembergen and Y. R. Shen, *Phys. Rev. Lett.*, **12**, 504, (1964).

[12] *Topics in Non-Linear Optics.*, Selected papers of N. Bloembergen, Indian Academy of Science, **Raman Professor, 1979.**, (1982).

[13] W. F. Hagen and P. C. Magnante, *J. App. Phys.*, **40**, 219, (1969).

[14] P. D. Maker and R. W. Terhune, *Phys. Rev.*, **137A**, 801, (1965).

[15] B. Champagne, E.A. Perpete, and J.M. Andre, *J. Chem. Phys.*, **101** , 10796, (1994).

[16] B. Champagne, *Chem. Phys. Lett.*, **261**, 57, (1996).

[17] D. A. Kleinmann, *Phys. Rev.*, **125**, 87, (1962).

[18] D. A. Kleinmann, *Phys. Rev.*, **128**, 1761, (1962).

[19] J. Zyss, *J. Chem. Phys.*, **98**, 6583, (1993).

[20] G. Alcaraz, L. Euzenat, O. Mongin, C. Katan, I.Ledoux, J. Zyss, M. B-Desce and M. Vaultier, *Chem. Commun.*, **22**, 2766, (2003).

[21] C. Fave, M. Hissler, K. Senechal, I. Ledoux, J. Zyss, R. Reau, *Chem. Commun.*, **16**, 1674, (2002).

[22] S. Fine and W. P. Hansen, *Appl. Opt.*, **10**, 2350, (1971).

[23] O. Bouevitch, A. Lewis, L. Pinevsky, J. P. Wuskell and L. M. Loew, *Biophys. J.*, **65**, 672, (1993).

[24] S. Maiti, J. B. Shear, R. M. Williams, W. R. Zipfel and W. W. Webb, *Science.*, **275**, 530, (1997).

[25] B. Champagne and D. M. Bishop, *Advances in Chemical Physics.*, **126**, 41, (2003).

[26] F. Castet and B. Champagne, *J. Phys. Chem. A.*, **105**, 1366, (2001).

[27] M. Guillaume, E. Botek, B. Champagne, F. Castet and L. Ducasse, *Int. Jour. Quan. Chem.*, **90**, 1378, (2003).

[28] S. Di Bella, M. A. Ratner and T. J. Marks, *J. Am. Chem. Soc.*, **114**, 5842 (1992).

[29] P. W. Fowler and P. A. Madden, *Phys. Rev. B.*, **30**, 6131, (1984).

[30] H. A. Kurtz, J. J. P. Stewart and K. M. Dieter, *J. Comput. Chem*, **11**, 82, (1990).

[31] K. B. Sophy and S. Pal, *J. Chem. Phys.*, **118**, 10861, (2003).

[32] J. Ward, *Rev. Mod. Phys.*, **37**, 1, (1965).

[33] B. J. Orr and J. F. Ward, *Mol. Phys.*, **20**, 513, (1971).

[34] *Polymers for Second-Order Nonlinear Optics*, edited by G. A. Lindsay and K. D. Singer (ACS Symposium Series 601, Washington D. C., 1995).

[35] E. Hanamura, *Phys. Rev. B.*, **37**, 1273 (1988).

[36] K. V. Katti, K. Raghuraman, N. Pillarsetty, S. R. Karra, R. J. Gulotty, M. A. Chartier and C. A. Langhoff, *Chem. Mater.*, **14**, 2436 (2002).

[37] S. Di Bella, M. A. Ratner and T. J. Marks, *J. Am. Chem. Soc.*, **114**, 5842 (1992).

[38] J. D. Augspurger and C. E. Dykstra, *Int. J. Quant. Chem.*, **43**, 135 (1992).

[39] L. Jensen, P-O Astrand, A. Osted, J. Kongsted and K. V. Mikkelsen, *J. Chem. Phys.*, **116**, 4001 (2002).

[40] H. E. Katz, William L. Wilson and G.Scheller, *J. Am. Chem. Soc.*, **116**, 6636 (1994).

[41] H. E. Katz, G. Scheller, T. M. Putvinski, M. L. Schilling, W. L. Wilson and C. E. D. Chidsey, *Science*, **254**, 1485 (1991).

[42] *Theory of Molecular Excitons* by A. S. Davydov (McGraw-Hill, New York, 1962).

[43] *Electronic Absorption Spectra: Geometry of Organic Molecules*, by H. Suzuki (Academic Press, New York, 1967).

[44] M. J. S. Dewar, E. G. Zoebisch, E. F. Healy, J. J. P. Stewart, *J. Am. Chem. Soc*, **107**, 3902 (1985).

[45] *Gaussian 03*, **Revision B.05**, M. J. Frisch, G.. W. Trucks, H. B. Schlegel, G. E. Scuseria, M. A. Robb, J. R. Cheeseman, J. A. Montgomery, Jr., T. Vreven, K. N. Kudin, J. C. Burant, J. M. Millam, S. S. Iyengar, J. Tomasi, V. Barone, B. Mennucci, M. Cossi, G. Scalmani, N. Rega, G. A. Petersson, H. Nakatsuji, M. Hada, M. Ehara, K. Toyota, R. Fukuda, J. Hasegawa, M. Ishida, T. Nakajima, Y. Honda, O. Kitao,

H. Nakai, M. Klene, X. Li, J. E. Knox, H. P. Hratchian, J. B. Cross, C. Adamo, J. Jaramillo, R. Gomperts, R. E. Stratmann, O. Yazyev, A. J. Austin, R. Cammi, C. Pomelli, J. W. Ochterski, P. Y. Ayala, K. Morokuma, G. A. Voth, P. Salvador, J. J. Dannenberg, V. G. Zakrzewski, S. Dapprich, A. D. Daniels, M. C. Strain, O. Farkas, D. K. Malick, A. D. Rabuck, K. Raghavachari, J. B. Foresman, J. V. Ortiz, Q. Cui, A. G. Baboul, S. Clifford, J. Cioslowski, B. B. Stefanov, G. Liu, A. Liashenko, P. Piskorz, I. Komaromi, R. L. Martin, D. J. Fox, T. Keith, M. A. Al-Laham, C. Y. Peng, A. Nanayakkara, M. Challacombe, P. M. W. Gill, B. Johnson, W. Chen, M. W. Wong, C. Gonzalez, and J. A. Pople, Gaussian, Inc., Pittsburgh PA, 2003.

[46] *Hydrogen Bonding: A theoretical perspective*, by S. Scheiner (Oxford, New York, 1997).

[47] *Hydrogen Bonding in Biological Structures*, by G. A. Jefferey and W. Saenger, (Springer-Verlag, Berlin, 1991).

[48] Z. Latajka, S. Scheiner and H. Ratajczak, *Chem. Phys. Lett.*, **135**, 367 (1987).

[49] M. Moet-Ner, *J. Am. Chem. Soc.*, **114**, 3312 (1992).

[50] K. Morokuma, *Acc. Chem. Res.*, **10**, 294 (1977).

[51] K. Morokuma and K. Kitaura, *Molecular Interactions: Ed. H. Ratajczak and W. J. Orville-Thomas*, Vol-1, 21, Wiley, New York (1982).

[52] J. Ridley, M. C. Zerner, *Theor. Chim. Acta.*, **32**, 111 (1973); A. D. Bacon, M. C. Zerner, *Theor. Chim. Acta.*, **53**, 21 (1979).

[53] R. J. Buenker and S. D. Peyerimhoff, *Theor. Chim. Acta.*, **35**, 33 (1974).

[54] Z. Shuai, D. Beljonne and J. L. Bredas, *J. Chem. Phys.*, **97**, 1132 (1992).

[55] D. Beljonne, Z. Shuai, J. Cornil, D. dos Santos and J. L. Bredas, *J. Chem. Phys.*, **111**, 2829 (1999).

[56] S. Ramasesha and Z. G. Soos, *Chem. Phys. Lett.*, **153**, 171 (1988); Z. G. Soos and S. Ramasesha, *J. Chem. Phys.*, **90**, 1067 (1989).

[57] S. Ramasesha, Z. Shuai, J. L. Bredas, *Chem. Phys. Lett.*, **245**, 224 (1995); I. D. L. Albert and S. Ramasesha, *J. Phys. Chem.*, **94**, 6540 (1990); S. Ramasesha and I. D. L. Albert, *Phys. Rev. B.*, **42**, 8587 (1990).

[58] S. K. Pati, S. Ramasesha, Z. Shuai and J. L. Bredas, *Phys. Rev. B*, **59**, 14827 (1999).

[59] S. K. Pati, T. J. Marks and M. A. Ratner, *J. Am. Chem. Soc.*, **123**, 7287 (2001).

[60] Oudar, J. L.; Chemla, D. S. *J. Chem. Phys.*, **1977**, *66*, 2664; Oudar, J. L. *J. Chem. Phys.*, **1977**, *67*, 446.

[61] M. Feyereisen, J. Nichols, J. Oddershede and J. Simons, *J. Chem. Phys.*, **96**, 2978 (1992).

[62] F. Sim, S. Chin, M. Dupuis and J. E. Rice, *J. Phys. Chem.*, **97**, 1158 (1993).

[63] V. Moliner, P. Escribano and E. Peris, *New J. Chem.*, 387 (1998).

[64] F. Spano, J. Kuklinski and S. Mukamel, *Phys. Rev. Lett.*, **65**, 211 (1990); V. Kamalov, I. A. Struganova and K. Yoshihara, *J. Chem. Phys.*, **100**, 8640 (1996).

[65] S. Yitzchaik, G. Berkovic and V. Krongauz, *Adv. Mater.*, **2**, 33 (1990); S. Yitzchaik, S. Di Bella, P. M. Lundquist, G. K. Wong and T. J. Marks, *J. Am. Chem. Soc.*, **119**, 2995 (1997).

[66] J. Zyss, J. F. Nicould, M. J. Coquillay, *J. Chem. Phys.*, **81**, 4160 (1984); B. R. Grubbs, S. R. Marder and J. W. Perry, *Chem. Mat.*, **3**, 3 (1991).

[67] J. D. Bierlein, L. K. Cheng, Y. Wang and W. Tam, *Appl. Phys. Lett.*, **56**, 423 (1990).

[68] S. C. Abrahams and J. M. Robertson, *Acta Cryst.*, **1**, 252 (1948).

[69] J. Donhue and K. N. Trueblood, *Acta Cryst.*, **9**, 960 (1956).

[70] G. F. Lipscomb, A. F. Garito, and R. S. Narang, *Appl. Phys. Lett.*, **38**, 663 (1981).

[71] G. F. Lipscomb, A. F. Garito, and R. S. Narang, *J. Chem. Phys.*, **75**, 1509 (1981).

[72] B. Tieke, *Adv. Mater*, **2**, 222 (1990).

[73] Sudharsanam, R.; Chandrasekaran, S.; Das, P. K. *J. Mol. Struct.*, **2003**, *645*, 51.

[74] Davydov, A. S. *Theory of Molecular Excitons* by A. S. Davydov (McGraw-Hill, New York, 1962).

[75] Harada, N.; Takuma, Y.; Uda, H. *J. Am. Chem. Soc.*, **1978**, *100*, 4029.

[76] *Circular Dichroic Spectroscopy: Exciton Coupling in Organic Stereochemistry* by K. Nakanishi; University Science Books, Mill Valley, CA, 1983.

[77] Scholes, G. D.; Ghiggino, K. P.; Oliver, A. M.; Paddon-Row, M. N. *J. Am. Chem. Soc.*, **1993**, *115*, 4345.

[78] McCullough, J. *Chem. Rev.*, **1987**, *87*, 811; Kasha, M. *Rev. Mod. Phys.*, **1959**, *31*, 162.

[79] Datta, A.; Pati, S. K. *J. Chem. Phys.*, **2003**, *118*, 8420.

[80] (a) D. Li, T. J. Marks and M. A. Ratner, J. Phys. Chem, **96**, 4325, (1992). (b) S. Ramasesha and Z. G. Soos, Chem. Phys. Lett, **158**, 171, (1988).

[81] M. G. Kuzyk, Phys. Rev. Lett, **85**, 1218, (2000).

[82] *Molecular Electronic-Structure Theory*, T. Helgaker, P. Jorgensen and J. Olsen (John Wiley & Sons, New York, 2000)

[83] B. K. Rao and P. Jena, J. Chem. Phys, **113**, 1508, (2000).

[84] (a) K. Wu, X. Chen, J. G. Snijders, R. Sa, C. Lin and B. Zhuang, J. Cryst. Growth, **237**, 663, (2002). (b) G. Maroulis and C. Pouchan, J. Phys. Chem.B, **107**, 10683, (2003).

[85] (a) S. Shetty, D. Kanhare and S. Pal, *Abstracts of Papers*, Symposium on Trends in Theoretical Chemistry, Kolkata, India, January 17-19, 2003. (b) S. Shetty, D. G. Kanhare and S. Pal, J. Phys. Chem. A, **108**, 628, (2004).

[86] A. Kuznetsov, K. Birch, A. I. Boldyrev, X. Li, H. Zhai and L. Wang, Science, **300**, 622, (2003).

[87] Z. Chen, C. Corminboeuf, T. Heine, J. Bohmann and P. V. R. Schleyer, J. Am. Chem. Soc, **125**, 13930, (2003).

[88] M. W. Schmidt, K. K. Baldridge and J. A. Boatz et al. J. Comput. Chem, **14**, 1347, (1993).

[89] S. Chacko, M. Deshpande and D. G. Kanhare, Phys. Rev. B, **64**, 155409, (2001).

[90] R. G. Pearson, Inorg. Chem., **27**, 734 (1988).

[91] *Advanced Organic Chemistry: Reactions, Mechanisms and Structure*, Jerry March, 4th edition, (John Wiley and Sons, 1992).

[92] S. R. Marder, J. W. Perry, G. Bourhill, C. B. Gorman, B. G. Tiemann and K. Mansour, Science, **261**, 186, (1993).

[93] A. D. Becke, J. Chem. Phys, **98**, 1372, (1993).

[94] T. Clark, J. Chandrasekhar and P.v.R. Schleyer, J. Comput. Chem. **4**, 294, (1983).

[95] M. J. Frisch, M. Head-Gordon and J. A. Pople, Chem. Phys. Lett. **166**, 281, (1990).

[96] (a) K. B. Sophy and S. Pal, J. Chem. Phys. **118**, 10861, (2003). (b) M. K. Harbola, Chem. Phys. Lett. **217**, 461, (1994).

[97] (a) S. J. A van Gisbergen, P. R. T. Schipper, O. V. Gritsenko, E. J. Baerends, J. G. Snijders, B. Champagne and B. Kirtman, Phys. Rev. Lett. **83**, 694, (1999). (b) P. M. Sanchez, Q. Wu and W. Yang, J. Chem. Phys. **119**, 11001, (2003).

[98] J. F. Ward and D. S. Elliot, J. Chem. Phys. **69**, 5438, (1978).

[99] J. M. Mercero and J. M. Ugalde, J. Am. Chem. Soc. **126**, 3380, (2004)

[100] A. Kuznetsov, K. Birch, A. I. Boldyrev, X. Li, H. Zhai and L. Wang, J. Am. Chem. Soc. **124**, 11791, (2002).

[101] G. Wilkinson, M. Rosenblum, M. C. Whiting and R. B. Woodward, J. Am. Chem. Soc. **74**, 2125, (1952).

[102] *Inorganic Chemistry: Principles of Structure and Reactivity*, James E. Huheey, E. A. Keiter and R. L. Keiter, 4th edition, (Pearson Education, 2000).

[103] S-Y. Chu, R. Hoffmann, J. Phys. Chem. **86**, 1289, (1982).